The Mitochondrial Protein Profile Changes during the Aging Process

Proteomic aspects and mathematical modeling

Vorgelegt von
Diplom-Ingenieur
Lei Mao
aus Pekin, China

angefertigt am Institute für Humangenetik
Charité Campus Virchow-Klinikum
Unter der Beteuerung von
Prof. Dr. Dr. Joachim Klose

Zur Erlangung des akademischen Grades
Doktor der Naturwissenschaften
- Dr. rer.nat. -
der Fakultät III-Prozesswissenschaften
Institut für Biotechnologie
der Technischen Universität Berlin
Univ.-Prof. Dipl.-Ing. Dr. U. Stahl

Genehmigte Dissertation

Promotionsausschuss:

Vorsitzender: PD Dr. rer. nat. Roland Lauster
Gutachter: Univ.-Prof. Dipl.-Ing. Dr. Ulf Stahl
Gutachter: Prof. Dr. Dr. Joachim Klose

Tag der wissenschaftliche Aussprache: 15.02.2005

Berlin 2005
D 83

Table of Contents

Summary

The accumulation of mitochondria bearing mutated genomes was proposed to be an important factor involved in aging (Wallace, 2001). In order to investigate the effect of mtDNA mutation at the protein level, we studied the mitochondrial proteome during aging with a mouse model (C57/BL6).

For the validation of the mouse model, histochemical staining was carried out to compare the cytochrome c oxidase (COX) activity on mouse muscle tissues of young (newborn) and old animals (24-months). No COX-negative myocyte was found in young mouse muscle tissue, whereas a significant part of the myocytes (43%) in the old-aged mouse muscle showed lowered COX-activity compared to the remaining cells in the same tissue. The senescent muscle tissue displayed typical “mosaic” pattern, similar to that has been described in previous studies using human material. This indicates that the mouse could be a valid model for human aging.

Mitochondria were isolated from mouse brain and liver at six different ages (newborn to 24-months, n=8 to 13) using continuous gradient centrifugation. Mitochondrial proteins were sequentially extracted using Tris-buffer (tris-(hydroxymethyl)-aminomethane buffer) (resulting “Fraction I”) and Triton-containing buffer (resulting “Fraction II”), while the remaining pellet underwent methanol-chloroform extraction (resulting “Fraction III”). Large-gel 2D-electrophoresis analysis and a modification of 2D-electrophoresis (employing Triton-X100) were utilized for the analysis of “Fraction I” and “Fraction II” proteins, respectively. Western immunoblotting was carried out on “Fraction III” samples to elucidate the changes in mtDNA-encoded protein COX subunit I.

The expression of two respiratory chain complex I subunits (NADH-ubiquinone oxidoreductase 13 kDa-A subunit and NADH-ubiquinone oxidoreductase 1 alpha subcomplex 5) and one complex IV subunit (COXVb) decreased with age. One subunit of complex III (ubiquinol-cytochrome c reductase binding protein), one subunit of complex V (ATP F0 subunit) and a mitochondrial ribosomal protein increased in expression during aging. Together, these data indicate that complex I and IV deficiency in aged tissue is accompanied by feedback regulation of other protein complexes in the respiratory chain. This is consistent with the previous prediction that accumulation of mtDNA deletion affect predominantly complex I and complex IV genes (Vu et al., 2000).

Furthermore, the observed down-regulation of the 10 kDa mitochondrial heat shock protein indicated an elevated level of oxidative stress in aged mouse brain and liver tissue, which

could be a common aspect in aging and neuronal degenerative diseases (Cottrell et al., 2000; Richter et al., 1988). The up-regulation of mitochondria-associated alpha-synuclein in brain tissue might indicate an enhanced susceptibility to protein aggregation with advanced age (Goedert, 1997; Ueda et al., 1993). The decrease of mitochondria-associated regucalcin in liver tissue indicates a lowered mitochondrial buffering capacity of calcium (Takahashi and Yamaguchi, 2000; Xue et al., 2000).

A mathematical model was developed to simulate the accumulation of defective mitochondria during aging. When we applied our quantitative data observed by 2DE to this model, the mtDNA mutation rate was estimated to be $1.2x10^{-8}$ per gene per day. This mutation rate is high enough to lead to the accumulation of defective mitochondria during the biological time scale.

The experimental data gained from our proteomic study were in accordance with the hypothesis that mitochondrial somatic mutations accumulate with age. This may explain the progression of mitochondrial dysfunction and increasing level of oxidative stress during the aging process. Future investigation will focus on the mtDNA-encoded protein changes and the in-depth mechanism of protein interaction during the aging process. This work would contribute to a better understanding of the mechanism of aging process, would also find application in the development of mitochondria-targeting therapies to prevent from insidious accompanies of aging process such like age-related degenerative diseases.

Keyword:
Mitochondria, aging, degenerative diseases, proteome, 2D-PAGE, mouse model, mathematical modeling.

List of Abbreviations

°C	degree Celsius
2D-electrophoresis	two-dimensional electrophoresis
8-OH-dG	8-hydroxydeoxyguanosine
A (mA)	ampère (milliampère)
ACN	acetonitrile
ADP	adenosine diphosphate
ATP	adenosine triphosphate
BCA	Bicinchoni acid
Bisacrylamide	N, N'-methylene-bis-acrylamide
BisTris	2-[Bis-(2-hydroxyethyl)amino]-2-(hydroxymethyl)propane-1,3-diol
bp (kbp)	base pair (kilo base pairs)
BSA	bovine serum albumin
CHAPS	3-[(3-cholamidopropyl)-dimethylammonio]-propan-sulfonate
cm	centimeter
CoA	coenzyme A
Complex I	NADH-ubiquinone oxidoreductase
Complex II	succinate-ubiquinone oxidoreductase
Complex III	ubiquinol-cytochrome c reductase
Complex IV	cytochrome c oxidase
Complex V	ATP synthase
CoQ	Coenzyme Q (ubiquinone)
COX	cytochrome c oxidase
Da (kDa)	dalton (kilodalton)
dAMP	deoxyadenosine 5'-monophosphate
dCMP	deoxycytidine 5'-monophosphate
dGMP	deoxyguanosine 5'-monophosphate
DHB	2,5-dihydroxybenzoic acid
DNA	desoxyribonucleic acid
Dpi	dots per inch
dpi	dots per square-inches
DTT	dithiotreitol
EDTA	ethylenediaminetetraacetic acid
EGTA	ethylene glycol-bis(beta-aminoethyl ether)-N,N,N',N'-t etraacetic acid
EMBL	European Molecular biology laboratory
ESI	electro spray ionisation
FADH2	reduced flavin adenine dinucleotide
g (mg, ng)	gram (milligram, nanogram)
h	hour
HPLC	high performance liquid chromatography
HTML	Hyper Text Markup Language
IEF	isoelectric focussing
IgG	immunoglobulin G
IPG	immobilised pH-gradient
l (ml, ml)	litre (millilitre, microliter)
M (mM)	molar (mill molar)
m/z	ratio of mass to charge
MALDI-TOF	matrix assisted laser desorption/ionisation-time of flight
min	minute
mRNA	messenger ribonucleic acid

MS	mass spectrometry
mtDNA	mitochondrial DNA
MPTP	1-methyl-4-phenyl-1,2,3,6-tetrahydropyridine
MW	molecular weight
NADH	reduced nicotinamide adenine dinucleotide
PAGE	polyacrylamide gel electrophoresis
PBS	phosphate buffer saline
PCR	polymerase chain reaction
PCR	polymerase chain reaction
pI	isoelectric point
PMSF	phenylmethylsulphonyl fluoride
RNA	ribonucleic acid
ROS	reactive oxygen species
rpm	rotations per minute
rRNA	ribosomale RNA
SDH	succinate:ubiquinone oxidoreductase
SDS	sodium deodecylsulfate
SDS-PAGE	sodium dodecylsulfate-polyacrylamide gel electrophoresis
SOD	superoxide dismutase
SPF	Specific pathogen Free
TEMED	N, N, N', N' – tetramethylethylenediamine
TFA	trifluoroacetic acid
TIM	translocases of the inner-membrane
TOM	translocases of the outer-membrane
Tricine	N-[2-Hydroxy-1,1-bis(hydroxymethyl)ethyl]glycine
Tris-base	tris-(hydroxylmethyl)-amoniomethane
Tris-HCl	tris (hydroxymethyl) aminomethane, Hydrochloride
Triton-X100	Polyethylene glycol tert-octylphenyl ether
tRNA	transfer RNA
Tween 20	Polyoxyethylene (20) sorbitan monolaurate
V(mV)	volt (mill volt)
v/v	volume per volume
w/v	weight per volume

1 Introduction

“Aging is the progressive accumulation of changes with time that are associated with or responsible for the ever-increasing susceptibility to disease and death which accompanies advancing age“ (Harman, 1981). As a biological phenomenon, aging exist in all sexually reproductive life forms, including unicellular organisms (Bowen and Atwood, 2004). The functional pathways involved in aging process may include responses to endogenous and exogenous changes, such like hormonal changes and damage accumulation (Finch, 1993). Aging and longevity are also influenced by genes (Finch and Tanzi, 1997).

1.1 Disposable soma theory of aging

Although no consensus of aging mechanism exist, it has been noticed that only species with a clear distinction between soma and germ line undergo somatic senescence (Kirkwood and Holliday, 1979; Le Bourg, 1998). Based on their observation, Lindop & Rotblatt proposed the *disposable somatic theory* (Henshaw, 1947; Lindop and Rotblat, 1961b), which states that aging may result from the accumulation of unrepaired somatic defects due to the reduced investigation for the somatic maintenance. For instance, telomerase, the enzyme that is responsible for the maintenance of the proper length of the chromosomal DNA does not function in somatic part (Harley et al., 1990; Hastie et al., 1990; Lindsey et al., 1991). This is also in accordance with the somatic theory of aging.

1.2 Free radical theory of aging

Respecting the reason of somatic damage, it is generally accepted that cellular DNA is constantly exposed to exogenous and endogenous DNA-damaging agents, with reactive oxygen species (ROS) as the most important contributors. This was deduced from the early observation of Lindop and Henshaw, who showed in their experiments that irradiation damage of DNA shortened lifespan in animal models and induced features of premature aging (Henshaw, 1947; Lindop and Rotblat, 1961a).

The direct relation of free radical and gene mutation has been proposed by Lindop & Rotblatt, who intensively studied the correlation between radiation and the concentration increase of 8-hydroxydeoxyguanosine (8-OH-dG), a marker of DNA oxidative damage. Later, Feeney suggested that free radicals are also involved in reactions that led to the damage of the biological membrane and proteins (Feeney and Berman, 1976).

1.3 The role of mitochondria in free radical production

As the major site of free radical generation in the eukaryotic cells, mitochondria have been pushed to the middle of the stage. Mitochondria are complex organelles bound by an inner and an outer membrane. They are involved in multiple cellular processes such as citric acid cycle, oxidative phosphorylation, β-oxidation, calcium homeostasis, urea cycle, heme biosynthesis, apoptosis and cell signalling (Green and Amarante-Mendes, 1998). Phylogenetic data support an origin of mitochondria from the bacteria of the Order Rickettsiales (Emelyanov, 2001).

The respiratory chain localized on the mitochondrial inner membrane is composed of five multi-polypeptide enzyme complexes. These include complex I (NADH-ubiquinone oxidoreductase), complex II (succinate-ubiquinone oxidoreductase), complex III (ubiquinol-cytochrome c reductase), complex IV (cytochrome c oxidase, or COX) and complex V (ATP synthase). Additionally, two mobile electron carriers (ubiquinone and cytochrome c) are also involved in the oxidative phosphorylation. The respiratory chain oxidizes electrons distributed from reduced nicotinamide adenine dinucleotide (NADH) or flavin adenine dinucleotide ($FADH_2$) to build the electro-chemical gradient across the mitochondrial inner membrane. This potential energy is utilized by complex V to synthesize ATP from ADP and orthophosphate.

Noteworthylly, the components positioned early in the respiration chain (Complex I and Coenzyme Q) leak some fraction of the electrons directly to molecular oxygen to form superoxide anion ($O_2^{\bullet}$-). Under physiological conditions, up to 2% of the total oxygen consumption was estimated to form superoxide radicals (Joenje, 1989). Besides, in the presence of reduced transition metals, H_2O_2 can also be converted to the highly reactive hydroxyl radical ($OH^{\bullet}$) by Fenton reactions. These are only partially detoxified by a variety of enzymes and free radical scavengers, including catalase, glutathione and peroxiredoxin (Joenje, 1989).

1.4 Involvement of mitochondrial mutation in aging

Except for Complex II, all respiratory chain complexes contain protein subunits that are encoded by mitochondrial genes on the circular mtDNA. These proteins are synthesized inside mitochondria by their own protein synthesis machinery (fig.1). The influence of mtDNA mutation on aging thus raised attention (Wallace, 1992).

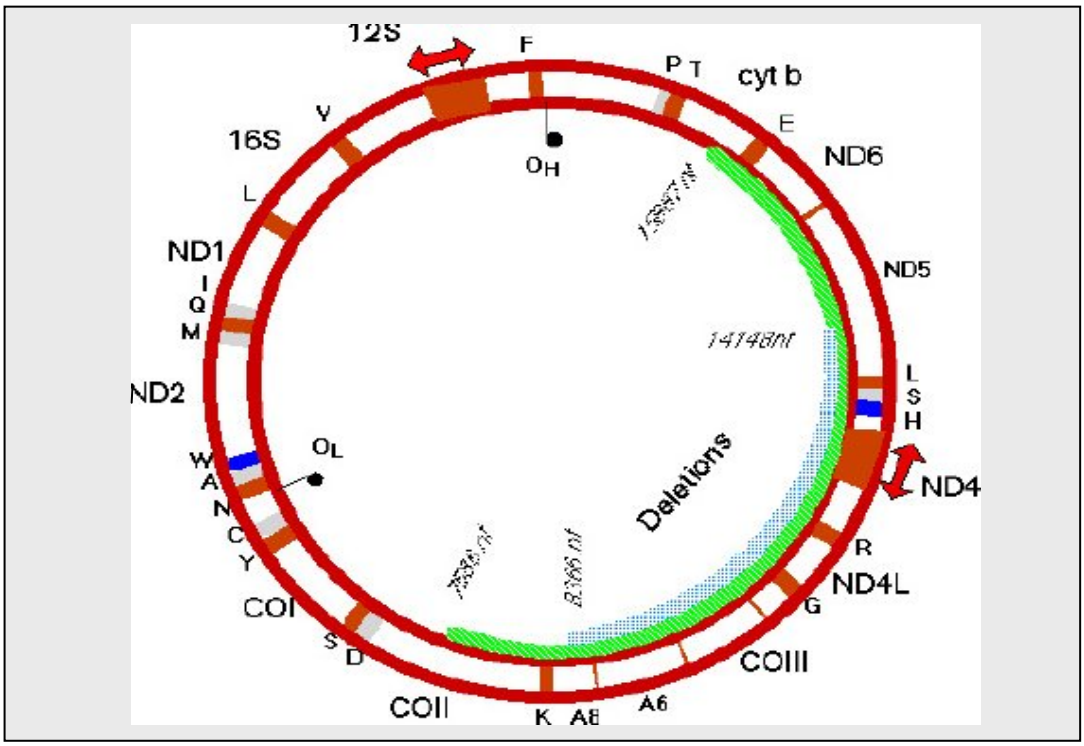

Fig.1: The human mitochondrial genome is a 16,569 bp molecule of double-stranded DNA. This mtDNA encodes for 13 essential components of the respiratory chain. DN1-ND6 and ND4L encode seven subunits of complex I, Cytb is the only mtDNA encoded complex III subunit. COXI-III encode for three of the complex IV subunits, whereas the ATP6 and ATP8 genes encode for two subunits of complex V. O_H and O_L are origins of replication from heavy and light strand mtDNA, respectively. Area marked in green shows the sequence range that is frequently been deleted (cited from web site of University of Minnesota, www.chem.umn.edu/groups/arriaga/mitochondria.htm).

Numerous mtDNA mutations have been observed in diverse mitochondrial diseases. These include large deletions (Lee et al., 1994), short duplications (Brockington et al., 1993) and point mutations (Munscher et al., 1993).

Interestingly, many mtDNA abnormalities that had previously been linked to a variety of clinical syndrome were also found to accumulate in normal aged individuals (Corral-Debrinski et al., 1992; Linnane et al., 1992). Particularly, a 4977bp large mtDNA deletion was most commonly found in aged individuals (Cortopassi and Arnheim, 1990; Linnane et al., 1990). This so-called “common deletion” occurs between two 13bp direct repeats located at nucleotide position 8470 to 8482 and at 13447 to 13459, respectively (Lee et al., 1994; Yen et al., 1991; Zhang et al., 1997a).

In 1997, Tengan observed the positive correlations between age and “common deletion” levels in both non-diseased controls (r=0.80) and patients with mitochondrial diseases (r=0.69) (Tengan et al., 1997). This led to the suggestion that there is an important connection between aging and the accumulation of mitochondrial DNA mutations (Wallace, 1992).

1.4.1 Possible mechanism of mtDNA mutation

The most likely cause of mtDNA rearrangement has been proposed to be the exposure to ROS ($O_2^{\bullet}$-, H_2O_2 and $OH^{\bullet}$) (Ames et al., 1993; Richter et al., 1988). In 1992, Hayakawa observed the clear correlation between the 8-OH-dG content in human heart and the amount of mtDNA with a deletion (r=0.93) (Hayakawa et al., 1992).

The mutagenic potential of 8-OH-dG is reflected by its miscoding properties: instead of dCMP, dAMP can be incorporated opposite the modified base 8-OhdG during replication (Shibutani et al., 1991), thus introducing point mutation. In turn, illegitimate recombination or strand slippage could happen during replication, which results in mtDNA deletion (Baumer et al., 1994; Taylor et al., 2001). The expression of mtDNA might also be compromised through interference in RNA polymerase bound with damaged nucleotides (Nagley and Wei, 1998). Furthermore, mtDNA molecules subjected to extensive oxidative damage can become cross-linked to other macromolecules such as proteins and lipids and this too could interfere with efficient mtDNA replication and transcription in mitochondria (Nagley and Wei, 1998).

1.4.2 mtDNA supposed to be especially vulnerable

The mutation rate of mtDNA is proposed to be 10 to 20 fold higher than in comparison to nuclear genes (DiMauro et al., 2000; Osiewacz and Hamann, 1997; Zeviani et al., 1998). This is due to the lack of histone protection on the mtDNA molecule, the proposed insufficient DNA repair mechanism in mitochondria (Cullinane and Bohr, 1998), and the extensive exposure of mtDNA molecules to ROS.

Additionally, since mtDNA molecules in mammals have a high information density with essentially no sequence redundancy, large-scale deletions and point mutation often cause the loss or truncation of not only structural genes, but also rRNA and tRNA genes. This will in turn have deleterious effects on mitochondrial protein production.

1.5 The mitochondrial theory of aging

Based on the observation that accumulation of mitochondrial somatic mutation is associated with the mitochondrial dysfunction that occur during the aging process, the

mitochondrial theory of aging was subsequently deduced by Harman as an extension of the *free radical theory* (Harman, 1972) (fig.2).

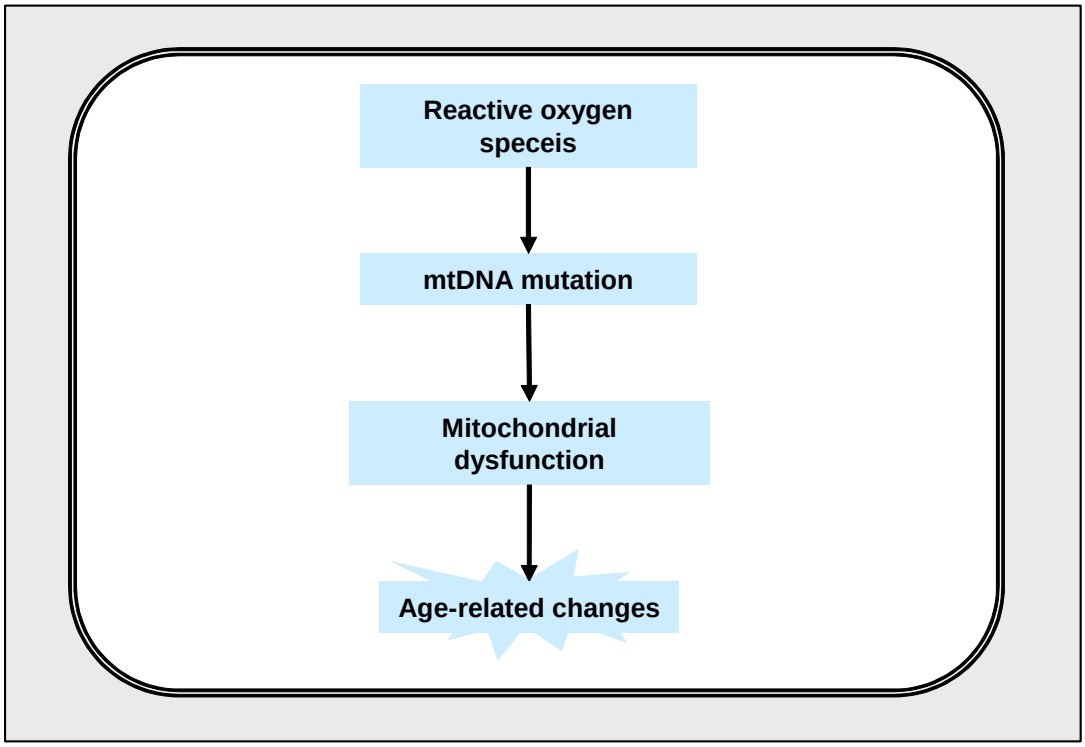

Fig.2: Mitochondrial theory of aging proposes that free-radical-induced mtDNA mutation is able to accumulate along with age. This could be the driving force leading to mitochondrial dysfunction and the phenomenon of aging.

The mitochondrial theory of aging states that the slow accumulation of impaired mitochondria due to free-radical induced mutation is the driving force of the aging process (Kowald and Kirkwood, 1999; Linnane et al., 1989; Richter, 1988). The theory foundations of mitochondrial theory of aging include two assumptions: firstly, mtDNA supposed to be more vulnerable than nuclear DNA respecting free radical induced mutations. Compared to nuclear DNA, human fibroblast mtDNA is damaged three times more by H_2O_2, 16 times more by ROS in general. More importantly, mitochondrial mutations have the potential of disrupting whole cellular physiology (Wallace, 1997).

1.5.1 Experimental evidences of mitochondrial theory of aging

Several lines of evidence support the view that the bio-energetic function of the mitochondria deteriorates with age (Boffoli et al., 1994; Brierley et al., 1998; Kopsidas et al., 1998). Histochemical staining has shown that aged muscle tissue show alternating cytochrome c oxdiase (COX)-positive and COX-negative regions, displaying a mosaic pattern (Kopsidas et al., 2000; Mita et al., 1989). In parallel, there exists a corresponding

“mosaic pattern” respecting mtDNA mutation. Those COX-negative regions contain high concentrations of the deleted mtDNAs (Shoubridge et al., 1990; Zhang et al., 1997b).

Accumulation of mtDNA mutations are widespread processes in various human tissues during the aging process. Age-dependent deterioration of mitochondrial respiration activity and age-associated mitochondrial DNA deletion were observed in human liver, heart, skin and brain tissues (Corral-Debrinski et al., 1992; Kovalenko et al., 1998; Yen et al., 1994).

Furthermore, it was demonstrated that mtDNA mutation does not occur uniformly in different tissues (Kovalenko et al., 1998). Liu and Pang observed that the slower growing normal skin tissues harbour higher level of the 4977bp deleted mtDNA than the faster growing skin tissues in cancerous and precancerous skin tissues (Liu et al., 1998; Pang et al., 1994). MtDNA rearrangement in tissues from aged human subjects occur in levels ranging from very low in liver, to considerable in cardiac muscle, to almost total in skeletal muscle (Kopsidas et al., 1998; Liu et al., 1998). Generally, it gives consensus that age-related mtDNA mutation occur more frequently and accumulate much faster in tissues of high energy-demand and low mitotic activity.

However, since most cells contain hundreds to thousands of mtDNA molecules, A single mutant molecule is unlikely to influence the physiology of the cell and thus cannot play a role in the aging process (Coller et al., 2002). To affect cellular physiology, the nascent somatic mutants must somehow accumulate in the cell to significant levels.

1.5.2 Theoretical supports of the mitochondrial theory of aging

In 1976, the mitochondrial theory of aging was refined by De Grey (de Grey, 1997), who reasoned the theoretical possibility of mitochondrial mutation accumulation. By proposing a slower degradation rate of defected mitochondria compared to wild type mitochondria, the defective mitochondria gain a selective advantage.

According to DeGrey’s idea, the mutated mtDNA molecules can eventually lead to a homoplasmic status of the cell. A mathematical model constructed by Kowald and Kirkwood (Kowald and Kirkwood, 2000) was able to simulate such dynamic processes theoretically.

1.5.3 Controversial observations

Whilst COX-deficient muscle fibres were a real finding in senescent tissues, the pivotal role of mtDNA mutations to the aging process is still controversial (Brierley et al., 1997). Some other investigations failed to detect age-dependent changes in mitochondria (Bodenteich et

al., 1991; Manzelmann and Harmon, 1987). Jazin found in the brain tissue that while the occurrence of sequence variation in mtDNA was significantly higher in the non-coding (D-loop) region of mtDNA of the aged individuals compared with that of the younger subjects, a very low occurrence of variation was found in coding regions of mtDNA segments (Jazin et al., 1996).

Kraytsberg argued that accumulation of defective mitochondria in cells is probably not the only and not the most important mechanism potentially relating mtDNA mutations to aging (Kraytsberg et al., 2003). They showed that mtDNA deletions co-locate not only with mitochondrial abnormalities, but also with thinned and degenerated fibre morphology.

Respecting the proposed lack of DNA repair mechanism in mitochondria, several repair pathways have been recently described for mtDNA, including double strand breakage repair (Bohr and Dianov, 1999).

1.6 Possible causes of these controversial observations

Reasons for the existence of these controversies could be two-fold: Firstly, the majority of the observations described above came from genetic analysis, mostly polymerase chain reaction (PCR) analysis on mtDNA and nuclear DNA encoded mitochondrial proteins (Cortopassi and Arnheim, 1992).

PCR methods have the advantage of selectively amplifying only mtDNA bearing certain range. However, mtDNA mutations appear to concentrate in certain “hotspot” areas, i.e., small regions of the genome with high incidence of mutations (Jazin et al., 1996; Nekhaeva et al., 2002). This implies that results of PCR are largely influenced by whether the applied primer contains certain mutation hotspots or not. Scoring mutations on a fragment that is too short can lead to the overestimation or underestimation of mutation events (Kraytsberg et al., 2003).

Furthermore, even though the recent development of whole range PCR is able to amplify the complete mitochondrial DNA molecule, it is still doubtful whether the genomic information alone is sufficient to clarify complete mechanisms of aging. The mtDNA genes need a whole repertoire of nuclear proteins for their protein transcription, translation and assembly (Sickmann et al., 2003; Zhao et al., 2000). The presence of a mitochondrial gene on the mtDNA molecule does not mean that this respective protein will be properly produced and assembled into functional protein complexes.

Expression levels of a protein depend not only on transcription rates of the gene, but also on additional control mechanisms, such as transcript stability, translational regulation and protein degradation. Moreover, both the activity and the function of proteins can be altered, mainly through post-transnational modification (glycosylation, phosphorylation) or proteolytic cleavage (Amson et al., 1996; Boguski and Schuler, 1995; Harry et al., 2000). All these points could contribute to the presence of largely controversial observations using genetic analysis (Rustin et al., 2000; Storm et al., 2002).

1.7 Proteomic analyses in aging research become obligatory

Based on the above consideration, the need of protein-level analysis arises because phenotypes of senescent cells appear through functions of expressed and modified protein networks. Transcription or translation products of genes in oxidative damaged or mutated mtDNA might deleteriously affect protein synthesis, protein complex assembly, and in turn respiratory enzyme function. An insufficient respiratory chain activity would consequentially further increase oxidative stress in the cells. Such phenomenon could be largely observed at the protein level, rather than in gene-based analysis. Therefore, research on age-dependent protein alterations in the cells is necessary in clarifying the involvement of mitochondria in the aging process.

As has been pointed out by Pirt, “The limiting factor is understanding not only the gene structure but also the gene expression, which varies in a most complex way. The new paradigm should be addressed to elucidation of the integrated functions of genes, enzymes, membranes and metabolites in the whole organism.” (Pirt, 1991).

The term “proteome” was first advocated by Marc Wilkins in 1995, defined as the entire protein complement in a given cell, tissue or an organism (Anderson and Anderson, 1996; Wasinger et al., 1995; Wilkins et al., 1996). In its wider sense, proteomic research also assesses protein activities, modifications, localization and interactions. By studying global patterns of proteins and their changes dynamically, proteomic research can improve our understanding of system-level cellular behaviour.

High throughput two-dimensional protein electrophoresis coupled with peptide mass fingerprinting analysis by mass spectrometry (MS) have become the most powerful techniques for morden proteome analysis (Gras et al., 1999) (fig.3).

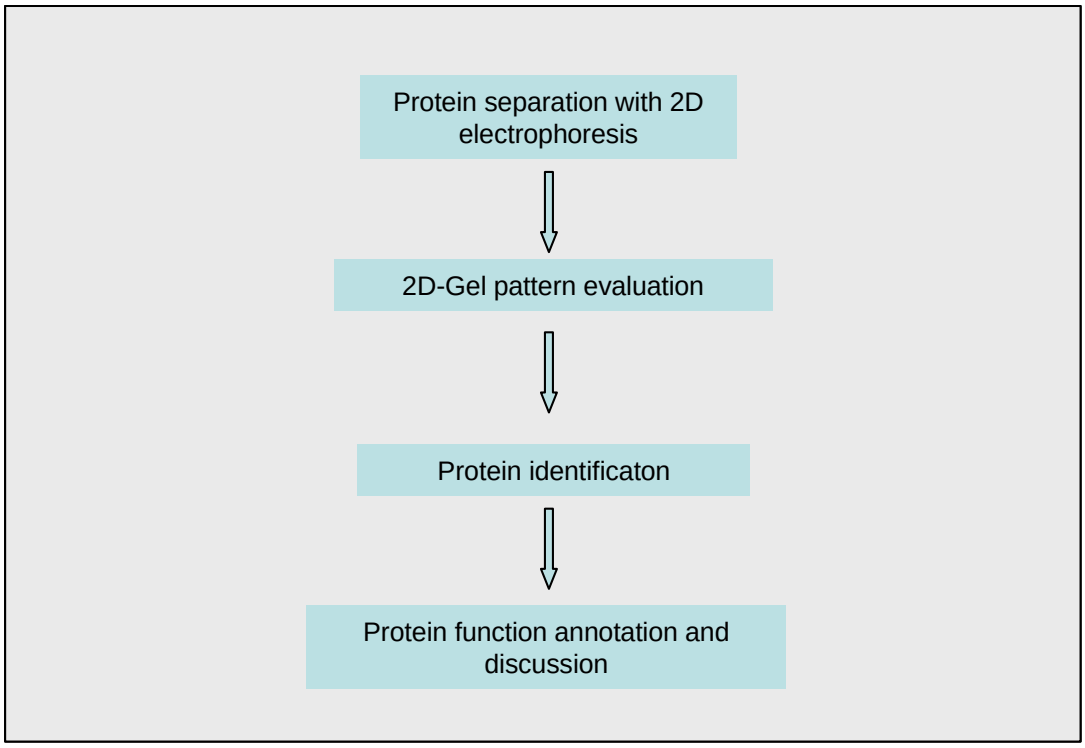

Fig.3: Strategy of differential protein display employing 2D-electrophoresis. Proteins are separated by 2D-electrohporesis, and proteomic profiles are displayed as spots on the gel slab. Quantitative and qualitative differences of corresponding spots among gels are accessed according to differences of protein spot patterns. Subsequently, proteins in the spot of interest are digested with an endoproteinase and subjected to mass spectrometry for identification by peptide mass fingerprinting.

1.8 Current state of mitochondrial proteomic research

The total number of different proteins or polypeptides in a mitochondrion was estimated to be around 1000 (Lopez and Melov, 2002). Mitochondrial proteome has been characterized on the human placental cells (Rabilloud et al., 1998), trans-human-mitochondrial cybrids (Lopez and Melov, 2002), human neuroblastoma cell line (Fountoulakis and Schlaeger, 2003), human lymphoblastoid cell line (Xie, 2003) and on human heart mitochondria (Taylor et al., 2002). Blue-native electrophoresis has greatly contributed to the mitochondrial protein complex investigations (Schagger and von Jagow, 1991), while Western immunoblotting remains to be an effective hypothesis-driven proteomic strategy.

So far, the largest proteomic study of purified mitochondria was performed by Sickmann on yeast mitochondria, leading to the identification of 750 mitochondrial or mitochondria-associated proteins with a coverage of up to 90% of predicted yeast mitochondrial proteome (Sickmann et al., 2003; Westermann and Neupert, 2003). Unfortunately, there is

still a lack of protein-level evidence of the accumulation of mutated mitochondria during the aging process (Wei, 1998; Zhang et al., 1998).

1.8.1 Why there has been a lack of protein-level analysis

The current lack of proteomic level investigation of the mitochondrial theory of aging is largely due to the lack of technical feasibility. First, it is likely that mutation rate of mtDNA is very small respecting a certain type of mutation, thus, more sensitive methods will be needed (such as pre-fractionation, mitochondrial sub-proteomics). Until now, it has been difficult to accurately assess spontaneous mtDNA mutation rate i*n vivo* in various organs and tissues during aging (Linnane et al., 1990).

Secondly, proteomic field has not been as powerful as the genetic method since very recently. Furthermore, many mitochondrial proteins of interest could be low abundant or membrane protein. This further escalates the difficulty of such projects.

1.8.2 Recent development of proteomic technology makes this study tractable

Only recently, sensitivity and effectiveness of proteomic analysis is rising through a whole new repertoire of high-throughput technical developments. Especially, large-gel 2D-electrophoresis analysis has now reached a technical state that offers the possibility to reveal the majority of the cellular proteins (Klose et al., 2002).

New protein analytical methods such like mass spectrometry compatible for macromolecules, computational tools, comprehensive databases for characterization of molecular structures of proteins led to large-scale strategies in protein identification. Other methods such like Blue-native electrophoresis and protein chip micro-arrays also provide the opportunity to directly test various proteomic aspects.

These made proteomics an attractive strategy of studying complex biology problems such like aging, in order to gain additional knowledge of protein localization, protein interaction and their influence on protein structure and function. In this study, we dared to challenge the mitochondrial theory of aging with an in-depth proteomic study. The goal of this proteomic study was to obtain a more global and integrated view of aging biology by studying dynamic protein networks, rather than certain protein individually.

1.9 Complexity of the system requires modeling

Upon obtaining the experimental data from proteomic studies, it would be necessary to determine a sequence of events that can elucidate the primary factors responsible for the cascade of complex events that accompany aging.

However, there is a range of factors that can potentially influence the abundance of mtDNA mutation. These include mtDNA mutation rate, metabolic rate, efficiency of mtDNA repair, propagation ability of mutant relative to that of normal mtDNA, influences of mutant mtDNA on cell proliferation and function, as well as mitochondrial degradation rates. For instance, a mitochondrial DNA mutation rate that is too small could make the influence of mitochondrial mutation negligible in the aging process, thus counteract the hypothesis of mitochondrial theory of aging.

Such a dynamic system defies understanding by verbal arguments alone. Quantitative tools would be necessary to probe reliably into the details of the system. From a mathematical point of view, the state of a dynamical system is specified by the concentration values of all biochemical species in the reaction network. After formulating the network into mathematical terms, its qualitative features can be demonstrated for comparison with experimental data, as well as for the generation of new parameter values. Sophisticated computational methods could be beneficial to interpret the complexity of biological information in aging studies.

2 Aim of the Study

The objective of this study was to access age-related changes of mitochondrial proteome. This could in turn reveal the influence of the proposed mitochondrial somatic mutation at the protein level.

In the first stage of this study, an inbreed mouse strain (C57BL/6) was to be validated as the model of human aging; the mitochondria isolation was to be optimized on the mouse liver and bran tissues. In addition, the influence of donor organism age and sample handling on the mitochondria isolation was to be investigated. In the mean time, proteomic analysis tools and protein pre-fractionation methods were to be optimized, in order to improve the resolution capacity of hydrophobic proteins in the 2D-electrophoresis analysis.

In the second stage, the mitochondrial proteins were to be analyzed by 2D-electrophoresis. Mass spectrometry was employed for databank-based protein identification. Special respect was paid on the mitochondrial-DNA-encoded proteins employing Western immunoblotting. Since all 13 mitochondrial-DNA-encoded proteins are localized in the mitochondrial respiratory chain protein complexes, preliminary application of Blue-native electrophoresis was to be conducted for protein complex analysis. A question of particular interest was whether there is tissue-specific property respecting mitochondrial protein profile change in the aging process. This was to be investigated through the parallel study of both brain and liver mitochondria.

Mathematical model has been employed previously to simulate the accumulation of mutated mitochondria in the aging process. However, validation of such model was hampered due to the lack of mtDNA mutation data. A parallel goal of this study was to utilize the data gained in experiment to estimate the mtDNA mutation rate. For this purpose, the hypothetical mechanisms involved in the mitochondrial theory of aging were to be converted into a mathematical model. By fitting the experimental data into this model, the mtDNA mutation rate of mouse tissue was to be calculated under the current modeling setting.

3 Animals, Materials and Methods

3.1 Animals and ethnical agreements

Experimental protocol of this study was approved by the Charité institutional review committee for the care of animal subjects and was performed in accordance with national animal care guidelines (Tierschutzgesetz, Germany).

Specific pathogen Free (SPF) C57BL/6 mice (*Mus musculus domesticus*) were provided by Charles River Germany (Sulzfeld, Germany) and Charles River France (Cedex France). All experimental animals were treated humanely. They received standard feed *ad libitum*, free access to water and human care. Animals were kept at constant temperature (22-24°C) and humidity and had a 12:12 hour light-dark cycle before entering the study.

For the current aging study, healthy mice with mixed gender of the following aging stages were used: newborn (0 to 2 weeks), 5-months, 10-months, 15-months, 20-months and 24-months. Three 22-months mice were used for the obtainment of muscle biopsies and the morphological control of mitochondria isolation from senescent tissues.

3.2 Materials and methods

All chemicals and reagents were purchased from Merck (Darmstadt, Germany) if not otherwise indicated.

3.2.1 Organ obtainment

The animals were sacrificed by swift de-capitalization with a sturdy dissecting scissors. The use of narcotic was avoided to eliminate possible influence on protein profile. Mouse liver perfusion was based on the method of Seglen (Seglen, 1976) with modifications. The abdomen was opened and the intestines gently moved aside to expose the hepatic portal vein and *inferior vena cava caudalis*. The portal vein was cannulated by a cannula (i.d. diameter 0.4mm, Terumo Leuven Belgium), the liver was perfused *in situ* with of 0.9% (w/v) NaCl until slightly distended. The *vena cava* was then cut and the perfusion continued until the liver was completely blanched. After 5ml of perfusion, the liver was freed from the connective membranes, surgically removed from the body and rinsed with cold (0°C) 0.9% (w/v) NaCl. Gall bladder was removed.

The obtainment of mouse brain tissue was conducted according to Klose (Klose, 1999). The muscle and membranous tissue from the posterior part of the skull was removed over

the cerebellum. Using a pair of small surgical scissors, the skull was cut from the *foramen magnum* to the *olfactory bulbs* and the flaps of skull were removed. Caution was exercised to keep the tips of the scissors away from the midline of the *cerebellum* and *cerebral cortex*. Subsequently, the mouse brain was gently pried from the skull, and immersed into a beaker of cold saline (0.9% w/v NaCl). The *trigeminal* and optic nerves were trimmed away, the *bulbi olfactorii* left intact. Spinal cord was cut off at the border to the *rhombencephalon*. For the obtainment of muscle biopsy, hind limb muscles were carefully excised surgically.

Organ weight of brain and liver tissues was controlled directly after organ obtainment for the calculation of mitochondrial yield. The extracted liver and brain tissues were either directly used for mitochondria isolation or shock-frozen in liquid nitrogen for later uses. Freshly extracted muscle tissue specimens without fixation were shock-frozen in isopentane cooled by liquid nitrogen and were stored at -80°C for the histochemcal demonstration of COX-activity.

3.2.2 Enzymatic histochemical staining of COX-activity

For the validation of the C57BL/6 strain as model of human aging, enzymatic histochemical staining of cytochrome c oxidase activity was carried out on the mouse muscle biopsies. Staining was performed on air-dried serial sections of muscle biopsies of young mouse (2 weeks) and old mice (22-months), according to Seligman (Seligman et al., 1968). The oxidation of 3,3'-diaminobenzidine (DAB, Sigma-Aldrich Steinheim Germany) at the site of cytochrome c oxidase activity results in a brown compound insoluble to ethanol.

8μm transverse frozen sections were cut with microtom Cyrostat (Microm, Walldorf Germany) and sections were attached to a cover slip (SuperFrostPlus, R.Langenbrink, Emmendingen Germany).

The incubation medium for the COX-staining consisted of 5mg 3,3'-diaminobenzidine tetrahydrochloride, 9ml of 50mM PBS (pH 7.6), 20μg/ml catalase (Sigma-Aldrich Steinheim Germany) solution, 10mg of practical grade cytochrome (Sigma-Aldrich Steinheim Germany) and 750mg sucrose. Sections were incubated in the incubation medium in a Columbia staining dish (Thomas Scientific, Swedesboro, NJ USA) for 60 minutes at room temperature. After washing with three changes of deionized water (Millipore Schwalbach, Germany), sections were dehydrated in alcohols with ascending concentrations: 50%, 70%, 80%, twice of 95% and twice of 100%, and subsequently cleared with 3 changes of RotiClear (Carl Roth, Karlsruhe, Germany). Section mounting was conducted in synthetic organic mounting medium (Permount, Fisher Scientific; Pittsburgh, PA).

Microscopic examination was carried out on a light microscope conjugated with digital camera under bright field illumination (Carl Zeiss, Oberkochen, Germany). Fibre numbers were determined on photographs (Magnification 100x and 200x) of 21 sections. Between 48 and 114 fibres were examined from each muscle biopsy.

3.2.3 Mitochondria isolation

The method of mitochondria isolation was adopted from Jungblut (Jungblut and Klose, 1985), with slight modifications. All procedures were carried out at 4°C, if not otherwise indicated, to minimize protease activity. Except for newborn tissue, mitochondria of each organ (either brain or liver) were isolated separately, without the pooling of different tissue samples.

Since part of the materials (24-months mice sample) used in this study were collected beforehand and frozen stored in our laboratory, a comparison of mitochondria isolation from fresh and snap frozen materials was carried out.

All solutions used in the centrifugal separations were iso-osmotic solutions (260 mOsm) to that of physiological condition of intact mitochondria, because indications of buoyant density of the organelle are meaningful only in conjunction with the osmolality of the medium employed.

3.2.3.1 Tissue homogenisation and crude mitochondria collection

In order to rupture the tissue and lyses the cell membrane without affecting most of the organelle structure, homogenization was carried out at 0°C with a gentle hand-held teflon-glass Dounce homogenizer (clearance 0.1mm) avoiding vacuum. For this purpose, the freshly removed or swiftly thawed brain or liver tissues were first suspended in three volumes of homogenisation medium (100mM KCl, 0.5M Tris-HCl, 5mM $MgCl_2$, 1mM ATP-Mg, 1mM ethylene glycol-bis(beta-aminoethyl ether)-N,N,N',N'-t etraacetic acid (EGTA), 0.08 v/v protease inhibitor cocktail Complete^{TM} table stock solution (solved in 2 ml 50mM PBS, Molecular Biochemicals Roche, Mannheim, Germany), pH 7.5). Protease inhibitors were added to prevent from protein degradation through biogenic proteases such like serine proteases, cysteine proteases and metalloproteases. The substances were added directly into the protein extracts of proper volume, and intensively stirred for 15 minutes. Up and down movement were carried out until no significant big tissue pieces could be seen by raw eye.

After homogenisation, the homogenate was centrifuged at 800xg (2400rpm, Kendro, Hanau, Germany) for ten minutes to sediment nuclei and debris. The supernatant was

collected. This step was repeated once. Subsequently, the final “post-nuclear supernatant” was collected and subjected to 10,000xg (10,600rpm, Type 50 Ti rotor, Beckman Coulter, Krefeld, Germany) for 15 minutes to obtain the crude microsomal fraction.

The crude microsomal fraction that contain multiple kinds of microsomes (mitochondria, lysosome, peroxisome, Golgi complex, etc.) was diluted with 7ml of 0.25M sucrose solution, and subjected to a serial of three wash steps: 8000xg, 5000xg and 3500xg (9600Upm, 7600Upm and 6300Upm, respectively, each for 15 minutes, Type 50 Ti rotor, Beckman Coulter, Krefeld, Germany). This was for the remove of most microsomal bodies other than mitochondria and lysosome.

After the last washing step, the supernatant was carefully removed by a Pasteur pipette without disturbing the pellet. Generally, only lysosome co-pellet with mitochondria at 3500xg since their similar density to that of mitochondria (Jungblut and Klose, 1985).

3.2.3.2 Purification of mitochondria using gradient centrifugation

In order to further purify mitochondria (separate lysosome from mitochondria), Percoll continuous gradient centrifugation was employed. The density gradient media Percoll (Sigma-Aldrich Steinheim Germany) is an inert colloidal suspension of silica particles coated with polyvinyl pyrrolidone (15-30nm in diameter), with virtually no osmotic effects (Sims, 1990). The low viscosity of Percoll ensures a fast establishment of continuous gradient body and quick centrifugal separation (Pascale et al., 1998; Sims, 1990).

For this purpose, approximately 700μl of suspended crude mitochondrial pellet (1:1 v/v, suspended with 0.25M sucrose with 0.1mM EGTA, pH7.2) was carefully topped on 7ml of 30% (v/v) Percoll solution (in 0.25M sucrose with 0.1mM EGTA) in a polycarbonate ultra centrifugation tube (Nalgene, Rochester, NY USA), avoiding any disturbance of the bottom phase. The centrifugal tube was subjected to 100,000xg (37,400rpm, Type 50 Ti rotor, Beckman Coulter, Krefeld, Germany) of ultra centrifugation for 15 minutes, with no mechanic brake applied upon deceleration.

During the centrifugation, the Percoll solution builds a continuous gradient body due to the migration of silicon particles in the strong gravity field. Meanwhile, the pellet materials co-migrate to their corresponding density layer. Only the intact mitochondria migrate to the density layer of 1.09-1.13 g/ml, while most lysosome and some broken mitochondria to the density layer of 1.05 g/ml above the mitochondrial layer (Jungblut and Klose, 1985).

After the gradient centrifugation, the lower band was aspirated with care and was washed with 0.25 M sucrose solution (10,000xg, 10 minutes Type 50 Ti rotor, Beckman Coulter, Krefeld, Germany) to obtain the mitochondrial pellet. One sample was taken from the upper band for microscopic control. An extensive dilution (1:5 v/v dilution of Percoll) using 0.25 M sucrose solution was necessary in order to sediment mitochondria effectively. This was due to the presence of remaining Percoll, which slowed down the centrifugation process by increasing the density of the surrounding medium.

If required for morphological control analysis using electronic microscopy, ca. 20μg of the pellet was immediately immersed in fixation solution of electronic microscopy. The remaining pellet of intact mitochondria was snap-frozen in liquid nitrogen for further proteomic analysis.

3.2.4 Electronic microscopic control of mitochondrial morphology

The electronic microscopic analysis was a collaboration with the Charité Institute of Anatomy. The mitochondria isolated from young (5-months) and old (22-months) organism (brain and liver tissues), as well as from fresh and frozen materials (brain and liver tissues) were controlled for their morphology and purity.

Portions of isolated mitochondria were fixated with fixation solution containing 60mM PBS and 2.5% glutaraldyhyde (v/v) at room temperature for 15 minutes. Mitochondria were then centrifuged at 15,800xg (20,000rpm, Ti50 rotor) for 5 minutes and the supernatant was discarded. The pellet was layered with fresh fixation solution and left overnight at 4°C. Two additional washing steps were carried out in 60mM PBS (15,800xg, 10 min each, Type 50 Ti rotor, Beckman Coulter, Krefeld, Germany). The specimen were post-fixed overnight in 2% (w/v) osmium tetraoxide (in PBS, pH7.2), and washed twice in water (five minutes each, Millipore Schwalbach, Germany).

Because the mitochondrial pellet displayed a diffused structure, it was necessary to embed it in agar before further processing. For this purpose, the pellets were resuspended in 4% (v/v) agar solution (Hobot et al., 1984). After the solidation of agar, the agar-embedded specimen was cut into $1mm^3$ blocks.

Dehydration of the specimen was carried out in a graded series of ethanol: 50% for 10 min, 70% for 10min, 95% for 10 min and twice of 100% for 30min. After dehydration, specimens were incubated in pure propylene oxide for 15 minutes, Epon/propylene oxide 1:2 for one hour, Epon/propylene oxide 1:1 for one hour and in pure Epon overnight. The resin-embedded specimen was heat polymerised at 60°C for 48 h.

Ultra-thin sections were cut on a Leica Ultramicrotome III (Leica, Wetzlar Germany), and counterstained with 4% (w/v) aqueous uranyl acetate for 5 minutes, followed by 30 seconds of incubation with a 1:5 dilution of lead acetate solution. Electronic micrographs were obtained using a transmission electron microscope (Carl Zeiss, Oberkochen, Germany) operating at 80 kV. The incidence of mitochondrial morphology was calculated by counting 100 mitochondrial cross-sections on six separate micrographs (10,000X original magnification).

3.2.5 Sequential extraction of mitochondrial proteins

The goal of sample preparation was to introduce proteins into a solution compatible to down-stream protein analyses, so as to enable high-resolution separation of the proteins. During this procedure, proteins should be kept intact, preventing from adverb modifications and degradations. In order to enrich low-abundant proteins and membrane proteins in the down-stream analysis, mitochondrial proteins were first separated into three different fractions.

The procedure for the sequential extraction of mitochondrial proteins was adopted from previous studies with modifications (Molloy et al., 2001; Ramsby et al., 1994; Weiss et al., 1992) (fig.4).

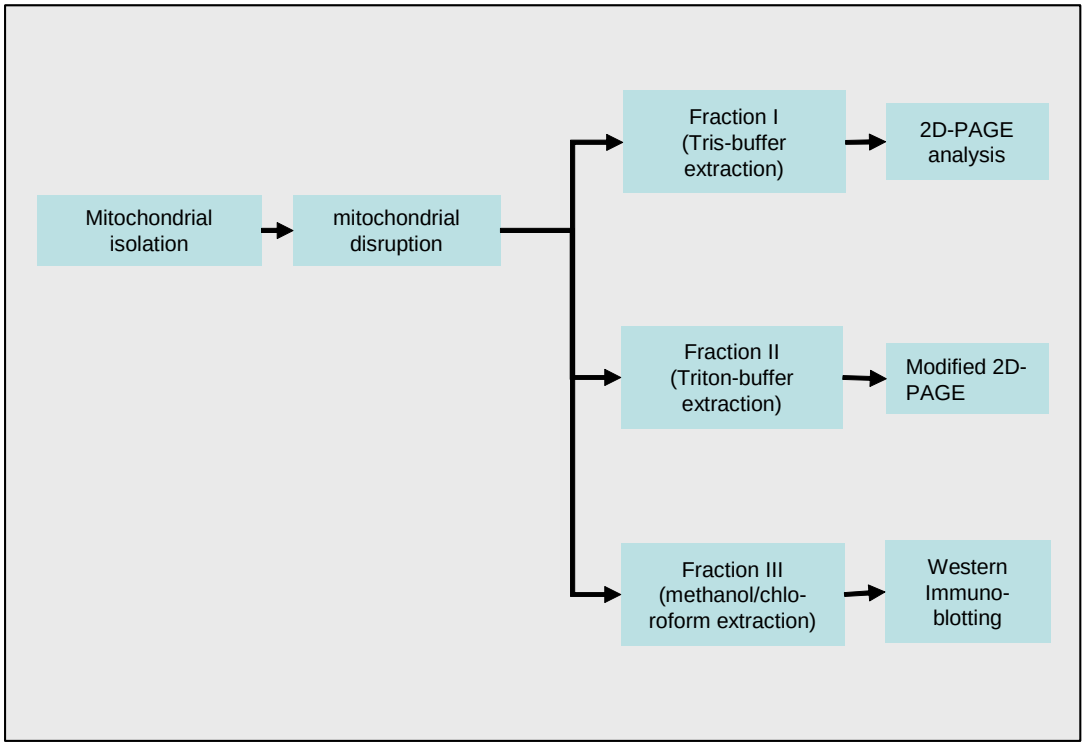

Fig.4: After isolation of mitochondria from mouse brain and liver tissues, the pooled mitochondrial samples were pre-fractionated into three different fractions using sequential extraction strategy. Different fractions were analysed with different analysis methods.

For the simultaneous processing of different mitochondrial samples, mitochondrial pellets from the same aging stage and tissue origin (brain or liver) were pooled into mixed samples. The mitochondrial membrane envelope was first disrupted by the addition of 0.5 volume of distilled water (Millipore Schwalbach, Germany), which acts as hypoosmotic medium. Afterwards, three times of freeze-thaw cycle (37°C to liquid nitrogen -156°C) were carried out to ensure the lyses of mitochondria (Jungblut and Klose, 1985).

3.2.5.1 Tris-buffer extraction

As the first step, 0.5 volume of 100mM Tris buffer (pH7.3) was added to extract soluble proteins. The mitochondrial whole lysate then underwent ultracentrifugation at 100,000xg for 45 minutes (Type 50 Ti rotor, Beckman Coulter, Krefeld, Germany) to sediment crude mitochondrial membrane pellet. Supernatant out of this centrifugation step was designated as “Fraction I”.

It was expected that the most soluble proteins were released from mitochondrial matrix and intermediate space by hypotonic and mechanic disruption, and that this “Fraction I” contained mainly hydrophilic proteins from mitochondrial matrix and membrane-associated

hydrophilic protein subunits (Molloy et al., 2001; Weiss et al., 1992). This fraction was further analyzed using large-gel 2D-electrophoresis method developed in our laboratory.

3.2.5.2 Triton buffer extraction

The crude mitochondrial membrane pellets were re-suspended with one volumes of 50mM Tris buffer (pH 7.4) containing 1mM dithiotreitol (DTT) and 0.1% (v/v) Triton-X100, stirred for 2 hours at 4°C, and centrifuged for one hour at 226,200xg (50,000rpm, Type 50 Ti rotor, Beckman Coulter, Krefeld, Germany) at 4°C. This was for the purpose of releasing the membrane-associated proteins of intermediate solubility (Santoni et al., 1999). The resulting supernatant was named “Fraction II” in the context of this study.

3.2.5.3 Methanol-chloroform protein extraction

Finally, the remaining pellet was subjected to methanol-chloroform extraction in order extract membrane-bounded proteins (Yerushalmi et al., 1995). For this purpose, four volume of deionised water (Millipore Schwalbach, Germany) was first added to the membrane pellet and suspended vigorously (Wessel and Flugge, 1984). This suspension was then aliquoted at 150μl portions in 1.5ml tubes. 600μl of methanol and 150μl of chloroform were added to each aliquot. After incubation on ice for 20 minutes under occasional vortexing, 450μl water (Millipore Schwalbach, Germany) was added to assist the phase separation.

The tubes then underwent centrifugation at 14,000xg (12,600rpm) for 2 minutes in order to separate different phases. After the centrifugation, the proteins were in the intermediate layer, with chloroform layer under it and the methanol-rich layer above it, which was carefully removed.

This protein pellet was washed once by the addition of 600μl methanol, so that protein pellet was left at the bottom of the tube. The ultimate pellet was designated as the “Fraction III” throughout this work. It supposed to contain mainly hydrophobic membrane proteins (Molloy et al., 1998). The protein pellets were allowed to dry under cold Argon for 10 minutes, before it was resuspended in either Laemmli buffer or in deionised water (Millipore Schwalbach, Germany) for protein concentration analysis.

3.2.6 Protein concentration analysis

Protein concentration measurement was carried out for “Fraction I”, “Fraction II” and “Fraction III”, accomplished before the addition of detergents or catropes. Bininchonicic acid (BCA, Perbio, Rockford, IL, USA) protein assay was employed.

This method combines the reduction of Cu^{2+} to Cu^{+1} by protein in an alkaline medium (the biuret reaction) with a colorimetric detection of the cuprous cat ion (Cu^{+1}) using a reagent containing bicichoninic acid. The chelating of two molecules of bininchonicic acid with one cuprous ion forms the purple-coloured reaction product of this assay (fig.5).

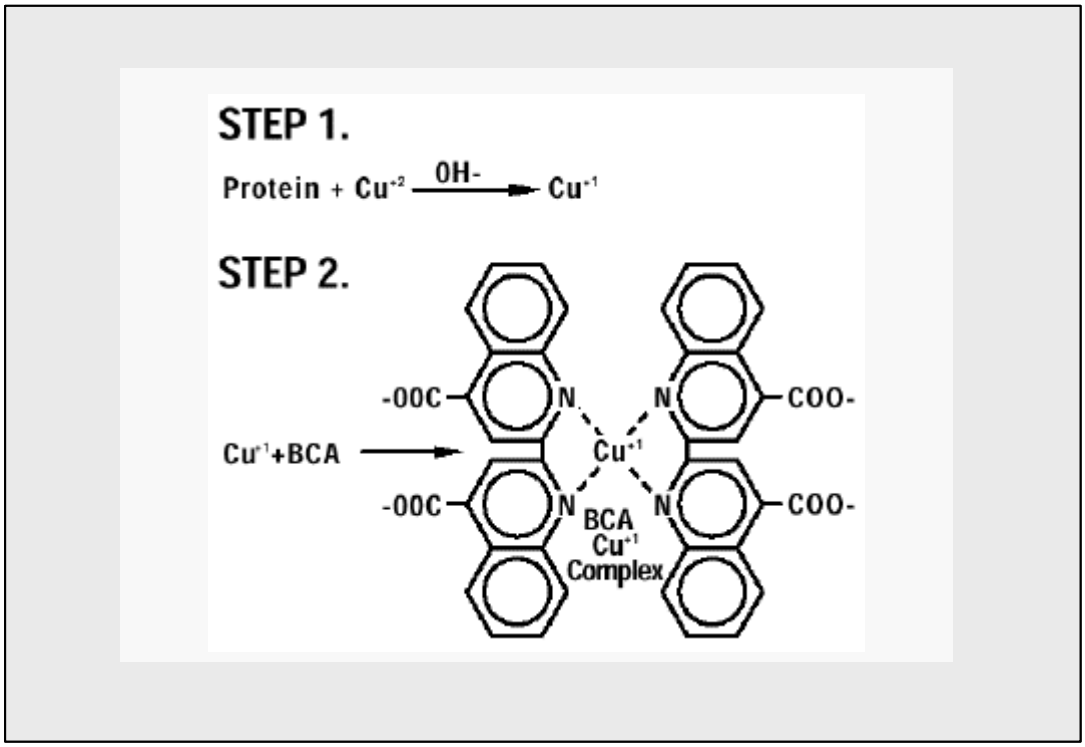

Fig.5: Chemical reactions involved in the protein concentration assay using bicinchoninic acid (cited from http://brahms.chem.uic.edu/~chem455/frames.html, University of Illinois at Chicago). Biuret reaction generates single-valent cuprous cat ion. Single valent copper ion reacts with two molecules of bicinchoninic acid to form BCA-Cu^{+1} complex, which has a maximum absorption at the wavelength of 562nm.

The water-soluble chromophore exhibits a strong absorbance at 562 nm that is linear with increasing protein concentration over a working range of 20μg/ml to 2000 μg/ml (Smith et al., 1985).

The protein standards were prepared by diluting a 2.0mg/ml bovine serum albumin (BSA) stock reagent serially with deionised water (Millipore Schwalbach, Germany), yielding a working range from 20 μg/ml to 1000μg/ml. Deionised water was used as blank.

The BCA working reagent was prepared by mixing 50 volumes of “reagent A” (containing BCA) with one volume of “reagent B” (containing $CuSO_4$). In a 96-well micro array plate, two times of 20μl of either sample (diluted 1:10 and 1:100 with deionised water (Millipore

Schwalbach, Germany) or standard was mixed with 300μl working reagent, and incubated for 30 minutes at 37°C. After cooling to room temperature, the plate was read at 570 nm with a spectrophotometer (Amersham Biosciences Freiburg, Germany).

3.2.7 Sample preparation for 2D-electrophoresis

A highly standardardized sample preparation protocol introduced by Klose was employed for the sample preparation of 2D-electrophoresis (Klose, 1999; Klose and Kobalz, 1995). The key feature of this protocol is to solubilize proteins and keep them soluble by the addition of zwiter-ion detergent and high concentrations of catropes.

200μg of protein extraction ("Fraction I", "Fraction II" and mitochondria pellet) was accommodated with the following substrates:

- 50mM phosphate buffer, pH7.1
- 100mM KCl
- 10% glycerol (v/v)
- 4% (w/v) 3-[(3-cholamidopropyl)-dimethylammonio]-propan-sulfonate (CHAPS) for mitochondrial pellets
- 1μM Pepstatin A (pre-solved in ethanol, Sigma-Aldrich, Steinheim Germany)
- 1.4μM phenylsemthylsulfonylfluorid (PMSF, Sigma-Aldrich, Steinheim Germany) (pre-solved in ethanol)
- 0.08 v/v protease inhibitor cocktail Complete^{TM} table stock solution (solved in 2 ml 50mM PBS) (Molecular Biochemicals Roche, Mannheim, Germany).

For mitochondrial total protein extract, a sonification treatment was carried out to maximize the membrane structure disruption and protein solubilization (Klose, 1999). Sonification was performed at 0°C for six times of 10 seconds (Ultrasonic bath, Bandelin, Berlin Germany), with 40-45 seconds of intensive stirring between each application and one minute keeping on ice. To enhance the sonification strength, 0.034 part (v/w) of glass beads with low sodium content (2.5 $\pm$ 0.05 mm diameter, Wolf Glaskugeln GmbH, Mainz, Germany) was added during the treatment (Klose, 1999). The glass beads were removed following the final sonification step.

Nucleic acids in the sample has been indicated to interfere with the isoelectric focusing process (O'Farrell, 1975). Upon further stirring at 4°C, 0.025 part (v/w) of Dnase (Benzonase) was added into the mitochondrial total protein extracts in order to degradate the mitochondrial DNA.

Subsequently, protein homogenates of all fractions were adjusted with 6M urea and 3M thiourea. After dissolving, 0.01 part (v/w) of 70mM DTT was added and stirring was continued at room temperature for another 30 minutes. A high concentration of catropes, such as urea or thiourea, function through the partial breaking of hydrogen bunds in the solution. The reducing agent DTT was essential for ensuring the breakage of disulfide bridges, which would otherwise oppose protein denaturation and prevent saturation of the polypeptide with sodium deodecylsulfate (SDS) in the following procedure. These protein denaturants could improve the unfolding of the protein secondary structure and thus keep the proteins in solution (Herskovits et al., 1985).

Finally, 1% (v/w) of ampholyte mixture Servalyte 2-4 (Serva, Heidelberg, Germany) was added as carrier ampholyte. The samples were stored at –80°C until Isoelectric focusing analysis.

3.2.8 Sample preparation for Western immunoblotting

20μg of "Fraction III" protein pellet obtained from methanol-chloroform extraction was suspended with 70μl Laemmli sample buffer (25mM Tris-buffer, 2% (v/v) SDS, 192mM DTT, pH 8.3) accommodated with10% (w/v) glycerol (Laemmli et al., 1976). The samples were heated at 95°C for 5 minutes to ensure the protein denaturation. After quick cooling on ice, the sample was ready for SDS-PAGE resolutions.

3.2.9 Sample preparation for Blue-native electrophoresis

Mitochondrial pellet corresponding to 1mg protein was suspended in 100 μl of extraction buffer comprising 0.75M aminocaproic acid and 50mM 2-[Bis-(2-hydroxyethyl)amino]-2-(hydroxymethyl)propane-1,3-diol (BisTris). 12.5μl n-dodecyl-β-D-maltoside (10% w/v) was added to the suspension, in order to solubilize mitochondrial inner membrane proteins (Schagger and von Jagow, 1991).

Following incubation on ice for 20 minutes with occasional vortexing, samples were centrifuged at 14,000xg (Heraeus, Hanau, Germany) for 10 minutes though a 100kDa molecular filter (Microcon, Millipore Schwalbach, Germany). 6.3μl of 5% (w/v) suspension of Coomassie brilliant blue G-250 in aminocaproic acid (0.5M) was added. Samples were kept on ice until Blue-native electrophoresis analysis.

3.2.10 Large-gel 2D-electrophoresis

Large-gel 2D-PAGE analysis was applied on whole mitochondrial protein extract, mitochondrial protein "Fraction I" and "Fraction II" protein samples. At least three times of 2D-PAGE analysis were carried out for each sample in order to access the reproducibility of the method and to exclude the artefact-deduced gel-to-gel differences. The large-gel 2D-

electrophoresis analysis of mouse brain total protein extract were carried out in our laboratory in the frame of a parallel project.

3.2.10.1 Principle of 2D-electrophoresis

The current modern 2D-electrophoresis was developed independently by Klose and O'Farrel (Klose, 1975; O'Farrell, 1975). It is a combination of isoelectric focusing with SDS-polyacrylamide gel electrophoresis. This method provides the opportunity to separate proteins from a highly complex protein mixture and make proteins accessible for further biochemical analysis. The modern large-gel 2D-electrohporesis allows the visualization of as many as 10,000 of protein-spots on a single gel (Klose and Kobalz, 1995).

In the isoelectric focusing electrophoresis, pH gradient can be established by applying a mixture of ampholytes (which is a mixture of synthesized oligoamino, oligoacarboxylic acids) with different isoelectric points to a polyacrylamide gel in an electric field. Upon the application of voltage, the carrier ampholytes stack according to their pI, and an increasing pH gradient is established within the gel. Migration of the proteins continue until all the components of the system reach a steady state, i.e., their isoelectric points. The rates of protein migration depend on the charge density (the ratio of charge to mass) of the individual proteins.

In the second dimension separation, the SDS-polyacrylamide gel electrophoresis (SDS-PAGE) utilizes SDS ($CH_3(CH2)_{11}SO^{4-}Na^{+}$) as an anionic detergent. Polypeptides bind SDS to the main chains in a constant weight ratio (1.4g SDS per gram protein) (Lottspeich and Zorbas, 1998). Due to the much higher anionic charge of SDS comparing to that of proteins, the charge difference between proteins can be ignored. All proteins have the similar charge to mass ratios at pH8.4.

In addition, upon binding to SDS, polypeptide chains are forced into extended cylindrical conformations with a constant diameter. SDS treatment thus eliminates the effect of differences in protein shape. So that chain length, which reflects mass, is the sole determinant of the migration rate of proteins in SDS polyacrylamide electrophoresis. Thus, the electrophoresis mobility of the proteins is only dependent on their molecular weight (Lottspeich and Zorbas, 1998).

3.2.10.2 Procedure of isoelectric focussing electrophoresis

The isoelectric focusing was performed according to protocol of Klose (Klose and Kobalz, 1995). High precision capillary glass tubes with internal diameter of 1.5 mm and a length of 20cm were used for the isoelectric focussing separation of "Fraction I" and "Fraction II"

proteins, while the 40cm IEF gels (0.9mm diameter i.d.) were used for mitochondrial total protein reference gel.

The gel solution contained 3.5% (w/v) acryamid, 0.3% (w/v) N, N'-methylene bisacrylamide (BisAcryamide), 9M urea and 2% (v/v) carrier ampholyte mixture, which was a mixture of:

- one part of Pharmalye pH3.5-10.0 (Pharmacias, Uppsala, Schweden),
- one part of Servalye pH2.0-11.0 (Serva, Heidelberg Germany),
- three part of Pharmalye pH4.0-6.5 (Pharmacias, Uppsala, Schweden),
- two part of Pharmalye pH5.0-8.0 (Pharmacias, Uppsala, Schweden), and
- one part of Pharmalyte pH6.5-9.0 (Pharmacias, Uppsala, Schweden).

In order to resolve more hydrophobic proteins on the 2D-PAGE gels, we included 2% (v/v) Triton-X100 in the isoelectric focusing gel solution (Stephenson et al., 1980) for the analysis of "Fraction II" protein extracts in this study.

Gel solution was filled into the tubes using accurately fitted nylon strings as plungers. The gels were left undisturbed for 30 minutes before the nylon strings were removed, allowing for polymerisation at room temperature. A further polymerisation for 3-4 days at room temperature was allowed before use.

Isoelectric focussing running buffer were made of purest water (Millipore Schwalbach, Germany) with electric resistance of 18.2mΩ. The anode buffer contained 4.25% (v/v) orthophospho acid and 2M urea (pH2); the cathode buffer contains 5% (v/v) ethylendiamin, 9M urea and 5% (w/v) glycerol (pH11).

200μg protein sample ("Fraction I" and "Fraction II") was applied on each 20cm 1.5mm diameter gel for preparative silver staining, whereas 100μg of total mitochondrial protein was applied on 40cm 0.9mm diameter gel for analytical silver staining. Prior to the loading of protein sample on the anodic end of IEF gel, a Sephadex (Sigma-Aldrich, Steinheim Germany) mixture (with 2% (v/v) carrier ampholyte mixture described above, 70mM DTT and 9M urea) was loaded to a height of 2mm. This Sephadex layer has shown to have positive effect on the isoelectric focussing, as it sieves up the possible granules in the sample, and in turn improves the entry of soluble samples into the IEF gel.

The isoelectric focusing was carried out at a series of increasing voltage: 100V for 1 hour, 200V for 1 hour, 400V for 17.5 hour, 650 V for 1 hour, 1000V for 30 minutes, 1500 V for 10 minutes and 2000V for 5 minutes. Immediately after isoelectric focusing electrophoresis,

the gels were expelled into the equilibration solution containing 125mM tris (hydroxymethyl) aminomethane, hydrochloride (Tris-HCl, pH 6.8), 40% (w/v) glycerol, 65mM DTT and 3% (w/v) SDS. Gel strips with the length of 40cm were cut at the middle. After 10 minutes of incubation under gentle shaking, the gel strips were stored at –80°C until SDS-PAGE analysis.

3.2.10.3 Second dimension of 2D-electrohporesis

The sodium dodecylsulfate polyacryamid gel electrophoresis was carried out in the format of 23.2cm x 30 cm x 1.0 cm gel cassette. The gel solution consisted of Laemmli buffer (25mM Tris, 192mM glycine, pH 8.3) containing 15% acrylamide (w/v) and 0.2% BisAcrylamide. Laemmli buffer was also used as electrophoresis buffer. One drop of bromophenol blue dye was added in the anode buffer as running state indicator.

Thawed at room temperature, the first dimension gel was gently transferred onto the surface of the SDS-PAGE gel, preventing the stretching of the gel and the introduction of air. Running buffer containing 1% (w/v) agarose was overlaid to restrict the movement of the IEF gel.

Electrophoresis was carried out at 15°C, first at 85mA for 15 minutes and then at 120mA for approximately five hours. This procedure was stopped when the bromophenol blue dye front reached 2cm short of the lower edge of the gel plate. After SDS-PAGE, the gels were transferred into fixation solution for staining procedure.

3.2.11 Silver staining

The 2D-gels bearing proteins separated by isoelectric focusing and SDS-PAGE were stained using either analytical silver staining or preparative silver staining protocol.

3.2.11.1 Analytical silver staining

In the silver staining procedure employing silver nitrate, silver ion binds to the amino acid side chains, primarily the sulfhydryl and carboxyl groups of proteins (Coligan et al., 1995). Since silver ions complexed with the protein undergo faster reduction than free silver ions, particles of colloid silver (between 20 and 80 nm in diameter) form preferentially at the site of proteins on the surfaces of the gel, leading to the deposition of silver grains.

The analytical silver staining is a sensitive staining method with a detection limit between 1 and 10 ng protein (Rabilloud et al., 1992; Switzer et al., 1979). This protocol was used to produce a master 2D-PAGE gel pattern for brain and liver mitochondrial total protein extract (Heukeshoven and Dernick, 1988; Jungblut and Seifert, 1990).

Directly after the SDS-PAGE separation, the proteins on the gels were fixed overnight with fixation solution containing 10% (v/v) acetate and 50% (v/v) ethanol under continuous shaking. This step immobilizes the proteins in the gel or retards their diffusion to a large extend, while at the same time removes substances such as SDS or glycerol that might interfere with the staining procedures.

Afterwards, the gels were incubated in a solution containing 30% (v/v) ethanol, 0.25M Sodium acetate, 0.8mM sodium thiosulfate and 20ml/l glutaraldehyde. Sodium thiosulfate was added to create latent images of protein spots by the precipitation of micro granules of silver sulfide, while the inclusion of glutaraldehyde promotes silver reduction (Rabilloud, 1990).

After the subsequent two washing steps in water (each for 10 minutes), the gels were incubated in silver-containing solution (0.1% w/v) for 45 minutes, with the addition of 0.01% (v/v) formaldehyde, which assists the silver ion reduction and the precipitation of metallic silver.

After a short rinse (one minute) with water, the gels were allowed to develop color (allow the reduction of silver ion to silver) in the presence of 2.5% (w/v) sodium carbonate, 0.02% (v/v) formaldehyde. 0.5mM Thimerosal (Mercury-[(o-carboxyphenyl)thio]ethyl sodium salt, Sigma-Aldrich, Steinheim Germany) was added as a preservative and colour enhancer. Since it was essential that the color development be carried out in an absolutely transparent solution, one change of development solution was carried out after one minute.

After the desired intensity of staining was achieved, this process was interrupt by the addition of 50mM of tetrasodium ethylenediamine tetraacetate (Titriplex III). Depending on the colour intensity, the colour development duration ranged between 3 to10 minutes.

3.2.11.2 Preparative silver staining

Mass preparative silver staining was performed using the protocol of Schevshenvo (Shevchenko et al., 1997) with slight modifications (Giavalisco, 2003). Compared to the traditional silver staining protocol (Klose and Kobalz, 1995; Rabilloud, 1990; Rabilloud et al., 1992; Swain and Ross, 1995), the Schevchendo method retains the possibility of diverse down-stream protein microanalysis. This is due to its omit of the sensitisation treatment with glutaraldehyde, which is known to attach covalently to the proteins through Schiff-base formation with the α and ε-amino groups (Shevchenko et al., 1997).

The fixed gels were first customerized in 30% ethanol (v/v) for 10 minutes, and then sensitised by a short incubation (one minute) with sodium thiosulfate (0.01% w/v). Two rinses with deionized water (Millipore Schwalbach, Germany, one minute each) were carried out to remove the unbound sodium thiosulfate. The incubation of silver (0.15% w/v) was carried out for 45 minutes at the absence of formaldehyde. The colour development procedure was identical to that of analytical silver staining.

3.2.12 2D-gel evaluation

The gel image evaluation remains a critical point of 2D-electrophoresis analysis. In this study, both visual gel evaluation and the gel image processing software were employed, in order to reduce artifacts.

For this purpose, the gel images were first digitalized using a densitometer (Umax Mirage-II DIN A3 scanner, Willich, Germany) with the resolution of 300 dots per square-inches (dpi). Respecting the similar gel patterns, the majority of spots were manually assigned to their counterparts in each of the age group according to their relative position on the gel pattern. Each set of homologous spot on different gels built a “super spot”. Comparison in each super spot was carried out respecting their intensity, their outward appearance and the variation type. Four categories of variation types were evaluated according to previous study (Kaindl, 2001):

- Presence/absence variants: whether a spot is visible;
- Amount variants: changes in size and intensity of protein spots;
- Mobility variants: alteration of spot position on the gel caused by possible changes of protein charge, molecular weight and conformation;
- Splitting variants: one of the two spots involved being split into to two or more spots.
- According to these findings, the protein spot changes during the aging process was postulated.

The comparison of brain mitochondrial 2D-gels to the total brain protein 2D-gels was carried out by Dr. Sagi in our laboratory.

For the quantitative analysis of protein concentration difference in different age groups, all gels were analysed using Proteomweaver (version 2.1, Definiens, Munich, Germany), which is a commercially available software for two-dimensional gel image analysis. Manuel correction was carried out after automatic spot recognition.

For this purpose, one average gel was generated for each age group by the software package in order to reduce the fluctuation of gel-to-gel variation inside the same group.

Average gels from six different age groups were matched to each other automatically, and the gel-matching pattern was controlled and edited manually to minimize software-induced artifacts.

Spot volumes were calculated with build-in feature for the spot quantification, which applied a fixed multiple of the Gaussian radius of the spot as background intensity function (Users' manual, Definiens, Munich, Germany). After spot volume calculation, the spot information was extracted and output by the ProteinWeaver. Properties of each "super spot", which was a serious of matched spot on different gels, was presented in a role, showing the super spot identity, Cartesian location, spot surface area and spot volume respecting the integration of intensity value of each pixel.

Spot intensities were normalized by calculating the "relative intensity", which was defined as percentage of the total spot volume on its parent gel. Coefficients of variance (CV=standard deviation/mean) of spot intensities in "super spots" were used to control the quality of automatic gel evaluation procedure (Challapalli et al., 2004). Scatter plots and correlation coefficients of relative intensities from different gel-pairs were calculated using StatView software package (Abacus, NC, USA). Ultimately, spot differences detected by visual gel evaluation were taken to statistical tests to determine the statistical significance (α<5%).

3.2.13 Protein identification

Presently, the most commonly used technique for protein identification is "peptide mass fingerprinting" employing mass spectrometry. This involves the generation of peptides using specific proteolytic enzymes (such as trypsin, chrymotrypsin), the determination of peptide masses and the matching against a theoretical spectrum of peptide fragments calculated from databases of known protein sequences (Mann and Wilm, 1994). Positive ionisation is generally used for protein and peptide analyses, because peptide possesses functional groups that readily accept protons (H+):

$R\text{-}NH_2 + H+ \rightarrow R\text{-}NH_3^+$ *(R: residual of protein or peptide)* *(eq.1)*

The Matrix-assisted laser desorption/ionisation time-of-flight mass spectrometry (MALDI-TOF-MS) (Fernandez et al., 1998) and the electrospray ionization iontrap mass spectrometry (ESI-Iontrap-MS) analysis were carried out by Mass spectrometry core facility of our institute.

MALDI is based on the bombardment of sample molecules with a laser light to bring about sample ionisation (Hillenkamp et al., 1991; Mann et al., 2001). The matrix substance transforms the photonic energy into excitation energy, which leads to sputtering of analyte and matrix ions from the surface of the co-crystal.

Electrospray Ionisation (ESI) is one of the Atmospheric Pressure Ionisation (API) techniques suitable for the analysis of polar molecules ranging from less than 100 Da to more than 1,000,000 Da in molecular weight (Wilm and Mann, 1996). The liquid sample is physically sprayed into an acidic environment. Rapid desolvation of sample droplet leads to the ionisation of sample molecules before their entering into a mass analyser.

The ions are then accelerated in an electric field and fly towards a detection board. The speed of flight depends on the mass-to-charge ratio. The detector monitors the ion current, amplifies it and the signal is then transmitted to the data system where it is recorded in the form of mass spectra. The mass spectrum gives information about mass-to-charge ratio (m/z) of each component, and the relative abundance of the various components in the sample.

3.2.13.1 In-gel trypsin digestion

The aims of in-gel tryptic digestion were two fold. The first is to eliminate the chemical substances (salts, detergents) remained from previous steps of sample preparation, 2D-electrophoresis and staining procedure, which could otherwise disturb the mass spectra and sensitivity. Another goal of tryptic digestion is to cut the protein into certain peptide mixtures according to the amino sequence pattern, so that the peptide mass fingerprinting analysis can be carried out.

Protein spots of interests were manually excised from the 2D-gel with a hand-held spot picker before proteolytic digestion using trypsin. Trypsin has the specific proteolytic activity for peptide bund at C-terminal lysine or arginine, provided that prolin is not the subsequent amino acid. It is useful for mass spectrometric studies because each proteolytic fragment contains a basic arginine or lysine amino acid residue, and thus is suitable for positive ionisation of mass spectrometric analysis.

The spots were desalted by the pendelling addition of 100µl acetonitrile (CH_3CN) and 100µl of 100mM ammoniumbicarbonate (NH_4HCO_3) for the total of six times, each with an incubation period of 10 minute at 37°C. This ensures the comprehensive removal of salt and detergents in the gel pieces.

The liquid phase was then removed and the gel pieces completely dried in a vacuum concentrator (Eppendorf, Hamburg, Germany). This ensures the complete permeation of the trypsin into the gel piece and thus prevent from extensive self-digestion of trypsin. Trypsin in-gel digestion was carried out in the trypsin solution (Seq. Grade modified Porcine trypsin, Promega WI, USA) containing 12.5ng/µl Trypsin in 50mM NH_4HCO_3 (pH8), at 37°C overnight, to ensure complete digestion.

After trypsin digestion, peptides were recovered by combining the liquid phases from several extractions of gel pieces with 50% aqueous acetonitrile containing 5% formic acid. Another desalting treatment was carried out using ZipPlate (Millipore Schwalbach, Germany) in case MALDI-TOF-MS analysis was carried out as the next step.

3.2.13.2 MALDI-TOF-MS analysis

Anchor Chip technology was applied for MALDI-TOF analysis. AnchorChips are equipped with hydrophilic patches (“anchors”) in a hydrophobic surrounding causing the relatively hydrophilic analyte to concentrate on the anchors (Karas and Hillenkamp, 1988). For this purpose, 1.5µl matrix material 2,5-dihydroxybenzoic acid (DHB) solution (3.3mg/ml DHB solubilzed in 90% (v/v) acetone and 0.05% (v/v) trifluoroacetic acid) was mixed with 1.5µl of the sample and allowed to co-crystallize on the anchored position.

MALDI-TOF mass spectra of the peptide mixture were obtained using the Bruker Reflex IV MALDI-TOF mass spectrometer (Bruker, Bremen, Germany), operated in the reflector mode in order to increase mass resolution. Signals corresponding to mass-to-charge (m/z) ranging from 0 to 3500 were monitored.

Each spectrum was the cumulative average of 50 to 100 laser shots (nitrogen laser, 337nm). An internal calibration using the monoisotopic peaks of trypsin self-digestion products (residues 108-115, $[M+H]^+$=842.509 Da and residues 58-77, $[M+H]^+$=2211.104 Da) as internal standards was carried out for each measurement.

The XMASS/NT software package (Bruker, version 5.1.16) was used for the data processing. Peptide peaks were de-isotoped and those exceeding 5% of full scale were submitted for database searching.

3.2.13.3 ESI-MS analysis

Nano-electrospray ionisation (Wilm and Mann, 1996) coupled to a reversed phase high pressure liquid chromatography (HPLC) was employed in this work (LCQ Deca ion trap mass spectrometer, ThermoFinningan).

10µl of the sample (ca. 75 fmol of each peptide) was injected into a pre-packed C-18 column (75µm inner diameter, LCPacking, Amsterdam, Netherlands). The separation of the peptides was performed with a gradient of 2-50% acetonitril containing 0.1% formic acid at a flow rate of 0.2µl/min. After the HPLC separation, a voltage of 1000 to 1200 V was applied on the gold-plated vial situated within the ionisation source of the mass spectrometer, resulting in sample spraying and ionisation.

3.2.13.4 Databank-based protein annotation

The obtained spectra of peptide masses were analysed by searching though databases to match the corresponding proteins. This is achieved through the comparison of *in silico* digestion product of protein in the non-redundant sequence database (NCBInr) with the help of online search engine Mascot (http://www.matrixscience.com). Several parameters were set before the Mascot search, including: the taxonomy of the specimen (mammalian), the used protease (trypsin), the number of accepted missed cleavages (one), the mass deviation tolerance (1.0 Da), and possible modifications (e.g., oxidation of methionine residue in a polypeptide increases its mass by 18 Da).

A protein was considered to be directly identified, in case at least four measured peptides match the *in silico* digestion peptide mixture and the probability based Mowse score was higher than the threshold value corresponding to $p<0.05$ (Pappin et al., 1993).

Respecting the spot homology in the gel evaluation, counterpart spots in a “super spot” were considered to be indirectly identified, if one of them had been directly identified (Kaindl, 2001).

3.2.13.5 Membrane protein prediction and protein sequence alignment

In order to identify putative membrane proteins, all the identified proteins were subjected to the Gravy value calculation and the prediction of putative trans-membrane domain using SOSUI tool (http://sosui.proteome.bio.tuat.ac.jp).

Gravy score, or general average hydrophobicity score, or, is a theoretical measurement of protein hydrophobicity according to their primary amino acid sequence. It is calculated as an arithmetic mean of the hydrophobicity of all amino acids of a protein sequence (Kyte and Doolittle, 1982). Integral membrane proteins typically have higher GRAVY scores than do soluble proteins. By definition, the Gravy factor does not consider any influence of protein secondary or higher-level structure. The SOSUI tool predicts the trans-membrane helices by calculating the hydrophobicity of the amino acid charges and the sequence

length of a candidate peptide (Hirokawa et al., 1998). Protein-protein sequence alignment was performed using Basic Local Alignment Search Tool (protein-protein, BLASTp (www.ncbi.nlm.nih.gov/BLAST/).

3.2.14 Western immunoblotting

Western immunoblotting employed in the current study involves transferring protein bands from the polycrylamide gel onto a nitrocellulose (Amersham Hybond ECL) membrane by electrophoresis (Towbin and Gordon, 1984), and the subsequent immuno-detection of protein of interest.

SDS-PAGE separation for Western immunoblotting analysis was carried out using the buffer system of Laemmli (25mM Tris, 192mM glycine, 2% SDS (v/v), pH 8.3) (Laemmli et al., 1976). Protein content was normalized by translocase of outer mitochondrial membrane 20kDa subunit (TOM20), which is part of the mitochondrial protein translocase machinery with one trans-membrane domain.

Samples were run though 4% loading gel (pH 6.8) and 15% running gel (pH 8.4) in the presence of 0.1% (v/v) SDS. Molecular weight markers (Rainbow, Amershan Biosciences, Freiburg, Germany) was employed for the confirming of protein transfer and the molecular weight orientation.

For the electro-blotting of proteins onto a nitrocellulose membrane (Amersham Hypond C), a two-pH Tris-glycine “semi-dry” electrophoretic transfer system containing 20% methanol was used. The pH value of the cathode buffer was 9.5 and the pH at the anode was 10.4, thus creating a pH-gradient which facilitates the electro-transfer of proteins. The use of methanol was shown to increase the binding capacity of nitrocellulose for proteins (Timmons and Dunbar, 1990).

The gel and membrane were saturated with transfer buffer and were stacked together horizontally between buffer-saturated filter paper pads (10mm thickness), then sandwiched between both planar electrodes. The electrodes were separated solely by the thickness of the stack, creating a uniform strength for protein transfer. Blotting was performed at 0.8mA/cm^2 for two hours. Analogue to SDS-PAGE, The protein mobility is a function of molecular weight, with the larger proteins being transferred more slowly.

After transfer of the proteins from the gel to the membrane, the remaining protein-binding sites on the membrane were blocked overnight at 4°C in 3% bovine serine albumin in a solution containing 10mM Tris-HCl, 133mM NaCl, 0.1% (v/v) Tween 20 (pH7.4) to avoid

non-specific binding of the antibodies or detection reagents in subsequent steps. BSA free of endogenous peroxidases was used for this purpose.

Immunoblots were incubated for one hour at room temperature with monoclonal mouse-anti-human cytochrome c oxidase subunit I IgG (dilution 1:100, Molecular Probes, Göttingen Germany), and polyclonal rabbit-anti-mouse TOM20 IgG antibody (Santa Cruz biotechnology, dilution 1:200) under gentle wagging. After intensive washing procedure (200mM Tris-Base, 9% (w/v) NaCl, 1% (w/v) Tween 20), one hour incubation was carried out with horseradish-peroxidase-conjugated secondary antibody (goad anti-mouse-IgG and goad anti-rabbit IgG, dilution 1:2000), which was included in the ECL detection kit (Amershan Biosciences, Freiburg, Germany).

Horseradish peroxidase (HRP) was used as a reporter enzyme to catalyse the oxidation of luminol in the presence of hydrogen peroxide (H_2O_2) (Motsenbocker, 1988; Whitehead et al., 1979). Immediately following oxidation, luminol is in an excited state that may decay to the ground state via a light-emitting pathway (fig.6).

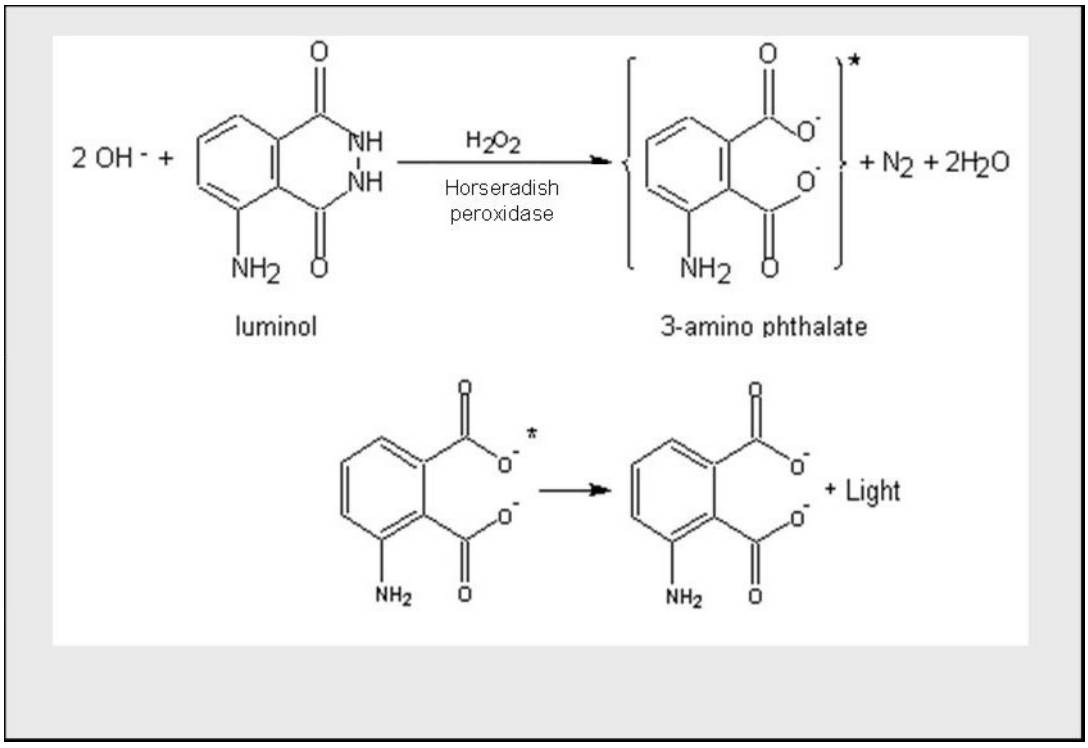

Fig.6: Chemical reaction involved in the oxidation of luminal and light emission in the presence of hydrogen peroxide (H_2O_2) and horseradish peroxidase (the asterisk denotes excited state of 3-aminophthalate). This reaction was involved for the fluorescent detection in Western immunoblotting analysis. Cited from website of Wageningen University (www.ftns.wau.nl/oc/research/phytochemistry/Antioxidants/lunteren/lunteren.htm)

For the fluorescent detection, the membrane was soaked briefly in the chemiluminescense detection reagent containing luminol and hydrogen peroxide (H_2O_2). The light output, which had a maximum emission at 428nm, peaked for 15 to 20 minutes before decaying. The resulting light was fluorographed using standard X-ray film (X-Omat, Kodak, Stuttgart, Germany). The approximate exposing time was 15 seconds.

Spot intensity of Western immunoblots was accessed using ImageQuant software package (Amershan Biosciences, Freiburg, Germany) after digitalizing the fluorographs (Umax Mirage-II DIN A3 scanner, Willich, Germany). The intensity ratio of COX I to TOM20 was calculated.

3.2.15 Blue-native electrophoresis

Blue-native electrophoresis is a charge shift method, where the electrophoresis mobility of protein complex is determined by the negative charge of the bound Coomassie dye, as well as the size and shape of the complex (Schagger and von Jagow, 1991). In a two-dimensional Blue-native/SDS-PAGE analysis system, monomeric proteins migrate within the hyperbolic diagonal, whereas protein spots below the diagonal indicate their protein complex nature.

Blue-native electrophoresis was scaled down to mini-gel system (0.75 x 70 x 82 mm, Bio-Rad, Munich, Germany). A non-linear 6-15% polyacrylamide gradient slab gel was used and 300μg protein (35μl) was loaded per slot (Brookes et al., 2002; Klement et al., 1995). The anode buffer contained 50mM BisTris, the cathode buffer comprised 50mM N-[2-Hydroxy-1,1-bis(hydroxymethyl)ethyl]glycine (Tricine), 15mM BisTris and Coomassie brilliant blue G-250 (0.02% w/v).

The gel was run for 30 minutes at 40V and then at 110V until the Comassie dye reached the end of the gel. Strips of first-dimension gel containing separated protein complexes were cut out, incubated with 3% SDS (w/v) and 1% β-Mercaptoethanol (w/v) for 20 minutes at room temperature. The gel stripe was subsequently subjected to 15% SDS-PAGE for the separation in the second dimension. The resulting second dimension gel was stained with preparative silver staining, as described in 3.2.11.2.

3.2.16 Mathematical modeling

We devised an abstract mathematical model in order to investigate the mechanism of wild type and mutated mitochondrial competition inside a post-mitotic cell during the aging

process. The main purpose of employing this model in this study was to apply the model on our experimental data to calculate the mtDNA mutation rate of mouse.

3.2.16.1 Modeling concept

This model was based on the following prerequisites: Free radicals induce both mtDNA deletions and mitochondrial membrane damage; Mitochondria with an intact genome have a growth advantage over mitochondria bearing genome damage; Mutated mitochondria produce less amount of free radicals compared to wild type mitochondria; Accumulation of membrane damage is proportional to free radical level. Besides, it was assumed that the degradation rate of mitochondria is positively correlated to their membrane damage level. Figure 7 gives an overview of the current model.

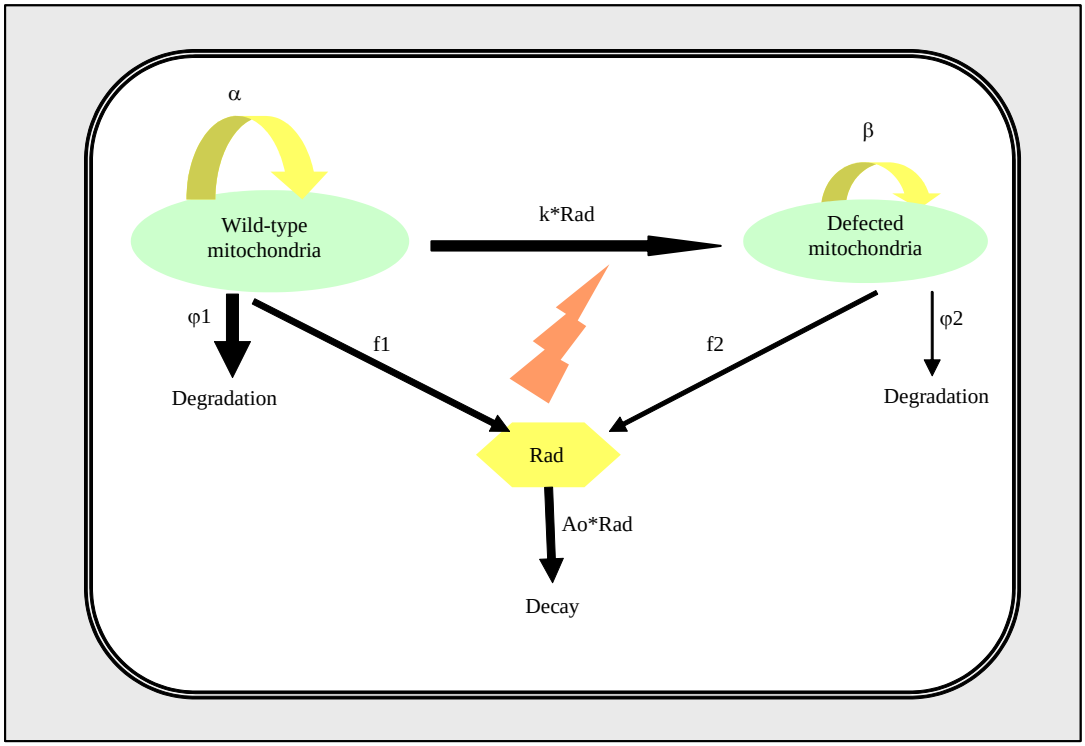

Fig.7: Biochemical reactions described by the current model. Two different classes of mitochondria were considered, those with intact genome (Mw) and those with mutated genome (Mm). Different classes produce different amounts of free radicals, which cause the transition of mitochondria from wild type to mutated type. Mitochondria are replicated and degraded with rate constants that are positively correlated to the amount of available mitochondria.

Mitochondria replication process is independent of the cell cycle in the relaxed condition. However, cell mitosis makes the replicate obligatory. In order to reflect the difference of post-mitotic tissue and mitotic tissue, the replication rate for mouse brain and liver were set

to 14 and 9.5 days, respectively. This is based on the consideration that cell division force mitochondria to replicate (Dallman, 1967; Neubert et al., 1966).

Since the mitochondria are not fully autonomous entities, but depend on the cytosolic protein synthesis, the investment of a cell for the production of mitochondria has an upper limit (Brown, 1991; Kowald and Kirkwood, 2000). The mathematical construct used to simulate this behaviour is given as the following control term:

Current proliferation rate = maximum proliferation rate x (A-Mw-Mm), *(eq.2)*

where "A" is the maximum number of mitochondria in a cell (we supposed here that there are a maximum of 1000 intact mitochondria in a cell, so A=1000), and the maximum proliferation rate for intact and mutated mitochondria were α and β, respectively. This construct reflects the dependency of mitochondrial proliferation rate on the remaining resource in the cell. It is a combination of product inhibition mechanism for the mitochondrial production reaction and a mass-dependence law (Brown, 1991).

Mitochondria are continuously degraded in the cell (Stryer, 1995). The rate of mitochondrial degradation is proportional to the amount of available mitochondria (Kowald and Kirkwood, 2000). Since the mitochondria bearing mutated genetic material also have defected respiratory chain, they generate less amount of free radicals. This deduces that compared with wild type mitochondria, defective mitochondria accumulate membrane damage more slowly. Therefore, they have a slower degradation rate ($\varphi 1 > \varphi 2$, where $\varphi 1$ and $\varphi 2$ are the degradation rate of wild type and mutated mitochondria, respectively). This is de Grey's idea of "survival of the slowest" (de Grey, 1997).

Through the continuous exposure to free radicals in the environment, mitochondrial genomes are cumulatively damaged during the aging process. This phenomenon was described by mutation reaction in the modeling system. Free radicals can damage the mtDNA with a rate "k", converting intact mitochondria into defective ones. The number of mutation event is proportional to the free radical level and the amount of intact mitochondria. For simplicity, a rate constant was set throughout this system for mtDNA mutation reaction, supposing that the strength of radical-induced damage remains the same.

As side-product of the respiratory chain enzyme activity, free radicals are produced by all mitochondria during the oxidative phosphorylation process. It is assumed that wild type

mitochondria generate more radicals than mutated mitochondria (f1>f2, where f1 and f2 are the free radical production rate of wild type and mutated mitochondria, respectively).

This model contains a constant number of antioxidant molecules that destroys radicals at a rate of φ3. In the radical clearance process, antioxidants act as enzymes that are not consumed in the reaction. The removal of free radicals is proportional to the existing amount of radicals and antioxidant level.

3.2.16.2 Differential equations and numerical solutions

To assist the deduction of numerical solutions from the assumptions described above, the ordinary differential equations (ODE) were developed. This model consists of two equations for the different mitochondrial sub-populations (wild type and mutated type), and one for the free radical level in a wild-type mitochondrion. The full set of differential equations reads:

$$\frac{dMw}{dt} = \alpha \cdot Mw \cdot \left(A - Mw - Mm\right) - k \cdot Rad \cdot Mw - \varphi_1 \cdot Mw$$
$$\frac{dMm}{dt} = \beta \cdot Mm \cdot \left(A - Mw - Mm\right) + k \cdot Rad \cdot Mw - \varphi_2 \cdot Mm$$
$$\frac{dRad}{dt} = f1 \cdot Mw + f2Mm - \varphi_3 \cdot Rad$$

(eq. 3, 4, 5)

In these equations, “Mw”, “Mm” and “Rad” are the concentrations (number of mitochondria per cell) of wild type mitochondria, mutated mitochondria and free radical level (in the unit of 10^6), respectively.

The first and third terms in eqn (3) and (4) are the synthesis and degradations of variables, respectively, with rates dependent on the Mw and Mm current concentration. The second term in eqn (3) and (4) describes the mutation reaction that rendering wild type mitochondria into pool of mutated mitochondria. Table 1 shows the parameters chosen to reflect the known features in the frame of the model:

Tab.1: Standard parameters used for the mathematical simulation:

Parameter name	Value	Description
α	Brain: 0.07 d^{-1} Liver: 0.073 d^{-1}	Replication rate of wild type mitochondria was set at 14 days for post-mitotic cells, 9.5 days for non-post-mitotic cells. According to Dallman (Dallman, 1967; Neubert et al., 1966).
β	0.035 d^{-1}	Replication rate of defective mitochondria was set at 28 days.
A	1000	Maximum number of total mitochondria in a cell.
$\varphi 1$	0.0693 d^{-1}	Degradation rate of wild type mitochondria. It corresponds to a half-life of 10 days (Menzies and Gold, 1971).
$\varphi 2$	0.0231 d^{-1}	Degradation rate of defective mitochondria, set to 25% of that of wild type mitochondria
$\varphi 3$	7000 d^{-1}	Rate of free radical removal by antioxidants (in the unit of 10^6), according to Rotilio (Rotilio et al., 1972).
f1	900 d^{-1}	Free radical production rate of intact mitochondria (in the unit of 10^6), according to Joenje (Joenje et al., 1985).
f2	300 d^{-1}	Free radical production rate of mutated mitochondria was set to one third that of intact mitochondria (in the unit of 10^6). According to Kowald (Kowald and Kirkwood, 2000).
k	to be calculated	Mutation rate of mouse mitochondrial DNA.

The initial values for wild type mitochondria, mutated mitochondria and free radical were set to 1000, 0 and 0, respectively:

$$Mw_{(t=0)} = 1000;$$
$$Mw_{(t=0)} = 0;$$
$$Rad_{(t=0)} = 0.$$

(eq. 6, 7, 8)

For the numerical integration of time evolution of different variables (wild type mitochondria, mutant type mitochondria and free radicals), the Runge-Kutta method was used. Based on the Euler method, the basic idea of the Runge-Kutta method is the adding up of the combination of the error terms of numerical integration, in order to decrease the error terms order by order. This method is suitable for non-oscillating functions and weak oscillating functions (Cartwright and Piro, 1992).

Parameter scanning respecting value “k” was carried out to determine the mouse mtDNA mutation rate. For this purpose, “k” values ranging from 10^{-3} to 10^{-12} per gene per day was simulated in a batch, the values of $Mw_{(t=newborn)}$, $Mw_{(t=5\text{-}months)}$, $Mw_{(t=10\text{-}months)}$, $Mw_{(t=15\text{-}months)}$, $Mw_{(t=20\text{-}months)}$ and $Mw_{(t=24\text{-}months)}$ calculated from these mathematical simulations were extrapolated. These sets of data were compared to the set of the experimental data gained from the 2D-electrophoresis through linear regression analysis.

As the experimental data set, the mean relative intensity values of mitochondrial NADH-ubiquinone oxidoreductase 13 kDa-A subunit, NADH-ubiquinone oxidoreductase 1 alpha subcomplex 5 and the COX Vb obtained through 2D-electrophoresis analysis were used. This was based on the reduced assumption that only wild type mitochondria contained respiratory complex I and complex IV subunits, wile mutated mitochondria were totally depleted of this subunits (di Rago et al., 1997). The “k” value bearing the simulated data set that best fits the experimental data set (with correlation coefficient nearest to 1) was considered as the mtDNA mutation rate of our mouse model. For this purpose, the linear regression with the highest correlation coefficients values (closest to one) was treated as the optimal fit.

4 Statistics

Sample dimension for all age groups in this study was eight (n=8), except for newborn group, which had a sample dimension of thirteen (n=13) (tab.2). The Western immunoblotting analysis was repeated six times. Histochemical staining of COX-activity was carried out for three times on muscle biopsies from three mouse individuals. Each large-gel 2D-electrophoresis analysis experiment was repeated at least three times (n=3 to 6, tab.3).

Tab. 2: Number of biological materials employed in this study:

Tissue Type	Newborn	5-months	10-months	15-months	20-months	22-months	24-months
Brain	13*	8	8	8	8	--	8§
Liver	13*	8	8	8	8	--	8§
Muscle biopsy	3	--	--	--	--	3	--

Note: * Sample pooled before mitochondria isolation; § these samples entered the current study as frozen materials.

Tab. 3: Sample dimension of different analysis carried out in this study:

Analysis	Sample type	Sample dimension
COX-activity staining	Muscle biopsy	n=3
2D-electrophoresis	Brain, liver	n=3 to 6
Western immunoblottong	Brain, liver	n=6
Blue-native electrophoresis	Liver	n=3

All metric values measured in this study were reported as mean ± standard error of mean (SEM) of the given number of experiments, while ordinal values were given as median together with quartile distance ($\Delta_{0.50}$). Median values were used for quantitative change of spot intensity.

For the gel image evaluation, relative spot intensity was used for the spot volume normalization, calculated as the ratio of individual spot volume to the sum of all spot volumes on its parent gel:

$$\text{Relative intensity} = \frac{\text{Intensity of this spot}}{\Sigma\,(\text{Intensity of each spot})} \qquad \text{(eq.9)}$$

For the access of reproducibility of 2D-electrophoresis, correlation coefficient of different gel pairs was calculated using the following formula:

$$r = \frac{\sum (X - \bar{X})(Y - \bar{Y})}{\sqrt{\sum (X - \bar{X})^2 \sum (Y - \bar{Y})^2}}$$

(eq.10)

where x and y values were the relative intensities of matched spots on each gel profile, and sums were taken ranging over all matched spots in each gel profile.

For all experiments besides 2D-gel spot evaluation, group-to-group difference investigation between more than two groups was performed with analysis of variance (ANOVA) ($p<0.05$), with the null-hypothesis that no difference exists. Difference analysis between two groups were performed with student's t-test ($p<0.05$).

Since the sample dimension of 2D-electrophoresis was small (n=3 to 6), Kruskal-Wallis test was employed for the access of variation in multiple-groups. In case significant variance was detected among the six age groups ($p<0.05$), non-parametric Mann-Whitney U test was further conducted for the pair-wise comparisons among different age groups to gain group-to-group difference information.

For the protein concentration assay, the calculation of average alteration rates of diverse proteins and for the model fitting, linear regression analysis according to "least squares" model was employed. The average change rates per day were determined by the slope of linear regression. Correlation coefficients were calculated for the control of regression quality.

5 Result

In this aging study, a mouse model (C57BL/6) was first validated as model of human aging by histochemical analysis of COX-activity. Then mitochondria from brain and liver tissues were isolated from mouse of different aging stages. The change of mitochondrial proteome during the aging process was accessed using proteomic approaches, including large-gel 2D-electrophoresis and Western immunoblotting. Preliminary studies employing Blue-native electrophoresis was carried out to investigate the possibility of accessing further protein subunits of respiratory chain complexes.

In parallel, a mathematical model was constructed to simulate the accumulation of defective mitochondria during the aging process through free-radical-induced mtDNA mutation. With the help of the mathematical model, the mouse mitochondrial DNA mutation rate was estimated.

5.1 Organ weight difference during development and aging

The brain, liver and muscle tissues of different mouse age groups ranging from newborn to 24-months were obtained. The average weight of brain and liver organs were 0.44 ± 0.08 g (n=43) and 1.25 ± 0.39 g (n=43), respectively, with a ratio of liver to brain as 2.84 (fig.8). Except for newborn stage, no significant difference of organ weight among all aging stages was observed.

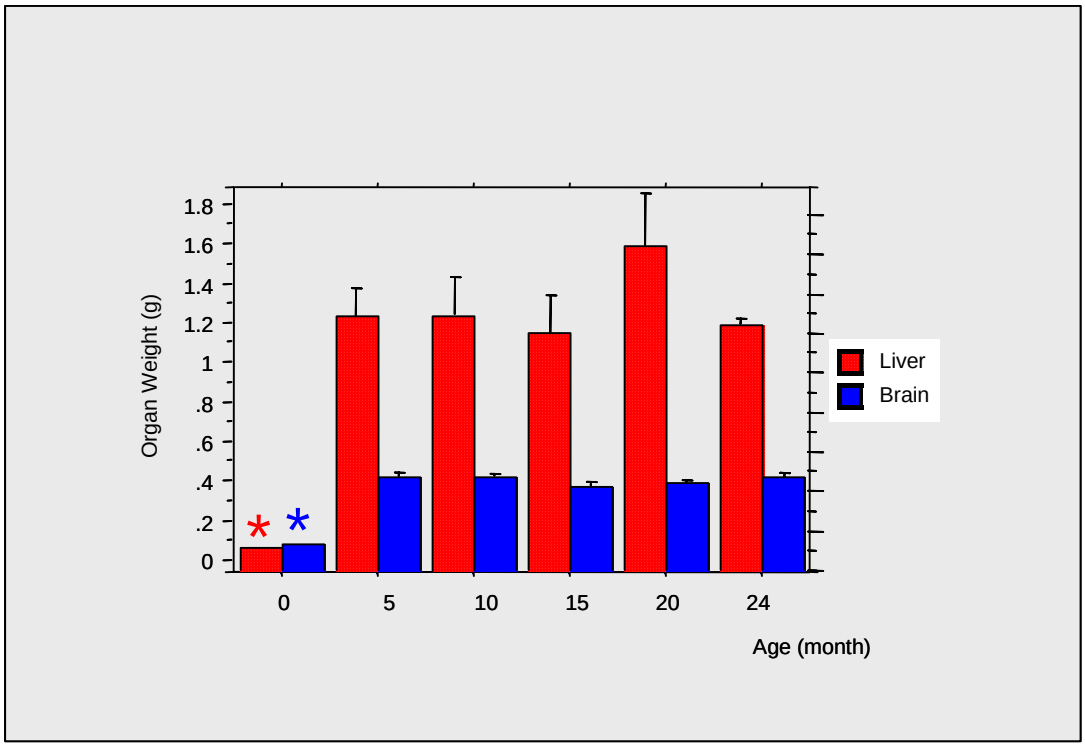

Fig.8: Weight-age relationship of the mouse brain and liver was evaluated in all experimental groups. No significant difference between all groups except for newborn stage was revealed.

5.2 Aging causes COX-activity deficiency on mouse muscle tissue

Mouse muscle biopsies with 79 ± 4 (n=21) muscle fibres per section underwent COX-activity staining and were examined under light microscope (100x to 200x magnification, fig.9). In sections from normal elderly subjects (22-months), there were muscle fibres with very low enzyme activity of cytochrome c oxidase (red arrow), displaying beige colour, while the other muscle fibres in the same section displayed dark brown colour, indicating normal or elevated COX-activity (blue arrow). The whole section showed “mosaic pattern” of alternating light and dark brown staining. The COX-positive ratio of 22-months-old mice muscle accounted $58.7 \pm 9.2\%$ (n=21), while that of young muscle (2 weeks) was 100% (n=21).

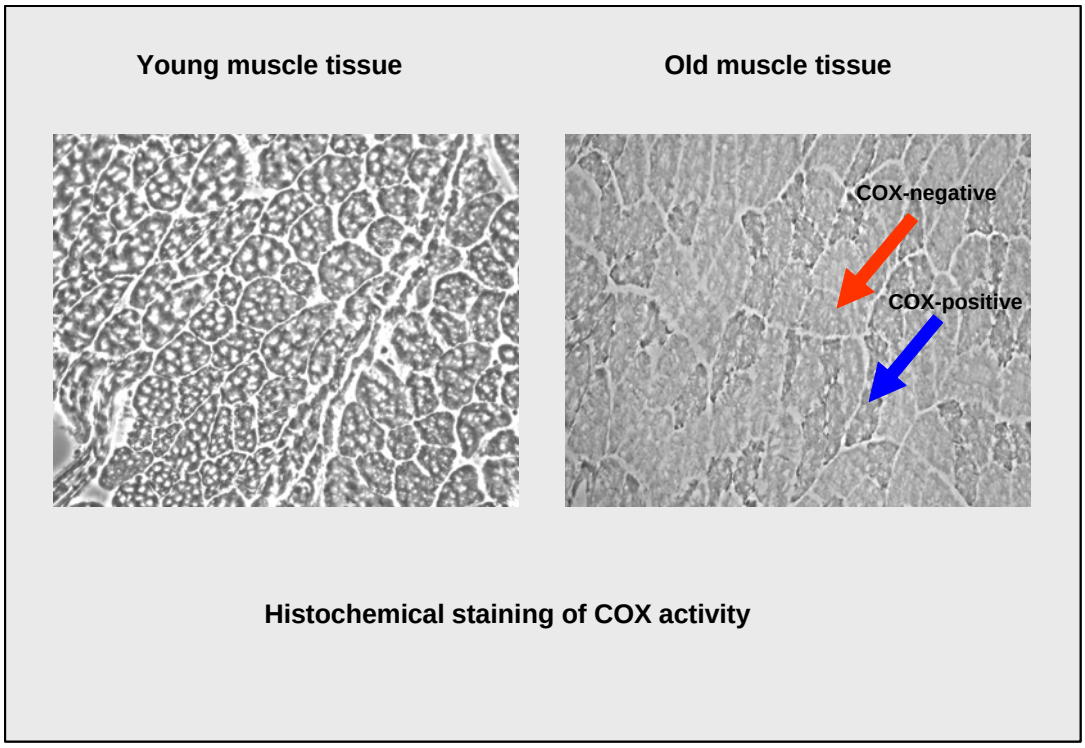

Fig.9: Histochemical staining of COX-activity on young (5-months, left image) and old mouse (22-months, right image) muscle sections. Abnormal muscle fibres with low or absent of COX-activity were detected in the rectus femoris muscle of a 22-months old mouse. Red arrow indicates a representative COX-negative myocyte displaying beige colour, the blue arrow shows a COX-positive phenotype stained brown.

Significant difference was observed between young and old muscle (student t-test, $p<0.0001$). However, histochemical staining of COX activity gives only ordinal results (positive or negative). No quantitative measurement could be conducted (fig.10).

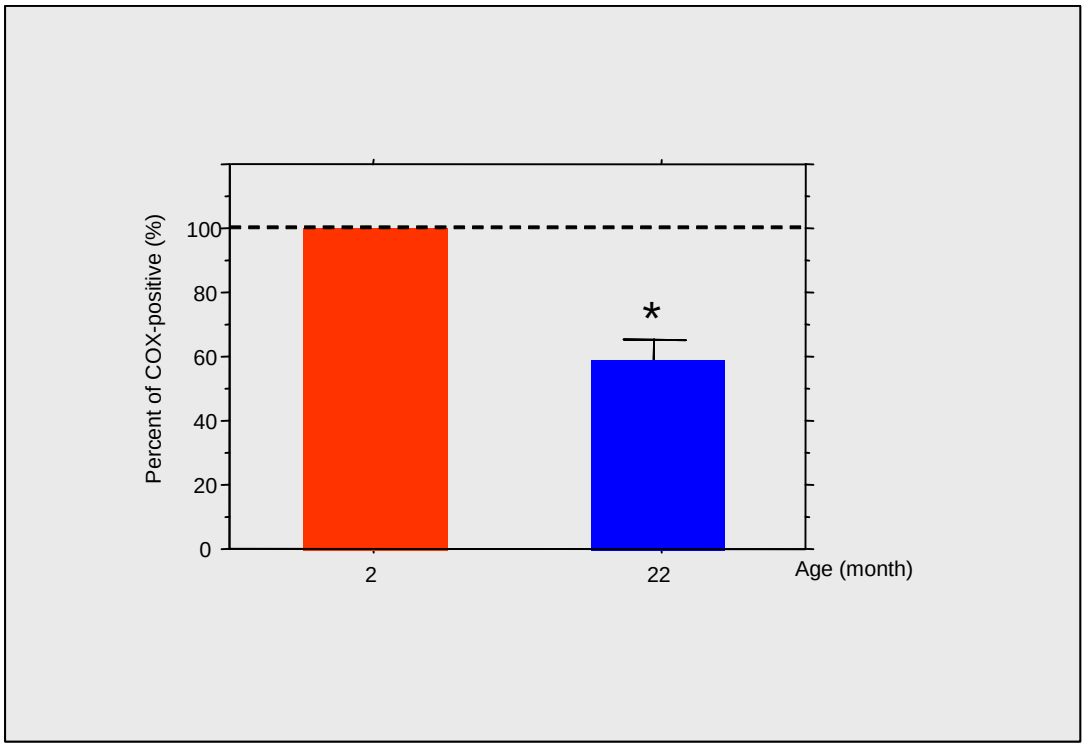

Fig.10: Bar chart showing the percentage of COX-positive muscle fibres measured in the COX-activity staining experiment. Significant difference between young (5-months) and old (22-months) muscle were observed. 41% of senescent myocytes were COX-negative, while no COX-negative myocytes were detected in young counterparts.

5.3 Result of mitochondria isolation

Mitochondria were isolated from mouse brain and liver tissues using the combination of gravity centrifugation and gradient centrifugation. After gradient centrifugation using 30% Percoll solution, two faintly white distinct bands could be observed in the continuous gradient body, with diffuse floating material between the two bands (fig.11). The two bands appeared at densities of 1.09-1.13 g/ml and 1.05 g/ml, respectively (Jungblut and Klose, 1985). Both the low-density fraction and the higher-density fraction were collected and investigated using electronic microscopy.

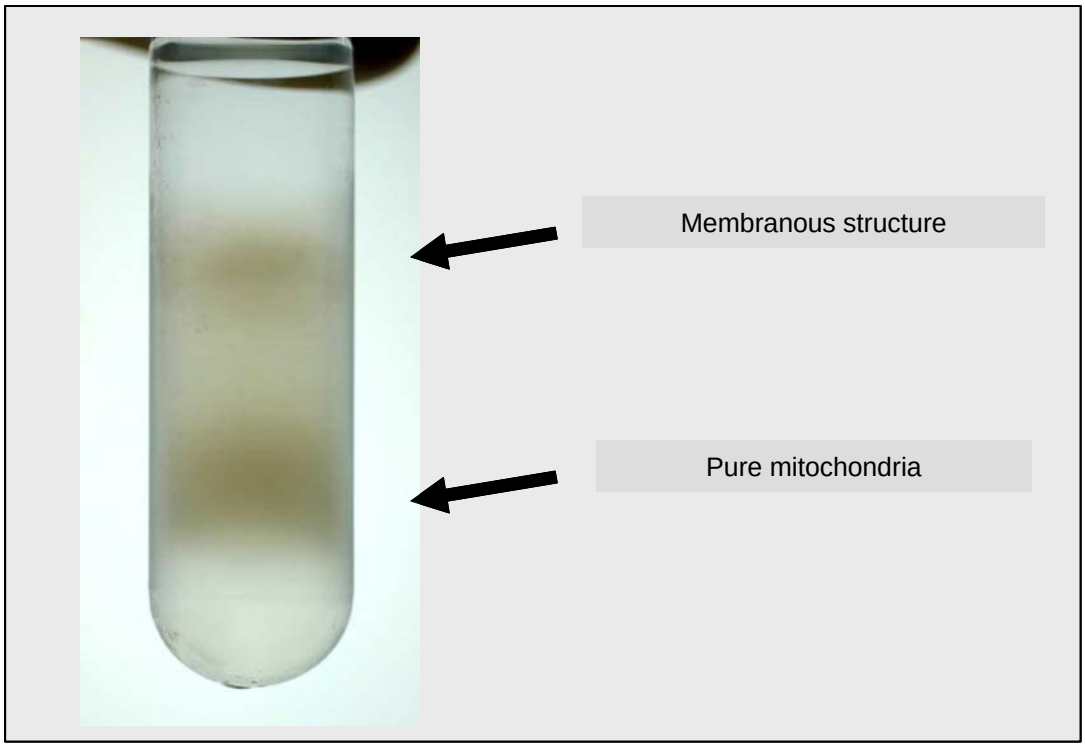

Fig.11: Image of a centrifuge tube after Percoll gradient centrifugation during the mitochondrial isolation procedure. Two bands were found, with some diffuse materials in the intermediate area. The upper band contained membranous structure and lysosomes, whereas the lower band was proved later to be highly purified intact mitochondria.

At the end of the washing step, the resulting mitochondrial fraction was diffuse, with pale white colour. Care was taken not to disturb the pellet during the aspiration of washing medium. Agar embedding procedure was necessary in the electronic microscopic analysis.

5.3.1 Morphology of isolated mitochondria

Through the electronic microscopic investigation, the upper layer in the Percoll gradient body was observed to contain mainly membranous structures, with a broad distribution of small vesicles and lysosomes, as well as damaged mitochondria (result not shown). The lower fraction with a narrow distribution of density range was highly enriched in intact mitochondria (fig.12). This shows that the intact mitochondria with higher density migrated to the lower layer during the continuous gradient centrifugation, while most lysosome and part of the broken mitochondria migrated to the upper layer. Based on this observations, only the lower fractions were used in the for subsequent proteomic analysis.

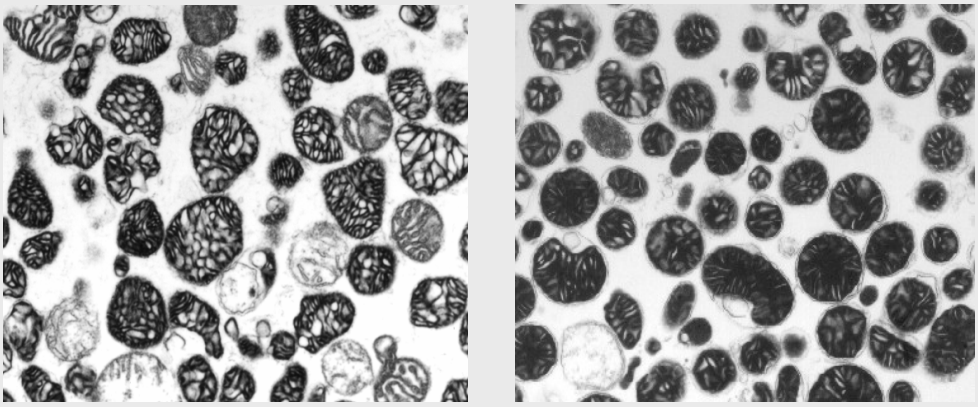

Mouse Brain Mitochondria **Mouse Liver Mitochondria**

Fig.12: Electronic micrographs of the lower fraction material obtained after Percoll gradient centrifugation. Left image: brain mitochondria, Right image: liver mitochondria. 10,000x original magnification.

On the electronic micrograph of isolated brain and liver mitochondria, the whole field demonstrated a highly homogeneous population of mitochondria (94.2 ± 0.7%, n=6) with inner and outer membranes intact. Only a small number (5.9 ± 1.4 %, n=6) of objects was other than mitochondria, among which mostly lysosomes (3.0 ± 0.6%, n=6) displaying regular round shape, homogeneously dyed grey. This showed that the mitochondria isolation from both mouse brain and liver tissues has been effective (fig.13).

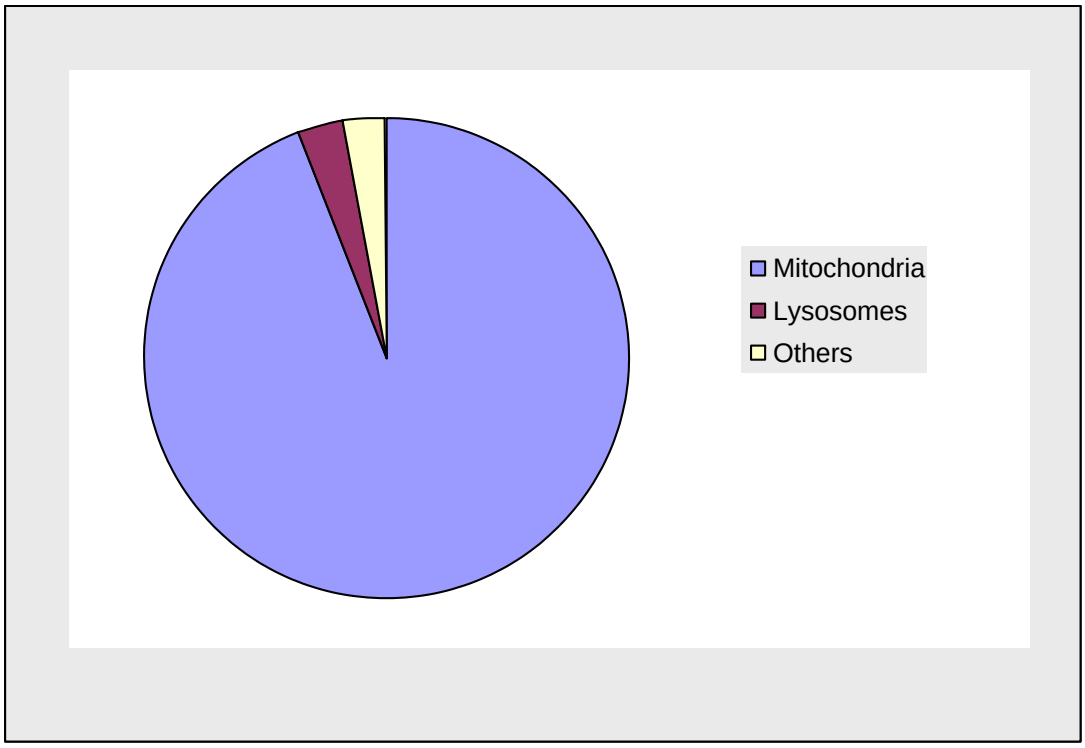

Fig.13: Percentage of mitochondria, lysosome, and debris in the mitochondrial fraction after Percoll gradient purification. 94% of particles were intact mitochondria, 3% were lysosome, others were undefined cell debris.

Both mitochondria isolated from brain and liver have the form of either round, or tube-like structure with a length of 1.8 ± 0.1 μm (n=100), and a width of 0.9 ± 0.03 μm (n=100). They consisted of double membranous structure that has been made contrast by osmium. The outer membrane built a round or oval envelope, while the inner membrane possessed pronounced cristae structure. In some electronic micrograph, the mitochondria were slightly rounded, indicating either a lower osmotic pressure of the surrounding medium, or the slight damage of mitochondria structure.

5.3.2 Yield of mitochondria

Together with the organ weight data collected in this study, the yield of mitochondria could be calculated as the “mg mitochondria per gram of wet tissue”:

$$\text{Yield of mitochondria} = \frac{\text{Amount of mitochondria [mg]}}{\text{Weight of wet tissue [g]}} \qquad \text{(eq.11)}$$

The yield of mitochondria was 4.21 ± 1.46 mg/g (n=41) from mouse liver tissue and 2.33 ± 0.97 mg/g (n=41) from brain tissue, respectively. Mitochondrial yield of liver was 1.8 times to that of brain. In both brain and liver tissues, the yields of mitochondria from newborn mice were significantly lower than that of the remaining aging stages (fig.14).

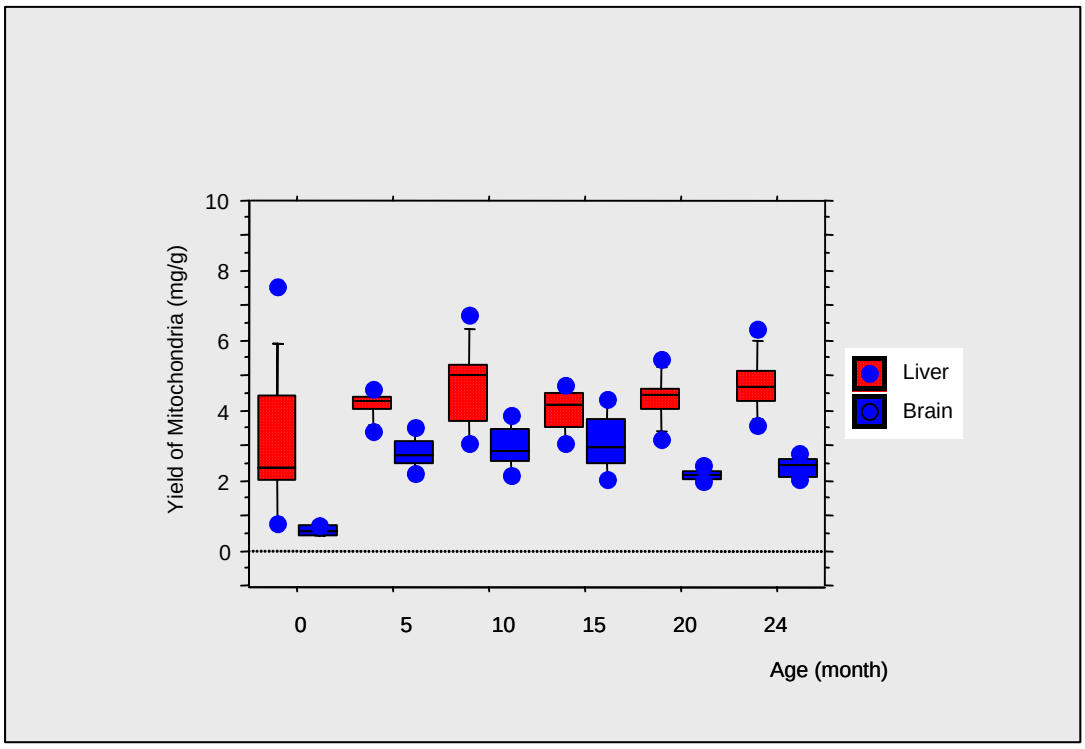

Fig.14: Mitochondrial yields from mouse brain and liver tissues of different age groups. Both brain and liver tissues from the newborn stage gave significant small yield of mitochondria.

Interestingly, for brain tissue, there was in addition an age-correlated difference of mitochondrial yield: significantly smaller yields of mitochondria ($p<0.05$) was obtained from the brain tissue of 20-months and 24-months mice. No similar tendency was observed in data of liver mitochondrial yields (fig.15).

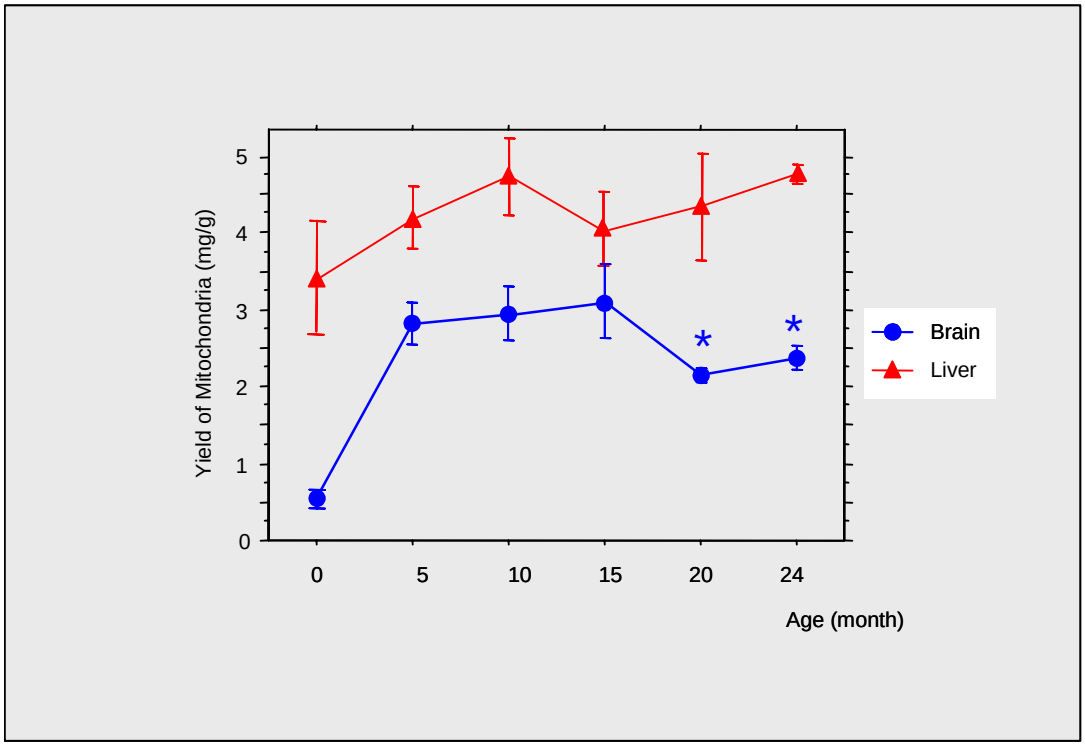

Fig.15: Yields of mitochondria respecting different age groups. For mouse liver tissue, only the newborn group had smaller yield compared to other aging stages. In brain, 20-months and 24-months aging groups gave significantly smaller yield of mitochondria compared to that of other stages aging (5-months, 10-months and 15-months). The asterisks indicate statistical significance ($p<0.05$).

5.3.3 Comparison of mitochondria isolation from fresh and frozen material

Since it was not always possible to obtain fresh materials for mitochondria isolation, frozen mouse organs were also employed in this study (24-months age group). The potential influence of this initial sample handling condition on the outcome of mitochondrial quality was taken into consideration. Upon comparing the mitochondria isolation result from fresh and frozen materials, part of the mitochondria isolated from frozen tissue showed slightly lower membrane integrity (fig.16). The yield of mitochondria gained from frozen material was smaller.

Mitochondria from fresh mouse muscle

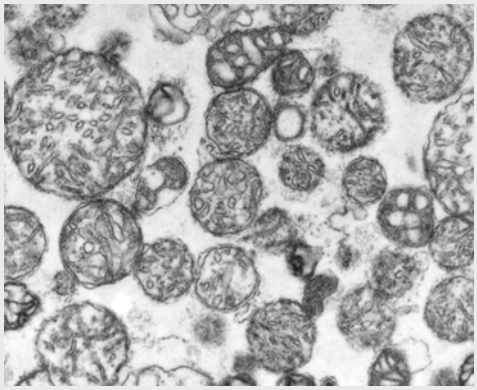

Mitochondria from frozen mouse muscle

Fig.16: Comparison of mitochondria isolation from fresh and frozen mouse muscle tissues. No substantial difference in quality of isolated mitochondria could be observed, although some of the mitochondria isolated from frozen tissue had slightly lower outer membrane integrity.

5.3.4 Comparison of mitochondria isolation from young and old organism

The subject of this study was to elucidate the protein profile changes of mitochondria in different aging stages. For this purpose, it was to be prerequisited at the first line that the mitochondria isolated from all aging stages were of comparable quality. Thus, a comparison of mitochondria isolation from young and old tissues was conducted.

Figure 17 shows the electronic microscopy of mitochondria isolated from young (5-months) and old (22-months) mouse brain tissue. No significant difference in mitochondrial morphology and purity could be observed from this comparison. This showed that it was tractable to isolate pure intact mitochondria from both young and old mouse liver and brain tissue.

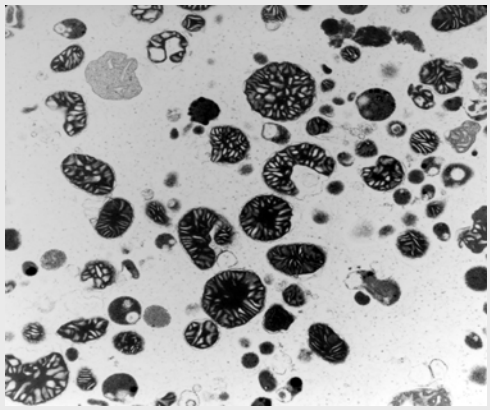

Mitochondria from
young mouse brain

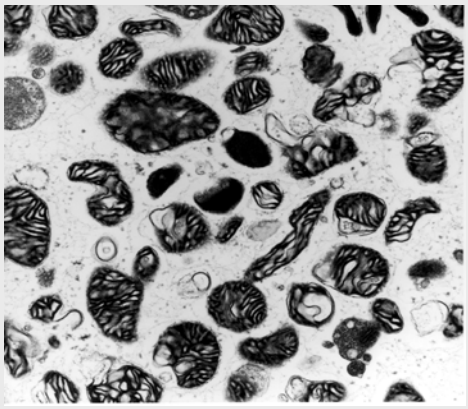

Mitochondria from
old mouse brain

Fig.17: Mitochondria isolated from young (left image, 5-months) and old (right image, 22-months) mouse organs (brain and liver) showed comparable quality under electro micrograph.

5.4 Result of protein pre-fractionation

In order to enrich low-abundant proteins and membrane proteins in the mitochondria proteomic analysis, we have separated the mitochondrial proteins into three fractions using the sequential extraction strategy. Tris-buffer was first used to extract soluble proteins, which resulted in “Fraction I”. This obtained supernatant after centrifugation was transparent, lightly pale white. Afterwards, Triton-X100-containing buffer was used to extract membrane-associated proteins, which resulted in “Fraction II”. Noticeably, this fraction had a darker colour compared to that of “Fraction I”. The remaining pellet fraction had a high viscosity, indicates the high content of lipids.

According to the protocol of Molly (Molloy et al., 1999), we carried out the methanol-chloroform extraction using the pellet obtained after Triton buffer treatment. As expected, a substantial amount of protein interface was precipitated between the methanol/water phase and chloroform phase, forming a solid pale white layer. This demonstrates that there was still considerable amount of protein in the membranous structures that could not be extracted by detergent-containing aqueous buffer system.

The extracted protein pellet was partially dried in cold Argon to reduce the amount of remaining organic solutions, and then resolved with Laemlli sample buffer or water. However, even after overnight stirring, not all pellet materials were resolved in the solution.

The protein concentrations of all three fractions (“Fraction I”, “Fraction II” and “Fraction III”) were measured by the BCA protein assay. The concentration of the protein “Fraction I” was measured to be 10.27 ± 2.17 mg/ml (n=12), while that of “Fraction II” was 5.76 ± 0.96 mg/ml (n=12). Noticeably, the protein concentration of “Fraction III” could not be measured successfully, possibly due to the presence of remaining organic solution, or due to the membrane protein property that was not compatible to the BCA assay or protein standard.

Respecting the total volume of both “Fraction I” and “Fraction II” samples, together with the assumption that there was approximately 280mg/ml protein in the mitochondrial pellet (Brown, 1991), Tris-buffer extraction proteins (“Fraction I”) and Triton-containing buffer extracted protein (“Fraction II”) accounted for 25.6 ± 2.8 % (n=11), 56.2 ± 5.5 % (n=11) of total protein present of the mitochondrial pellet, respectively. This led to our prediction of the percentage of “Fraction III” (methanol-chloroform extracted) to be around 17%. This, again, demonstrate that a considerable part of protein remained in the protein pellet extracted using methanol-chloroform. Figure 18 shows the percentage of protein present in three different fractions.

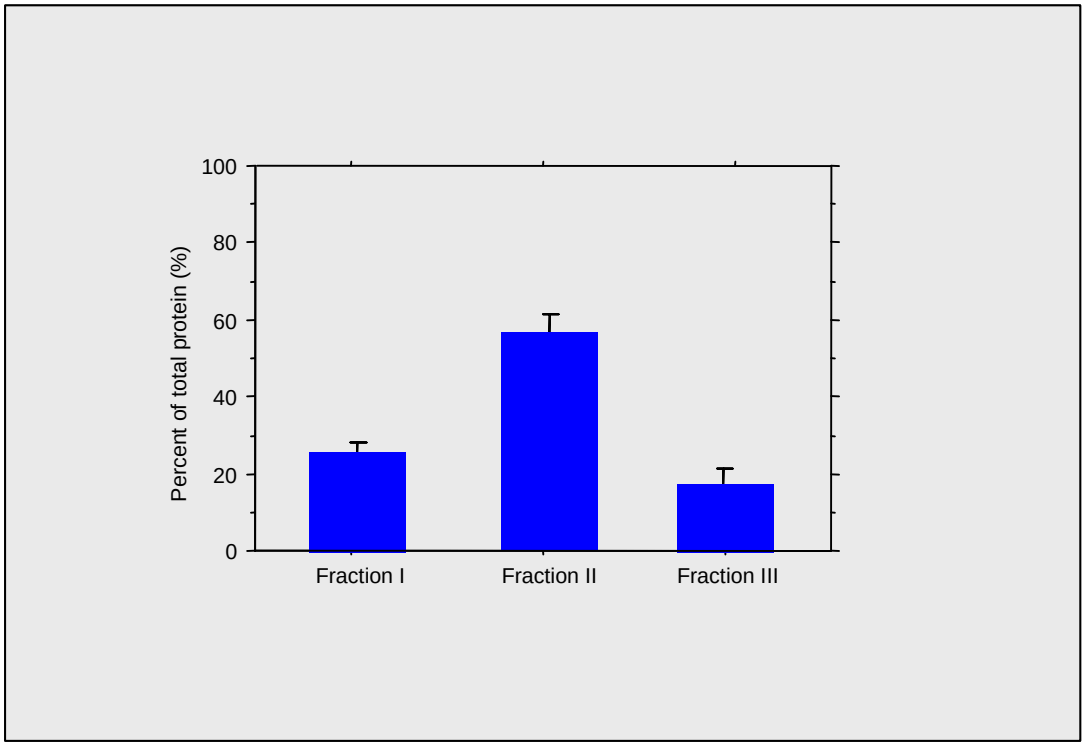

Fig.18: Mitochondrial proteins were fractionated into three different fractions using sequential extraction strategy. Tris-buffer extracted proteins ("Fraction I"), Triton-containing buffer extracted protein ("Fraction II") account for 25.6 ± 2.8% (n=11) and 56.2 ± 5.5 % (n=11) of the total protein present of the mitochondrial pellet. The percentage of "Fraction III" (methanol-chloroform extracted) was estimated to be 17.0 ± 3.1% (n=11) respecting the starting material amount.

Due to the lack of protein concentration data of "Fraction III" samples, weight of protein pellet instead of protein amount was used as the sample amount orientation in the subsequent Western immunoblotting analysis.

5.5 Result of 2D-electrophoresis analyses

2D-electrophoresis analysis was employed for the quantitative analysis of "Fraction I" and "Fraction II" mitochondrial proteins of different age groups. A broad carrier ampholyte mixture with pH value ranging from 2-11 was used as carrier ampholites in order to get a panorama view of the mitochondrial proteins. Figure 19 shows the reference gel patterns of brain and liver mitochondrial total protein extract. By convention, the resulting high-resolution spot patterns of a 2D-electrophoresis were oriented with the low, acidic isoelectric points on the left and the lowers molecular weight proteins at the bottom.

a) 2D-gel pattern of mouse brain mitochondrial total proteins

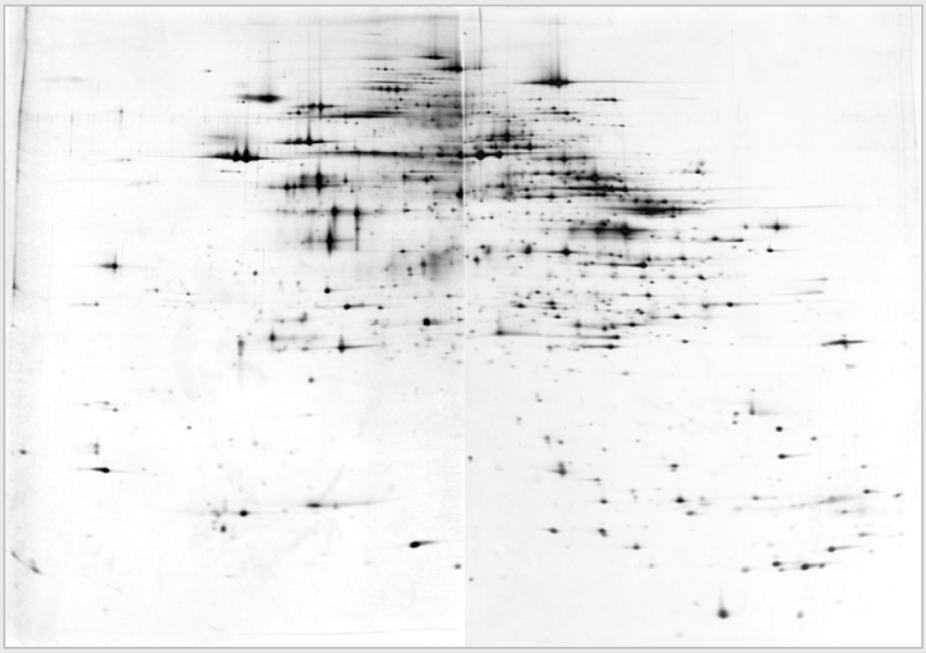

b) 2D-gel pattern of mouse liver mitochondrial total proteins

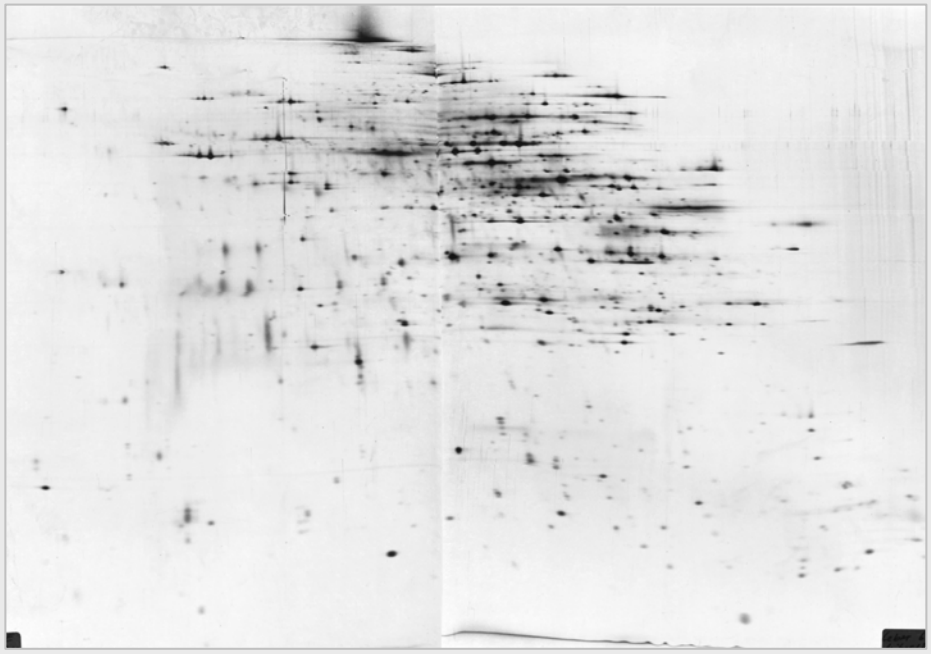

Fig.19: The mouse brain (upper image) and liver (lower image) mitochondrial protein total extract (from 5-months old mouse brain and liver tissues) were separated by large-gel 2D-electrophoresis (40x30 cm). Shown are representative analytical silver stained gels at protein load of 100μg.

After the preparative silver staining, ampholyte running front gave hill-form background at the lower side of the gels (see fig.20). This is specific for preparative silver staining due to the short rinsing period. Since the carrier ampholyte contain both amino- and carboxyl

residues, they behave like small proteins that also bind to SDS. Due to their small size, the vast majority migrate at the dye front (O'Farrell, 1975). In the analytical silver staining method, these small ampholytes were washed out of gels though the application of long incubation period.

5.5.1 Reproducibility of 2D-electrophoresis carried out in this study

In order to study primary variability of the 2D-electrophoresis method carried out in this experiment, the gel-to-gel difference of the large-gel 2D-electropheresis analysis was first accessed with six different gels generated from a single sample, run on different days spreading in the time span of six months.

Although the contrast level of the gels was slightly different, the majority of analogous protein spots showed only minimal differences in relative location and shape. The average correlation coefficient of these six 2D-gels was 0.98 ± 0.05. Figure 20 shows an example of wrapped image of two 2D-gels from this same sample, created by the image software ProteinWeaver. On this wrapped image, single gel image bears either blue or orange, which is the complementary colour of blue. Analogous spots on different gels with similar spot pattern and location display black colour, which is the optical addition of blue and orange.

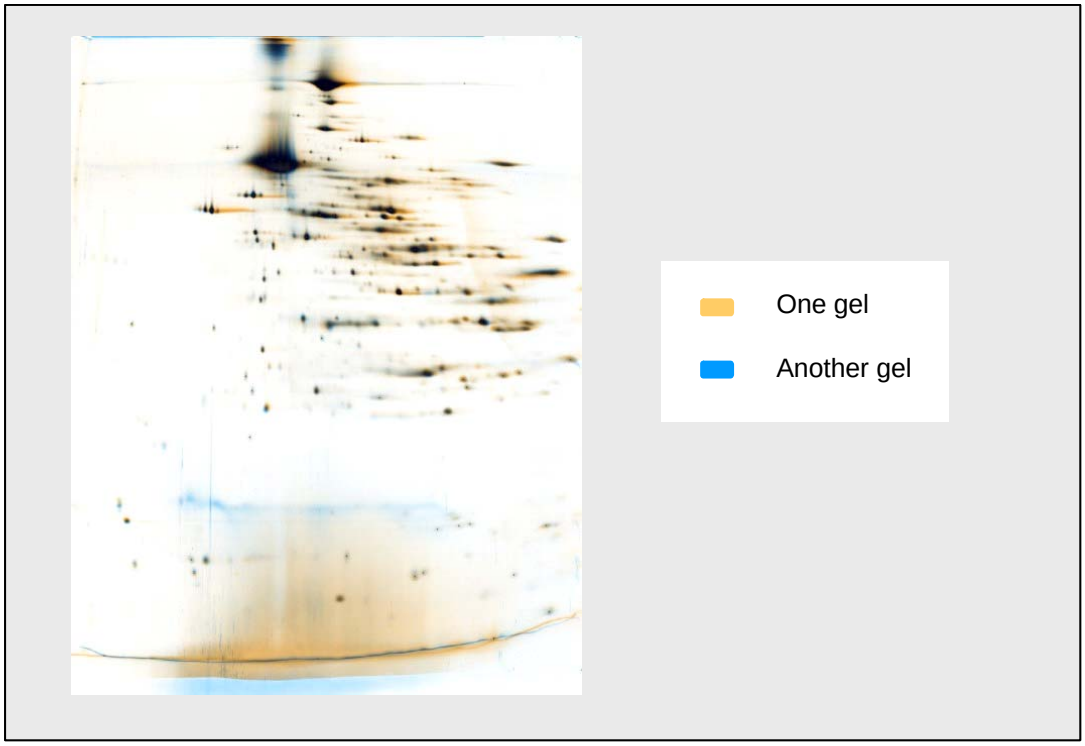

Fig.20: The wrapped image of two 2D-gels (20x30 cm) run from the mouse liver mitochondrial protein sample (5-months of age, "Fraction I") displays minimal spot pattern

difference of the two gels. The matched spots were displayed in black colour, which account for the vast majority of spots. This indicates a high reproducibility of the 2D-electrophoresis method. The spots that could not be matched were either orange or blue.

Using the relative intensity of one gel as X-axis, and that of the other gel as Y-axis, the majority of the matched spots of the gel pairs were localized close to the diagonal line (fig.21). This indicates that the matched spots show correlated intensity.

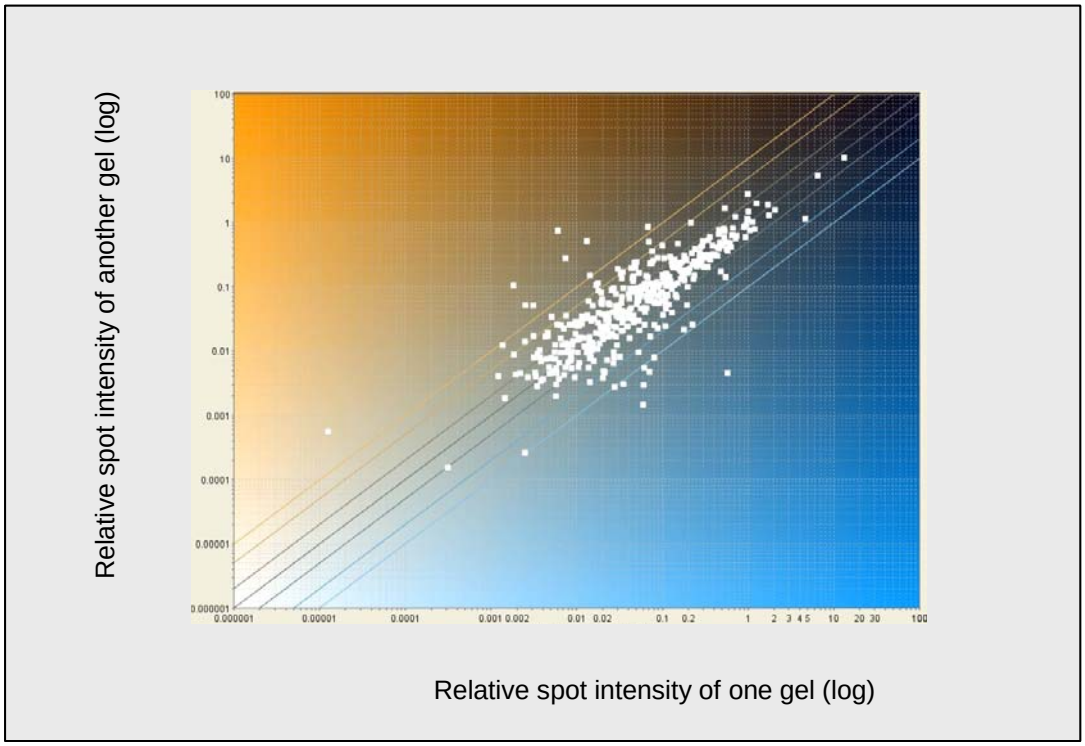

Fig.21: Scatter plot of the relative spot intensities of two 2D-gel patterns of brain mitochondria (Fraction I protein) from a same mitochondrial sample. The x-axis shows the intensity of the gel image on one gel, the y-axis shows the spot intensities on another 2D-gel. Spots with the same relative intensity on both gels were found on the diagonal of the scatter plot. The distance from the diagonal is a measure of the intensity difference of the protein spots in the two gels.

The same tendency was observed in 2D-gels from different age groups in our experiment. In order to access the comparability of 2D-gels generated in our current experiment, we defined “spot matching rate” as the percent of corresponding spots on two different 2D-gels from different mitochondrial protein samples. The average spot matching rate of liver mitochondrial 2D-gels among different age groups was 91 ± 4% (n=15), that of brain mitochondrial gels were 79 ± 8% (n=15). The average spot matching rate of the whole

study accounted 80 ± 13% (n=66) (fig.22). The 2D-gels from brain mitochondria had a slightly less satisfactory spots matching quality compared to that of liver.

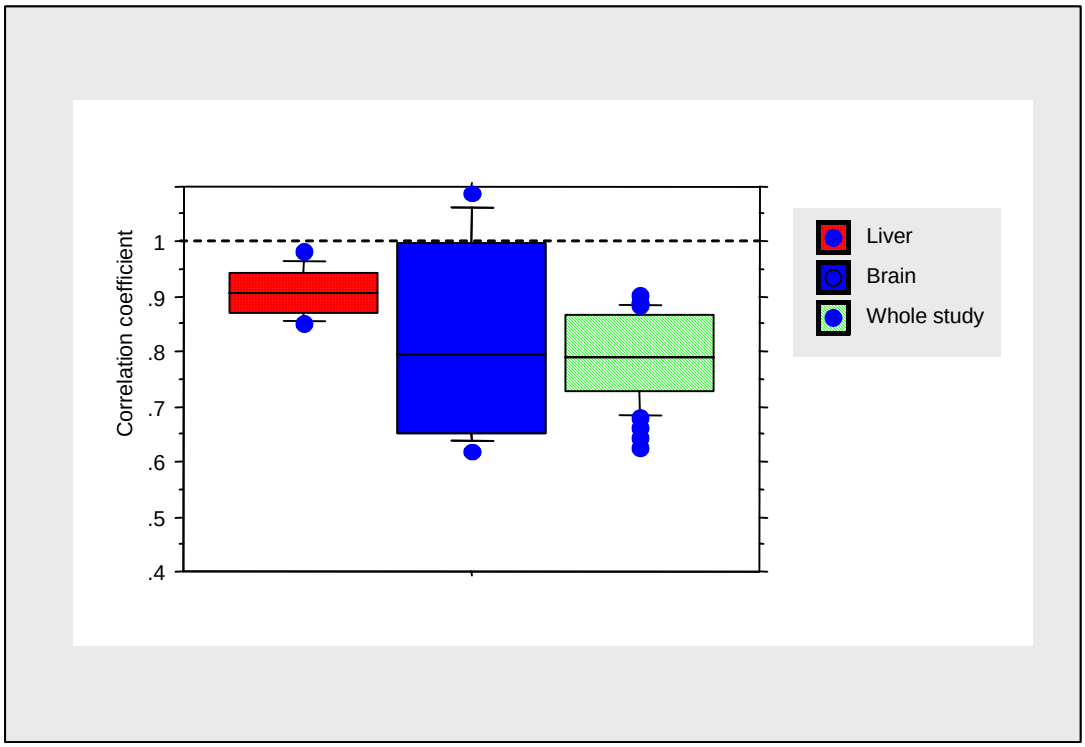

Fig.22: Box chart showing the value distribution of "spot matching rates" of 2D-gels in this aging study. The mean value of "spot matching rates" for liver-to-liver gel matching, brain-to-brain gel matching were 0.91 and 0.79, respectively. The average "spot matching rates" of the 2D-gels throughout this study was 0.80.

Respecting the matching quality of 2D-gels from different age groups, the best match of brain mitochondrial 2D-gels was obtained between the 10-months age group and the 24-months age group (spot matching rate 99.3%). In liver, the 2D-gels of newborn stage matched best with 20-months aging stage (spot matching rate 98.3%). There was no correlation of gel image matching quality to the age distance. Larger age difference does not correlate to a smaller matching quality. Specifically, there was no significant difference in protein spot patterns between 2D-gels of 24-months samples (which entered this study as frozen materials) compared to that of all other age groups.

5.5.2 Comparison of whole tissue 2D-gel to mitochondrial 2D-gel

In order to investigate whether the isolation of mitochondria allowed us to access changes of additional protein spots on the 2D-gels, the 2D-electrophoresis gel patterns of the brain total protein extract and brain mitochondria were compared to each other (fig.23). The two-

dimensional protein spot pattern of mitochondria was largely reduced compared to that of brain whole tissue spot pattern. While the 2D-gel of mouse brain total protein extract contains over 6000 spots, 626 protein spots were found on the 2D-gel map of mitochondrial total protein extract.

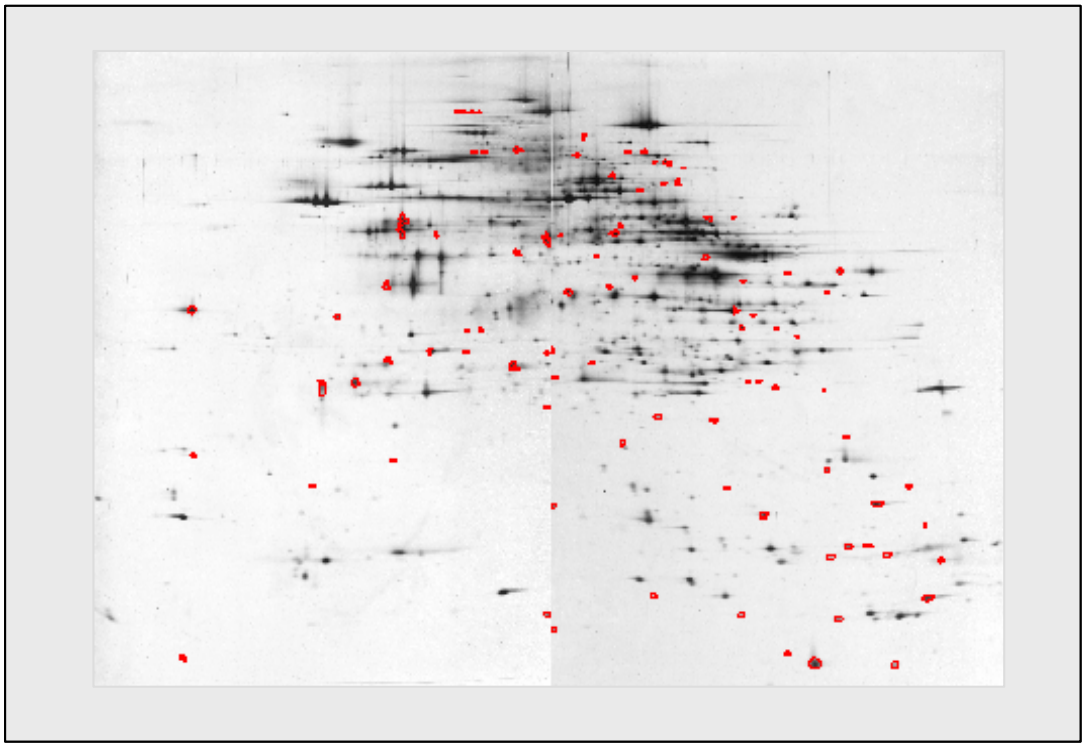

Fig.23: Comparison of brain mitochondrial total protein extract to brain total protein using 2D-electrophoresis (40x30 cm). All protein spots shown in black colour were also visible on the 2D-gel of mouse brain total protein extract (shared spots). Red dots indicate spots that are additional or demonstrated enhanced intensity on the mitochondrial 2D-gel (courtesy of Dr. Sagi).

Despite the reduced protein spot pattern on the mitochondrial gel, 90 spots, which were barely visible on the whole organ gel, showed up intensely on the mitochondrial gel. Another 26 spots were completely additional on the mitochondrial 2D-gel, supporting the effect of sub-cellular fractionation on the enrichment of low-abundant proteins (courtesy of Dr. Dijana Sagi in our research institute).

5.5.3 Effect of protein pre-fractionation on protein resolution

Through the 2D-electrophoresis separation carried out in our current study, 556 protein spots were resolved from the mitochondrial “Fraction I” protein samples (fig.20), while 149 spots were resolved from “Fraction II” protein samples (fig.24).

In order to target membrane proteins, we employed Triton-X100 in the 2D-electrophoresis separation of “Fraction II” proteins obtained through the sequential protein extraction procedure. Consequently, it was our interest to investigate how many hydrophobic proteins were resolved on the “Fraction II” 2D-gels.

As shown in fig.24, very different protein spot pattern was obtained from “Fraction II” proteins (compared to fig.19, fig.20). Due to the drastic difference of spot patterns, it was not feasible to compare the 2D-gel patterns of “Fraction II” proteins to other 2D-gel pattern of our study. Thus, all 80 spots with relatively high intensity on the 2D-gels of “Fraction II” were taken to mass spectrometric protein identification.

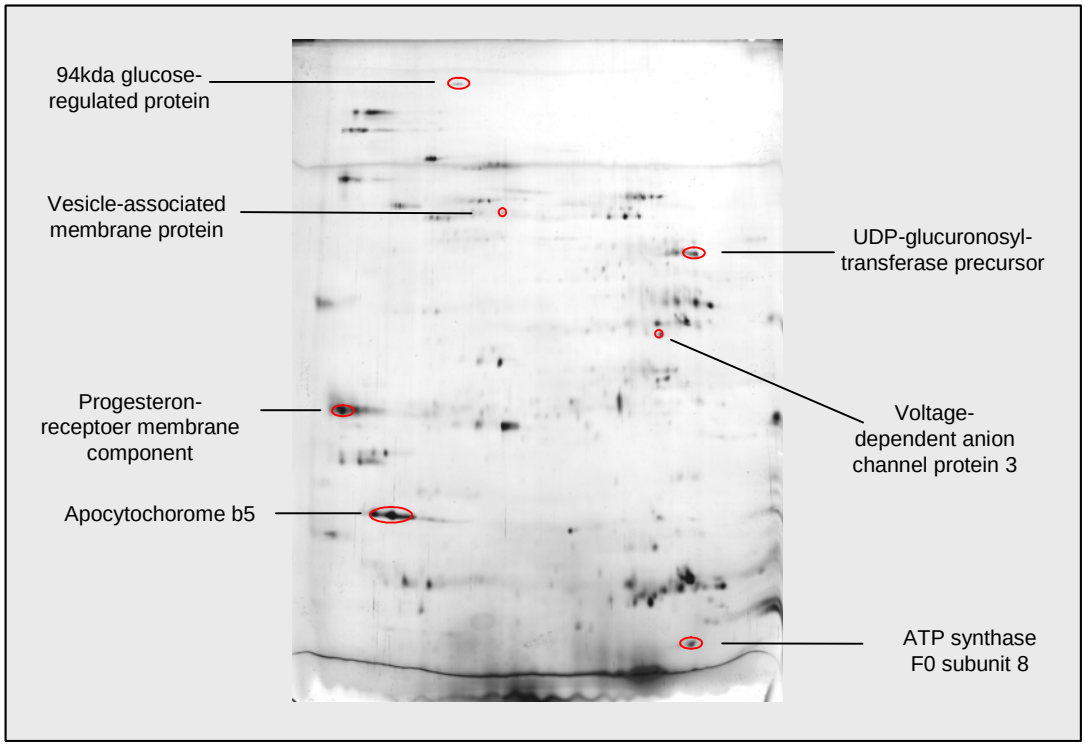

Fig.24: An example of 2D-gels (20x30 cm) from “Fraction II” sample of mouse liver mitochondria. Very different pattern was gained compared to that of “fraction I” or standard pattern. Seven proteins that later predicted to be membrane proteins are marked on the gel image.

Though the comparison of 2D-gel patterns generated from pre-fractionated mitochondrial proteins to that of mitochondrial total protein extract, six additional protein spots were gained though the fractionation of brain mitochondrial proteins. Among these, two additional proteins were only visible on 2D-gels of “Fraction I” samples, while four protein spots were only visible on 2D-gels of “Fraction II”.

Analogously, four protein spots were additionally gained though fractionation of liver mitochondrial proteins. Among these, two protein spots were only visualized on 2D-gels of "Fraction I" proteins (one of them later identified to be mitochondrial ribosomal protein L12); one protein spot was not visible on 2D-gels of liver mitochondrial total protein extract, but visible in both 2D-gels of both "Fraction I" and "Fraction II" (later identified to be NADH dehydrogenase 1 beta subcomplex 7). The other protein spot was only visible on the 2D-gels of "Fraction II" sample (later identified to be mitochondrial DNA topoisomerase).

5.5.4 Access of possible proteomic changes based on protein spot pattern

Pursuing our initial interest of age-related changes in mitochondrial proteome, we evaluated two-dimensional mitochondrial protein patterns of six different age groups, generated from either "Fraction I" and "Fraction II" samples of mouse brain or liver mitochondria. Through visual comparison of the mitochondrial protein spot patterns of different age groups bearing the same fraction number and organ type, numerous differences among the different age groups were detected in both brain and liver mitochondria.

Intensities of some of the spots were observed to decrease or increase with age, indicating the change of steady state concentration of the corresponding proteins in mitochondria during the aging process. Specifically, 26 changed spots were detected in brain "Fraction I" gels; 16 changed spots were found in liver "Fraction I" gels; 19 spot changes were observed in brain "Fraction II" 2D-gels, while 34 spot changes were annotated in liver "Fraction II" 2D-gels (tab.4). Noticeably, eight protein spots showed only decreased profile from 20-months age group to 24-months group.

Tab.4: Protein spot changes from newborn to 24-months group detected on 2D-gels of different mitochondrial protein fractions:

Alteration	Brain mitochondria		Liver mitochondria	
	"Fraction I"	"Fraction II"	"Fraction I"	"Fraction II"
Up-regulation	3	3	5	5
Down-regulation	9 (4)*	6	9 (1)*	10 (3)*
Other changes	14	0	2	19
Not visible in newborn	8	8	2	8
Visible only in newborn	12	4	1	6

Note: * among the down-regulated protein spots, number of spots showing only a decrease from 20-months to 24-months of age are listed in the parenthesis.

For the access of tissue-specifity respecting mitochondrial aging profile, we compared the cross differences of 2D-gels respecting brain or liver mitochondrial sample origin. Eight protein spots appeared to be enhanced in brain or liver mitochondrial 2D-gels, respectively. Seven of these protein spots were on the liver mitochondrial protein 2D-gels, while one was brain mitochondria-specific. Together with the 80 selected protein spots on the “Fraction II” 2D-gels, 173 protein spots underwent mass spectrometric identification (tab.5).

Tab.5: Protein spots from 2D-gels that underwent mass spectrometric protein identification:

Categories	Number of spots
Changed spots in brain “Fraction I”	26
Changed spots in brain “Fraction II”	9
Changed spots in liver “Fraction I”	16
Changed spots in liver “Fraction II”	34
Spots from “Fraction II” proteins	80
Possible liver mitochondria-specific	7
Possible brain mitochondria-specific	1
TOTAL	173

5.6 Result of protein identification

For protein identification, we employed both MALDI-TOF-MS and ESI-Iontrap-MS analyses. MALDI-TOF-MS is fast and effective method, but needs larger amount of peptide sample. Besides, MALDI-TOF-MS is not suitable for the identification of protein mixture. For this reason, intensive spots on the 2D-gels were identified with MALDI-TOF-MS, whereas ESI-Iontrap-MS was employed for protein spots with less intensity, especially those spots that were partially merged to adjacent ones.

5.6.1 Quality of MS-spectra

Figure 25 shows an example of mass spectra of the MALDI-TOF-MS experiment. Comparing to the *in silico* digested peptide list, measured peptide was highlighted on the peptide sequence. The methionine-containing peptides and their corresponding oxidized derivates, which leads to a (m/z) mass increase of 18 Dalton, were marked blue with their non-oxidized counterparts at the left side. Although it was not expected that all methionine residuals have their oxidized counterparts, this pair-wise representation of methionine-containing peptides strongly confirmed the identity of these peptides.

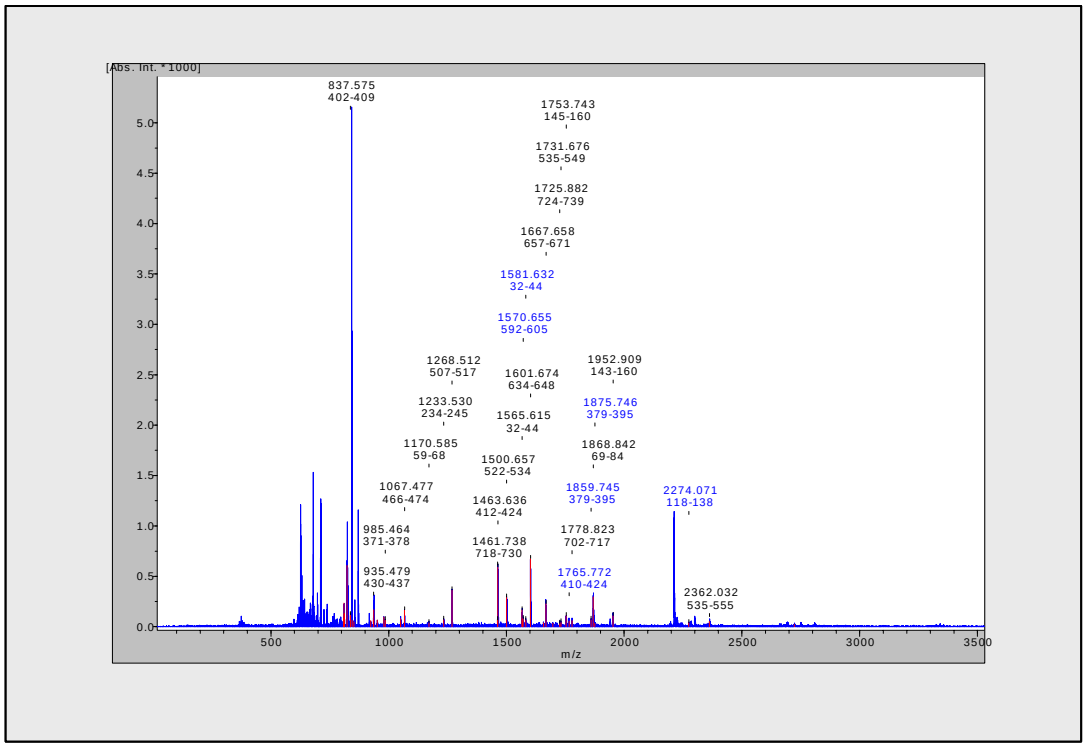

Fig.25: An example of MS-spectra obtained in this study. 34 mass peak signals were measured. Among these, 20 peaks (labelled black) were able to be assigned as tryptic digested peptide sequences of aconitase (gi 18079339). Another six masses (labelled blue) could be orientated as modification of existing peptide peaks. Three of the peaks were identified as endo-digestion product of trypsin.

5.6.2 Databank-based protein identification

The obtained mass spectrometry raw data (peak list and relative intensities) were used to search against the National Centre for Biotechnology Information non-redundant protein database NCBInr (all mammalian species) with the Mascot search engine.

Mascot incorporates a probability-based implementation of the Mowse (mol. Wt. Search) algorithm (Pappin et al., 1993). It calculates a p-value describing the absolute probability that the observed match is a random event (with the assumption that the entries in the sequence databases are random sequences). The Mowse score displayed in the result sheet was reported as $-10\log_{10}(p)$. The significant threshold value for Mowse score is thus a function of the size of the sequence database being searched. In the current study, a threshold value of 61 corresponded to a match with statistical significance ($p<0.05$) for searching all mammalian species of NCBInr database.

For the majority of cases in our study, four or five measured peptides were sufficient to confirm the identity of the protein satisfactorily. Of the 173 protein-spots-of-interest

prepared from the 2D-electrophoresis analysis, 123 spots were successfully identified, which account for 71% of all the 173 protein identifications. The number of matched peptide masses was 13.8 ± 0.6 (n=123). The average percentage of the sequence coverage was 51.3 ± 1.5 % (n=123). The median of Probability Mowse score accounted as 102, with a quartile distance $\Delta_{0.50}$=69 (n=123). This corresponds to an expected probability value (p) as 1.15 E-5. Nonetheless, some spot could not be identified despite multiple efforts.

Among the 50 proteins that were not identified successfully, 10 protein spots were from the 2D-gels of brain mitochondrial “Fraction I” protein; 13 spots were from the 2D-gels of brain mitochondrial “Fraction II” protein. Two protein spots were from the 2D-gels of liver mitochondrial “Fraction I” protein, while 25 spots were from the 2D-gels of liver mitochondrial “Fraction II” protein.

5.7 Prediction of hydrophobicity of identified proteins

In order to access the efficiency of membrane protein resolution of 2D-electrophoresis analysis and sequential protein pre-fractionation strategy carried out in this study, all 123 identified proteins were subjected to Gravy score prediction. Only seven of the identified proteins in this study were predicted to contain trans-membrane domains (ranging from one to two), with Gravy scores ranging from 0.139 to -0.72. Among them, the ATP synthase F0 subunit 8 is one of the 13 mtDNA-encoded proteins. Noticeably, all these seven spots were additional spots on the 2D-gel pattern of “Fraction II” proteins. The annotation of these membrane proteins, together with their number of trans-membrane domain (TMD) and Gravy factor are listed in the following table (tab.6).

Tab.6: Properties of membrane proteins identified on the 2D-gels of "Fraction II" samples:

Protein name	gi number	TMD number	Gravy factor
ATP synthase F0 subunit 8 (mtDNA encoded)	gi 5834958	1xTMD	+0.139
UDP-glucuronosyltransferase 1-1 precursor	gi 2501472	2xTMD	+0.087
Vesicle associated membrane protein 2	gi 2253399	1xTMD	+0.003
Voltage-dependent anion-selective channel protein 3	gi 12643945	1xTMD	-0.280
Cytrochorme b5 outer mitochondrial membrane precursor	gi 31542438	1xTMD	-0.602
Progesterone receptor membrane component	gi 31980806	1xTMD	-0.604
Endoplasmin precursor (94kDa glucose-regulated protein)	gi 729425	1xTMD	-0.72

5.8 Quantitative changes of protein spots observed

Among the 123 identified spots (see table A1 for summary), 27 spots were determined to be cellular contaminations. These include hemoglobin, alpha globin, cytoplasmic ribosomal proteins, myosin, major urinary proteins, albumin, beta tubulin and mouse keratin. Since these cellular proteins are not mitochondria-specific, they were not further analyzed in the current study. Five protein spots that were additional on the 24-months age group 2D-Gels were identified to be QIL1; Heat-responsive protein 12; annexin A2; dimethglycine DH and citron-kinase K.

Compared to other age stages, 23 protein spot changes were observed only in the newborn sample, while 26 protein spots were absent in newborn state. Since these changes could reflect possible influence of pre- and post-natal switch, these 49 protein spots were excluded in our downstream analysis.

Specifically, inconsequence of visual gel evaluation and computer-aided gel evaluation was observed. According to protein quantification using ProteinWeaver software, seven protein spots that were evaluated visually as either with age-related decrease or increase profile showed fluctuating behavior inside certain age groups without detectable rules. These

seven proteins were not further analyzed in detail. Table 7 shows a summary result of protein spots that underwent mass spectrometric identification.

Tab.7: Identification results of protein spots that underwent MS-identification:

Category	Number of spots
Not identified	50
Cytosolic contamination	27
Additional protein spots in 24-months sample	5
Changes only in newborn	23
Absent in newborn	26
With fluctuating profile	7
Not statistical significance	25
Statistical significant	**10**

The concentration profile changes of the remaining 35 protein spots were taken to statistical test as described in chapter 4. Among these observations, alterations of only ten protein profile changes demonstrated statistical significance. Table 8 is a summary of proteins that demonstrated reproducibly quantitative and qualitative changes along with age ($p<0.05$ during the aging process). To access a general alteration profile during the whole time range, linear regression analysis was carried out to obtain the percent change per day respecting the protein concentration of newborn samples.

Tab.8: Proteins on mitochondrial 2D-gels that showed significant alteration among different age groups. The average change rates were determined by linear regression analysis:

Protein name	gi number	Change	
		in Brain [d^{-1}]	in Liver [d^{-1}]
NADH-ubiquinone oxidoreductase 13 kDa-A subunit	38075371	-0.429%	-0.028%
NADH-ubiquinone oxidoreductase 1 alpha subcomplex 5	13386100	-0.657%	ND
Cytochrome c oxidase, subunit Vb	6753500	-0.342%	-0.022%
Ubiquinol-cytochrome c reductase binding protein	133885726	ND	0.557%
ATP synthase, H+ transporting, mitochondrial F0 complex, subunit F	7949005	0.314%	ND
Mitochondrial ribosomal protein L12	22164792	ND	0.357%
10kDa Mitochondrial heat shock protein	6680309	-0.057%	-0.714%
Regucalcin	6677739	ND	-0.057%
Alpha-synuclein	6678047	0.071%	ND
Peroxiredoxin 1	6754976	ND	-0.014%

Note: Only proteins with statistically significant changes in different age groups were listed ($p<0.05$). Negative sign indicates decrease tendency. ND: not detected.

In the following chapters, the concentration profile of these ten proteins against age were graphically presented, that of brain and liver mitochondria were presented separately with different curves.

5.8.1 Alpha-synuclein increased with age in brain mitochondria

Alpha-synuclein, which represents itself as a prominent spot on the acidic side of brain mitochondrial 2D-gels (pI: 4.74, MW: 14kDa), was hardly detectable in the newborn group. However, the relative intensity of this protein spot increased significantly with age. Upon evaluating the protein spot of alpha-synuclein on the 2D-gels of brain total proteins, this protein was present during the whole time range on 2D-gels of brain total proteins. Less prominent increase tendency along with time was observed (fig.26).

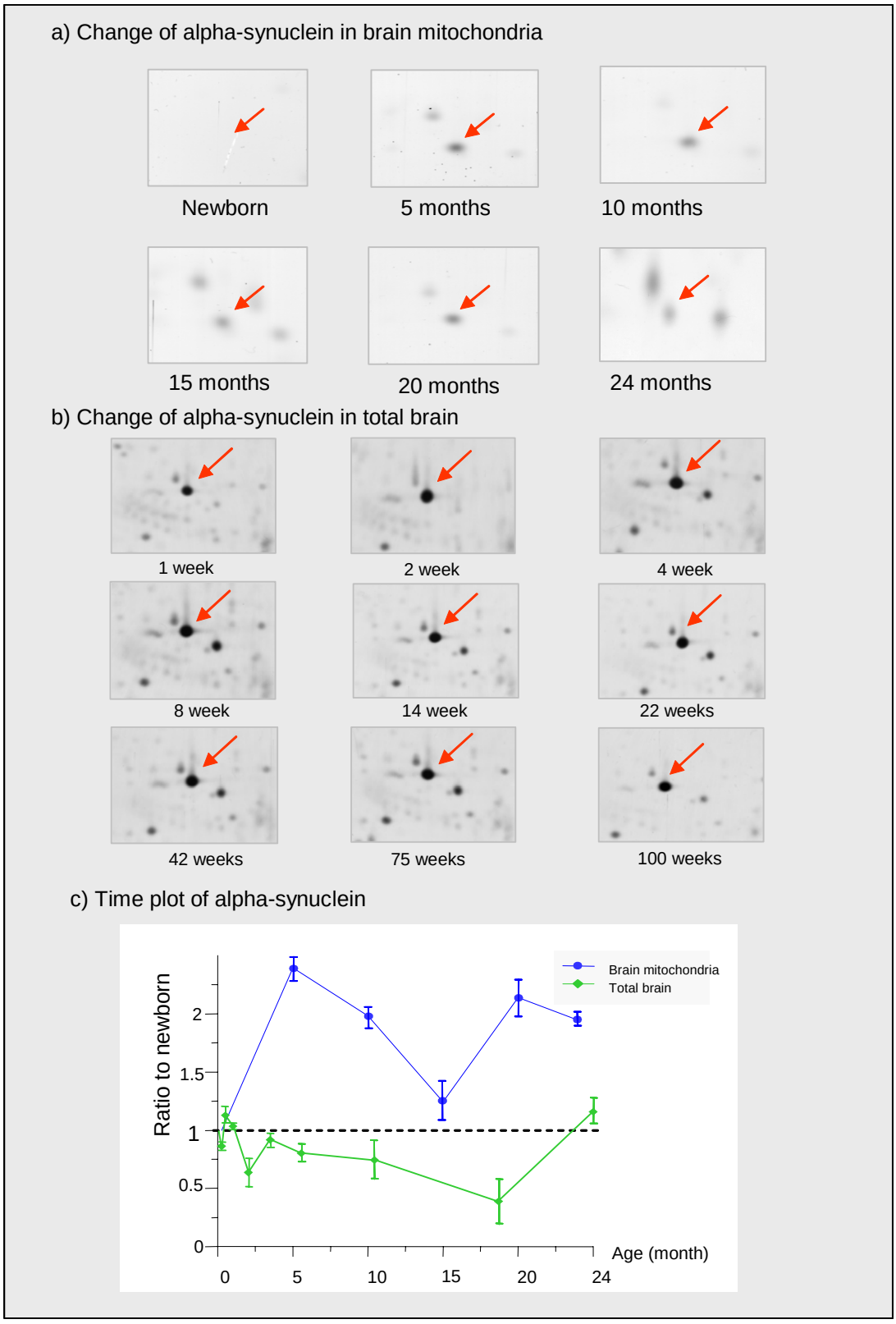

Fig.26: Time-dependent alpha-synuclein level in brain mitochondria compared with that of total brain. No significant difference of protein level was observed in brain total protein extract throughout the lifespan (new born to 100 weeks, b). On the contrary, there was a significant increase in mitochondria-associated alpha-synuclein level (a). The time-plot of synuclein is shown in c.

5.8.2 COX subunit Vb decreased with age

The relative intensity of COX subunit Vb (pI: 8.69, MW: 14kDa) in brain mitochondria was not changed significantly from newborn stage to 10-months stage. However, pronouced decrease was observed in the 15-months groupe. In liver mitochondria, the COX Vb level first showed an increase at 5-months group. The decrease tendency of relative intensity sustained until 24-months of age (fig.27).

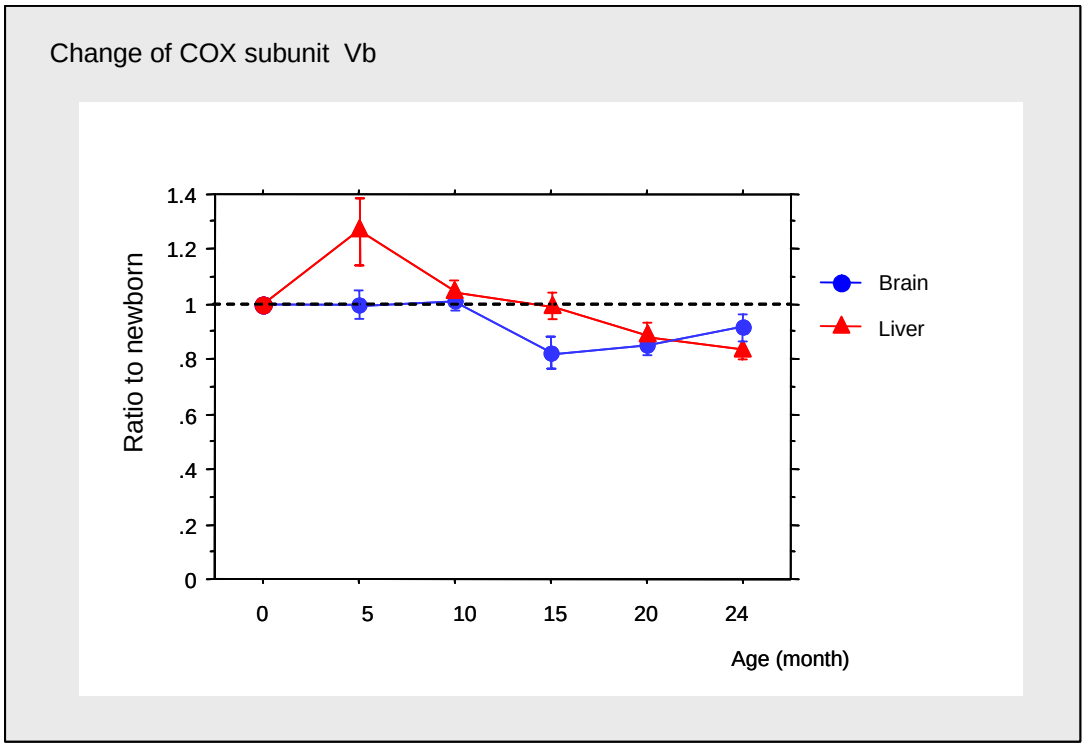

Fig.27: Time-dependent level change of cytochrome c oxidase subunit Vb protein spot on the 2D-gels. Shown are relative spot intensity ratios compared to that of newborn stage. A decrease tendency was observed in both brain and liver mitochondrial 2D-gels (a and b, respectively).

5.8.3 10kDa heat shock protein decreased with age

Spot intensity of the 10kDa mitochondrial heat shock protein (pI:7.93, MW: 11kDa) showed decreased profile in both brain and liver mitochondria throughout the time range measured in this study. The decrease was more pronounced in liver mitochondria (fig.28).

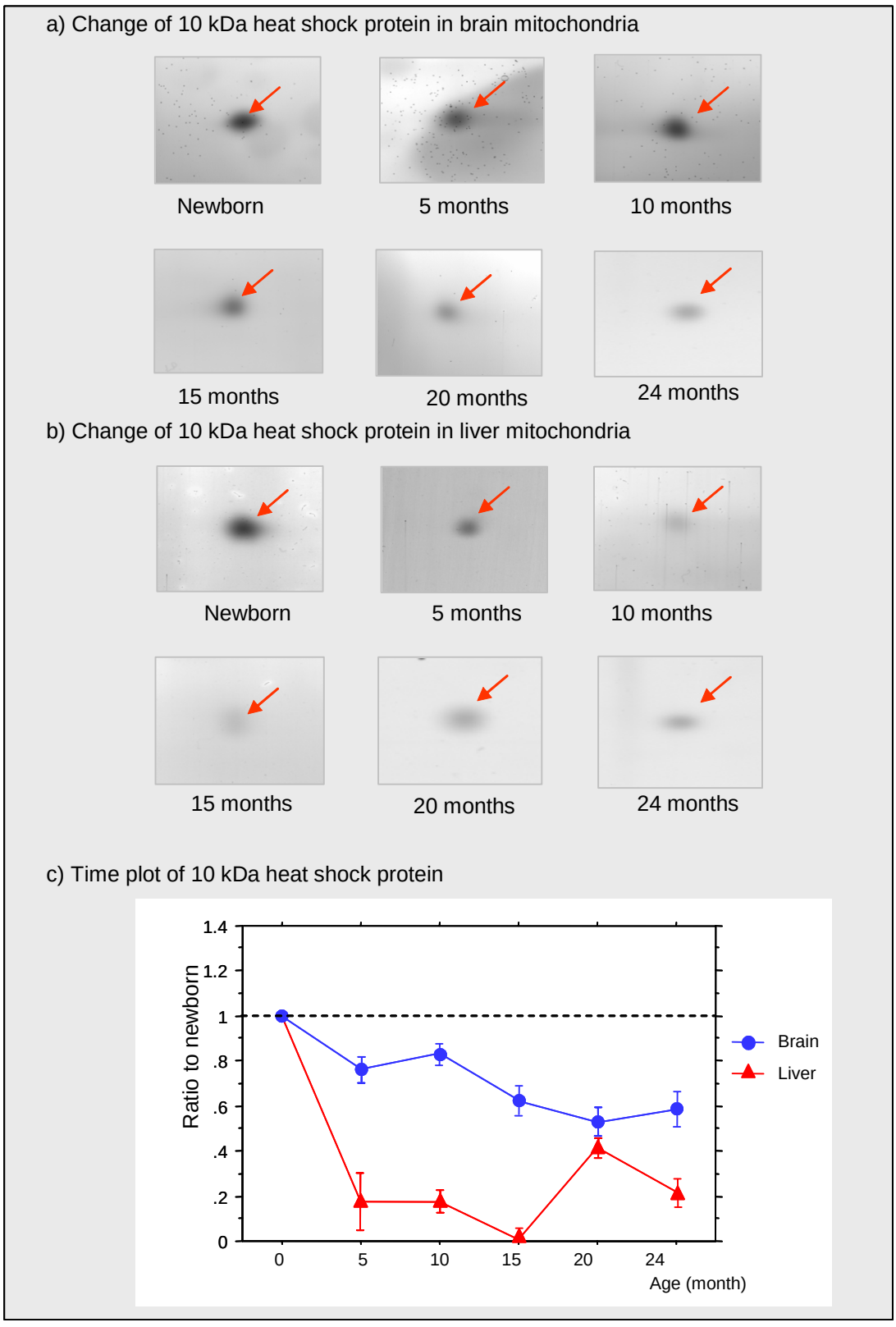

Fig.28: Two-dimensional gel image insets of mitochondrial 10 kDa heat shock protein in brain and liver mitochondria (a and b, respectively). The partial 2D-gel images are shown and the protein spot corresponding mitochondrial 10kDa heat shock protein were indicated with arrows (a: brain; b: liver). The corresponding time-plot is shown in c.

5.8.4 Two complex I subunits decreased with age

Two protein subunits of NADH-ubiquinone oxidoreductase were observed to decrease with age. The decrease tendency of NADH-ubiquinone oxidoreductase 13 kDa-A subunit (pI: 10.32, MW: 18kDa) was observed in both brain and liver mitochondria (fig.29), whereas the alteration of NADH-ubiquinone oxidoreductase 1 alpha subcomplex 5 (pI: 7.82, MW: 13kDa) was detected only in brain mitochondria (fig.30).

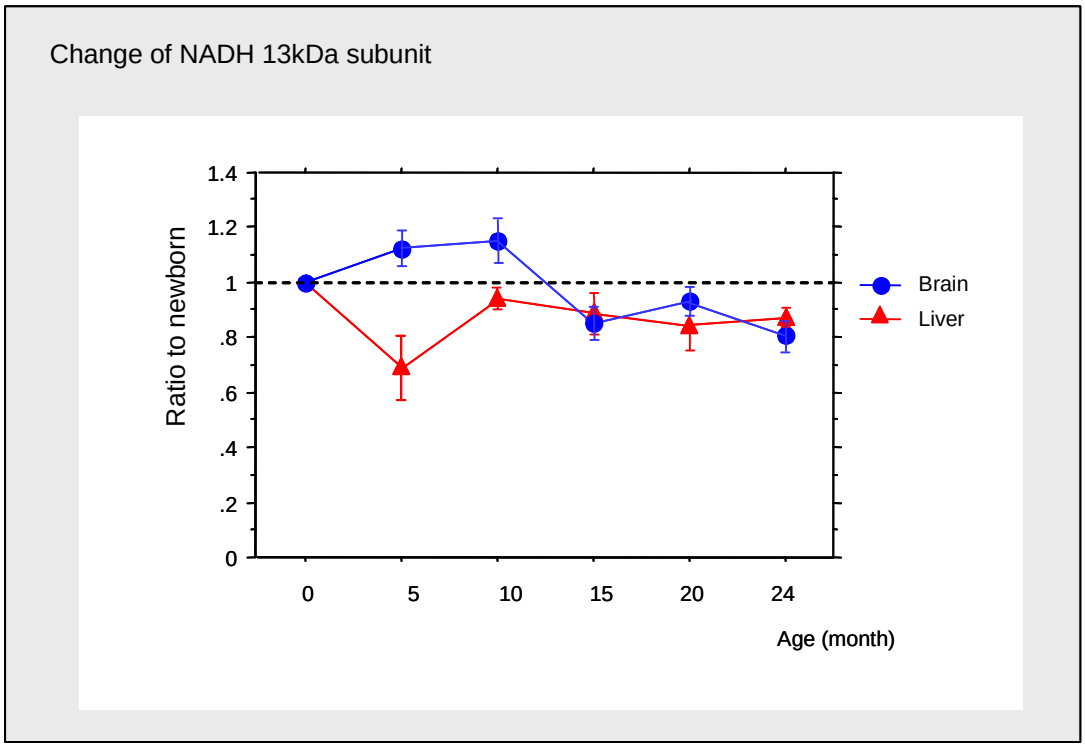

Fig.29: Time-dependent level change of NADH-ubiquinone oxidoreductase 13 kDa-A subunit in brain and liver mitochondria. Data were obtained through evaluation of 2D-electrophoresis gels of mouse brain and liver mitochondria of six different ages.

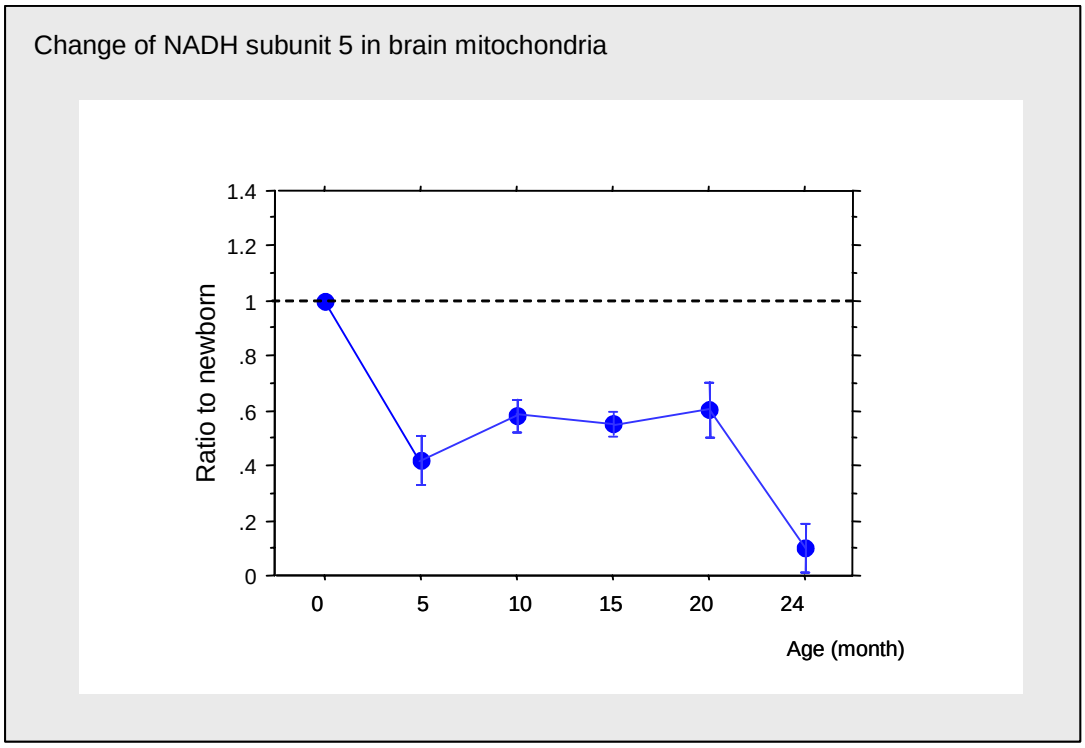

Fig.30: Time-dependent level change of NADH-ubiquinone oxidoreductase 1 alpha subcomplex 5 in brain mitochondria. Data were obtained through evaluation of 2D-electrophoresis gels of mouse brain mitochondria of six different ages.

5.8.5 Peroxiredoxin 1 decreased with age in liver mitochondria

On the basic side of the mitochondrial 2D-gel, a prominent decrease of protein spot was detected in the liver mitochondrial 2D-gels. This spot was identified to be peroxiredoxin 1 (pI: 8.26, MW: 22kDa, fig.31). Since peroxiredoxin 1 is an abundant antioxidant in cytoplasm, we performed protein-protein sequence alignment in order to verify the protein annotation result. Peroxiredoxin 1 could be aligned to two mitochondria-associated proteins with high similarity scores: substrate protein of mitochondrial ATP-dependent proteinase [bovine] (gi627764, score 260, 1e-68), and the putative mitochondrial peroxiredoxin (gi 16751316, score 245, 5e-64).

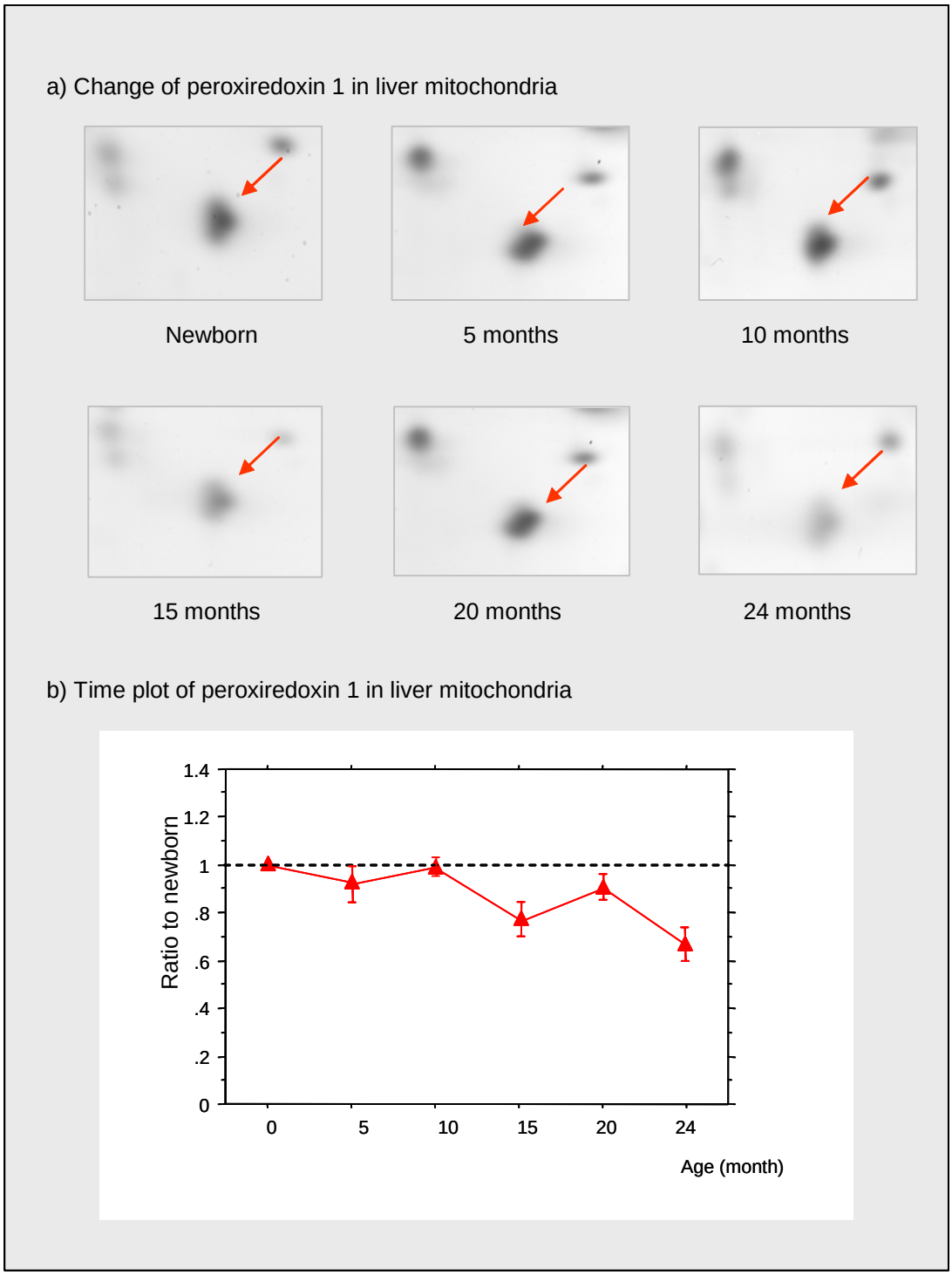

Fig.31: Two-dimensional gel images of peroxiredoxin 1 of liver mitochondria. The gels were prepared and protein spots were analyzed as described in experimental procedure. The partial 2D-gel images are shown and the corresponding protein spots were indicated with arrow. The corresponding time-plot is shown in sub-figure b.

5.8.6 Regucalcin decreased with age in liver mitochondria

Again on the 2D-gels of liver mitochondria, a significant decrease of regucalcin protein spot (pI: 5.15, MW: 33kDa) was observed (fig.32). The relative intensity of regucalcin dropped along with age. In the 24-months group, only 65% of the regucalcin amount was available compared to that of newborn group.

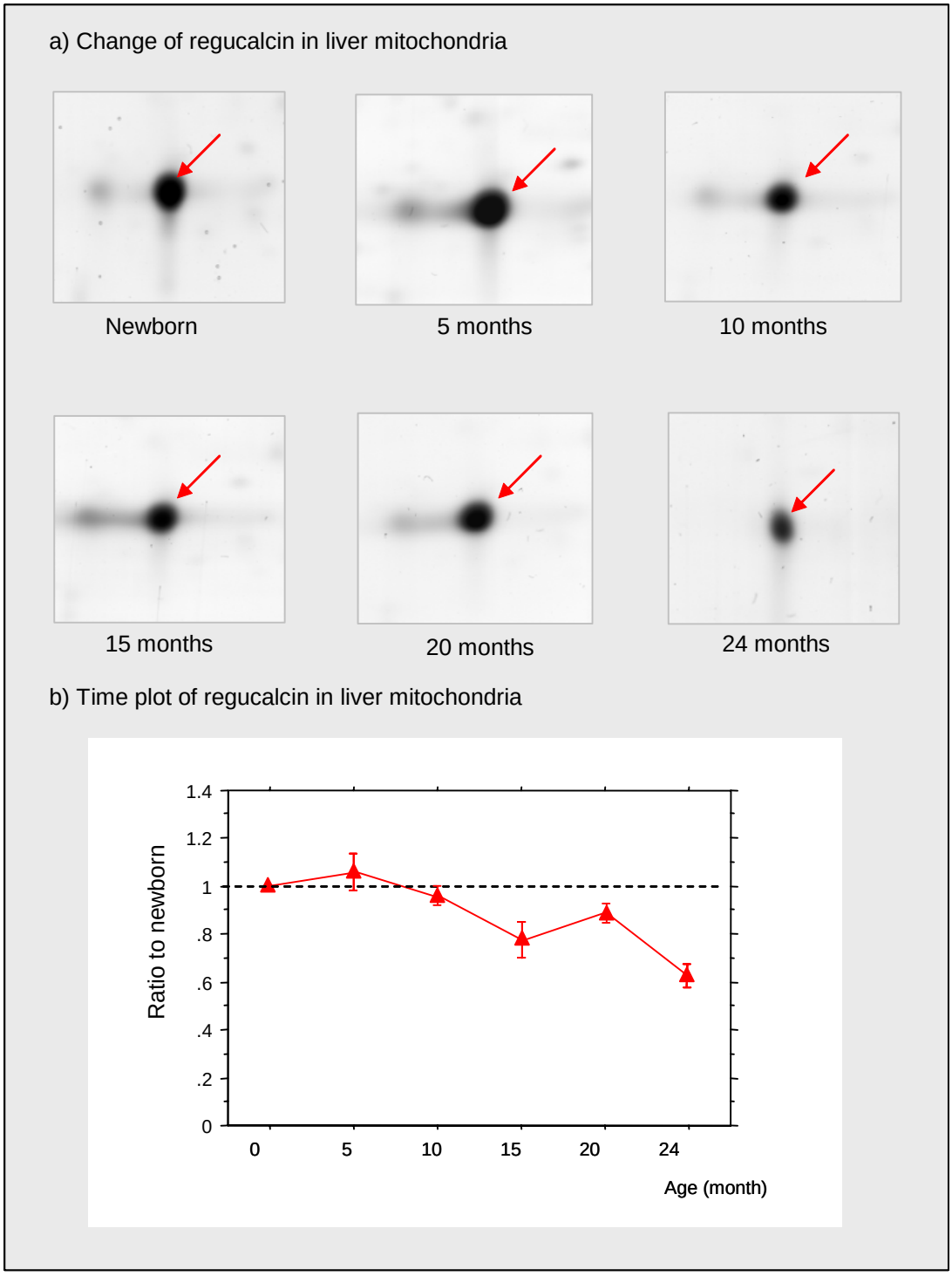

Fig. 32: Two-dimensional gel image insets of regucalcin protein spot in liver mitochondria (a). The protein spot corresponding to regucalcin were indicated with arrow. The time-plot of synuclein is shown in b.

5.8.7 Increase of a mitochondrial ribosomal protein in liver

Further rightward on the liver mitochondrial 2D-gels, increase of relative intensity of a protein spot was detected. This protein spot was identified to be a mitochondrial ribosomal

protein L12 (pI: 9.34, MW: 22kDa). The increase level was especially pronounced at the 20-months age group, which accounted for more than three times compared to the newborn age stage (fig.33). A significant decrease from 20-months to 24-months was followed.

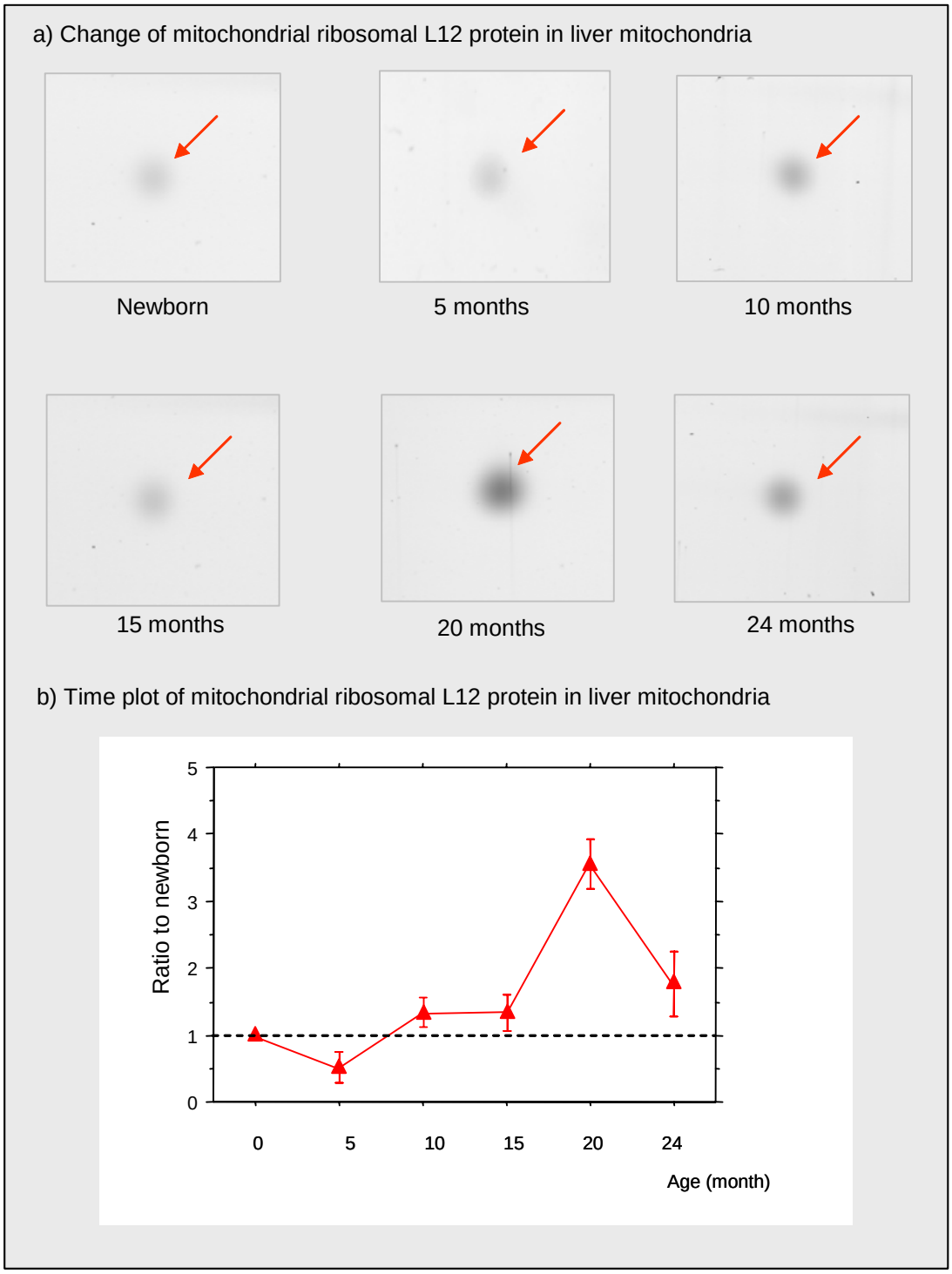

Fig.33: Two-dimensional gel images of mitochondrial ribosome L12 protein in liver mitochondria. The partial 2D-gel images are shown and the corresponding protein spots were indicated with arrow. The time-plot of this spot is shown in b.

5.8.8 Alteration of ubiquinol-cytochrome c reductase binding protein and ATP synthase subunit

On the liver mitochondria 2D-gels, one of the respiratory chain complex III subunit, the ubiquinol-cytochrome c reductase binding protein (pI: 9.1, MW: 14kDa) showed significant increase profile at 20-months age stage (fig.34a). In brain mitochondrial 2D-gels, the subunit F of ATP synthase F0 complex (pI: 9.36, MW: 12kDa) showed increased level at both 5-months and 20-months age groups (fig.34b).

a) Change of ubiquinol-cytochrome c reductase binding protein in liver mitochondria

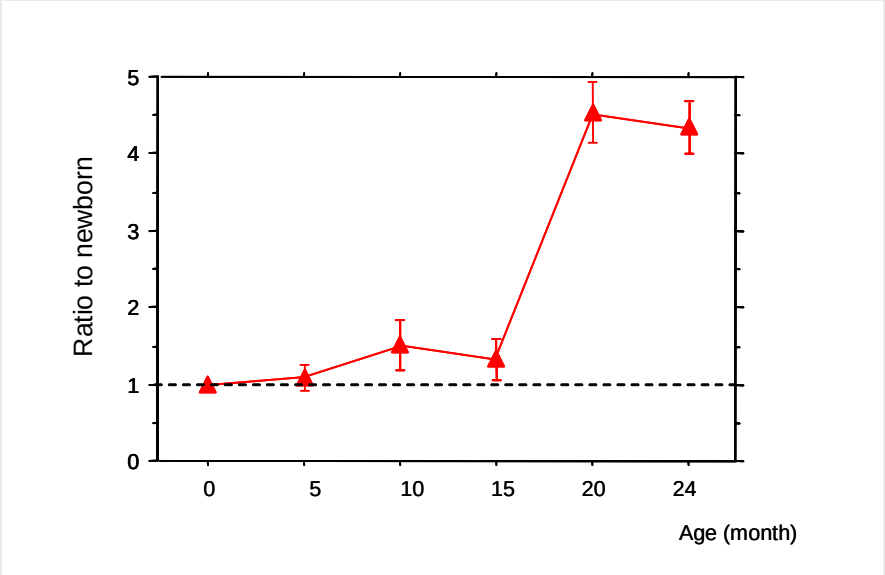

b) Change of ATP synthase F0 subunit F in brain mitochondria

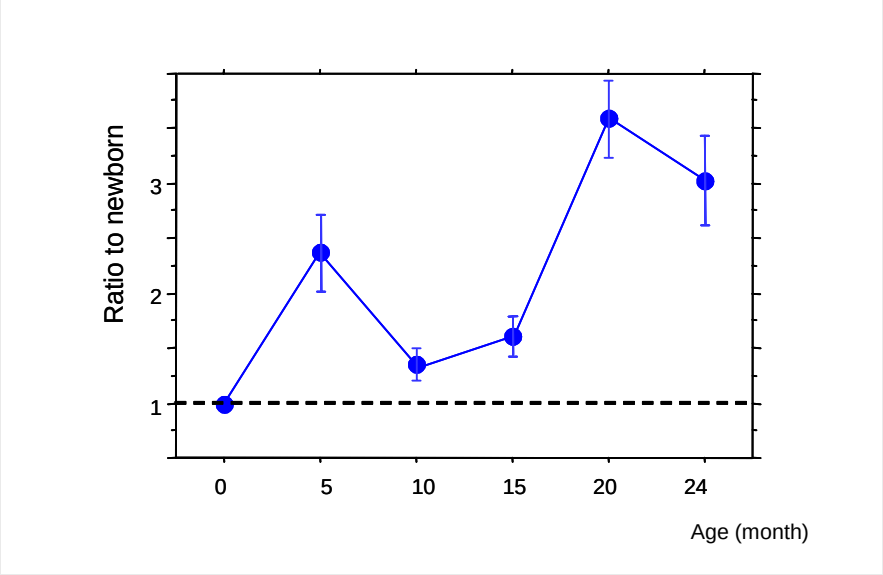

Fig.34: Time-dependent level change of ubiquinol-cytochrome c reductase binding protein in liver mitochondria (a) and ATP synthase F0 subunit F in brain mitochondria (b). Data were obtained through evaluation of 2D-electrophoresis gels of mouse brain and liver mitochondria of six different ages.

5.9 Result of Western immunoblotting

Using the Western immunoblotting method, we tested all three commercially available antibodies against mtDNA-encoded proteins: anti-human COX subunit I, II and III (Molecular Probes, Göttingen Germany). Among these three antibodies, only anti-COX I specifically cross-react with mouse mtDNA-encoded COX subunit I. The possible change of COX subunit I, a mtDNA encoded protein, was analysed using the TOM20 as an internal control for protein amount. The quantitative results are shown in figure 35.

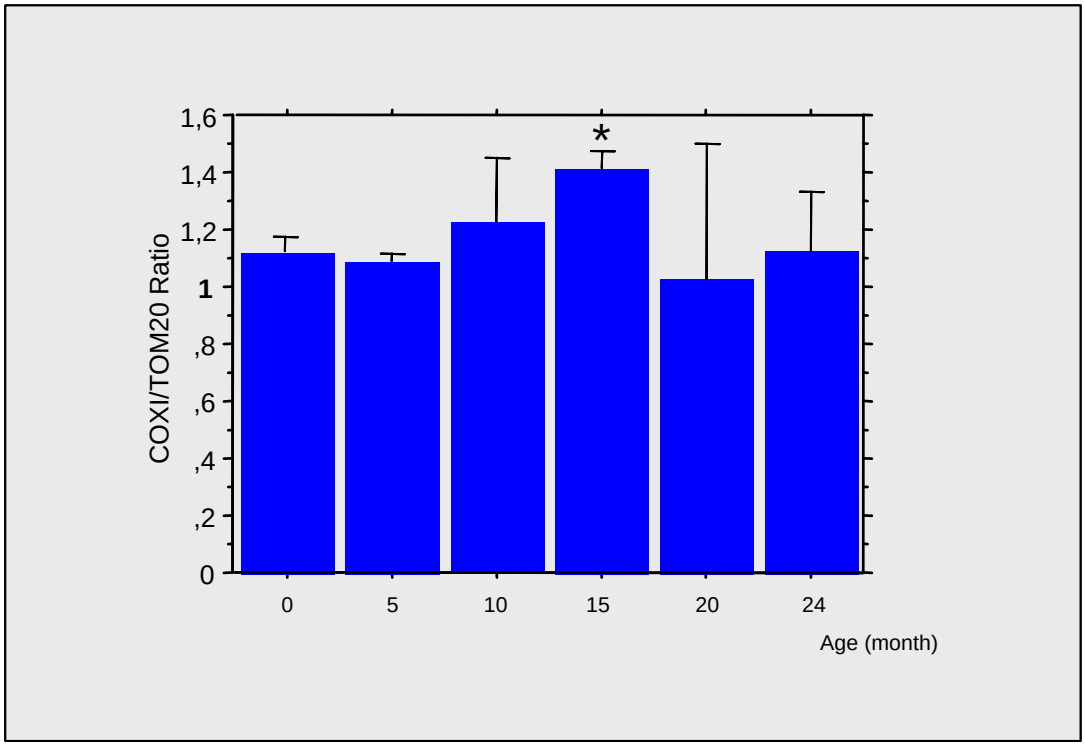

Fig.35: Immunoblotting analysis of the brain mitochondrial "Fraction III" (20μg) from pooled sample of different age groups. The anti-COX subunit I antibody recognized specifically the mtDNA-encoded COX I (57 kDa) protein in the mitochondrial inner membrane. Quantification was performed by reference to mitochondrial translocase of outer membrane TOM20. An asterisk showing the significant increase at 15-months ($p<0.05$).

As can be seen in fig.35, there was no significant change in COX I level among all aging stages except for 15-months stage. A pronounced increase at 15-months aging stage compared to other aging stages was observed. This was followed by a drop-back at 20-months group. This phenomenon was observed in Western immunoblots of both brain and liver mitochondria. This increase of COX I level at 15-months aging stage was shown to be significant comparing to other groups ($p<0.05$).

5.10 Preliminary result of Blue-native electrophoresis

In the last stage of this study, we explored the possibility of quantitatively study of further respiratory chain subunits in the frame of protein complex. For this purpose, we first estimated the mitochondria complexes with the help of a 100kDa molecular sieve using Blue-native electrophoresis analysis.

After the first dimension of Blue-native electrophoresis, proteins bands with molecular weights similar to those of complexes I, V, III and IV (complex I >910 kDa; complex V > 550 kDa; complex III 490 kDa; complex IV 204 kDa (Arnold et al., 1998; Ludwig et al., 1998)) were clearly visible on the stained gel slab (result not shown). After the second dimension separation using SDS-PAGE, protein subunits of different complexes were resolved into individual subunits (fig.36).

Over 34 protein spots were resolved on the mini-scale gel. Among these, 26 protein spots, corresponding to 37 proteins were successfully identified using MALDI-TOF mass spectrometry (tab.A2 in appendix). This suggests a complex protein mixture property of protein spots. At least 28 of the 37 identified proteins are known mitochondrial proteins. Among them, seven proteins were mitochondrial respiratory chain subunits, including one protein (COX subunit IV) that was a membrane protein containing two trans-membrane domains. Another calcium-binding protein calreticulin (with two trans-membrane domains) was also identified. However, no mtDNA-encoded protein was detected.

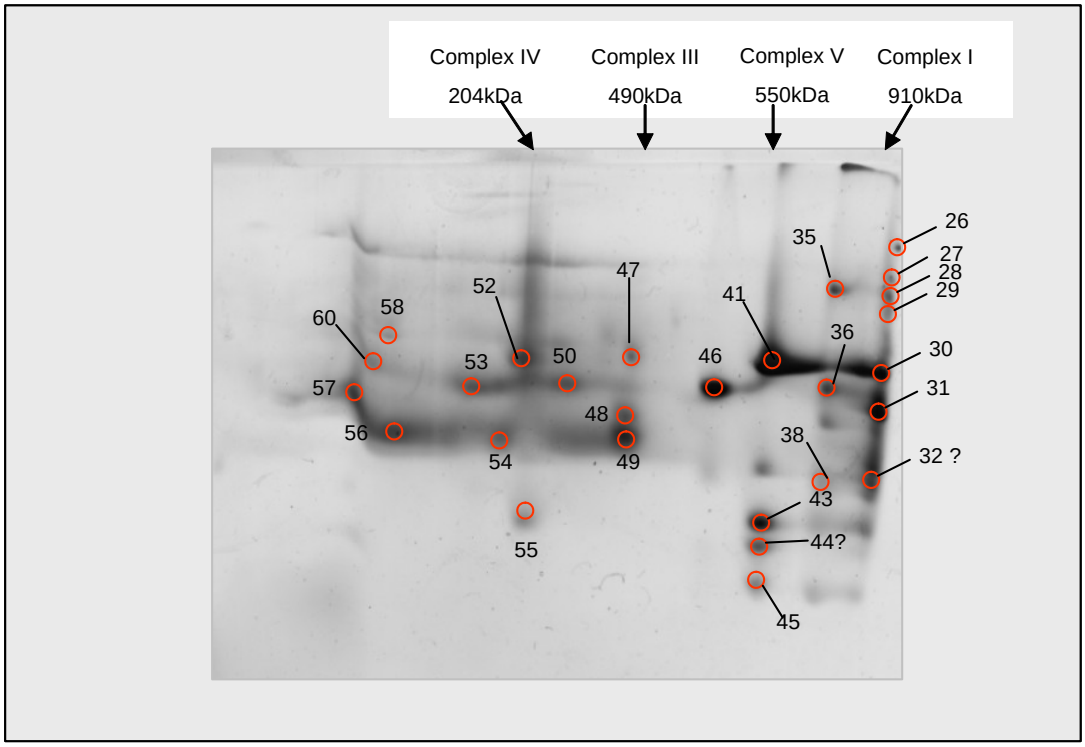

Fig.36: Two-dimensional Blue-native electrophoresis of the mitochondria fraction from mouse muscle mitochondria. Protein (1mg mitochondrial pellet as starting material) was separated in the first dimension by Blue-native electrophoresis and in the second dimension by SDS-PAGE as detailed in chapter 3.2.15. The protein spots were visualised using preparative silver staining. The position of complexes I, III, IV and V were indicated. The protein identification results of marked protein spots are shown in table A2.

5.11 Mathematical simulation and model fitting

We used a mathematical model that describes the relationship between the mtDNA mutation and the mitochondria population dynamics. This model was proposed whereby the rates of mitochondrial replication were under feedback control of the available mitochondria in the cell (Kowald and Kirkwood, 2000). Given initial values and standard parameters, the equations could be solved numerically for different variables against time (fig.37).

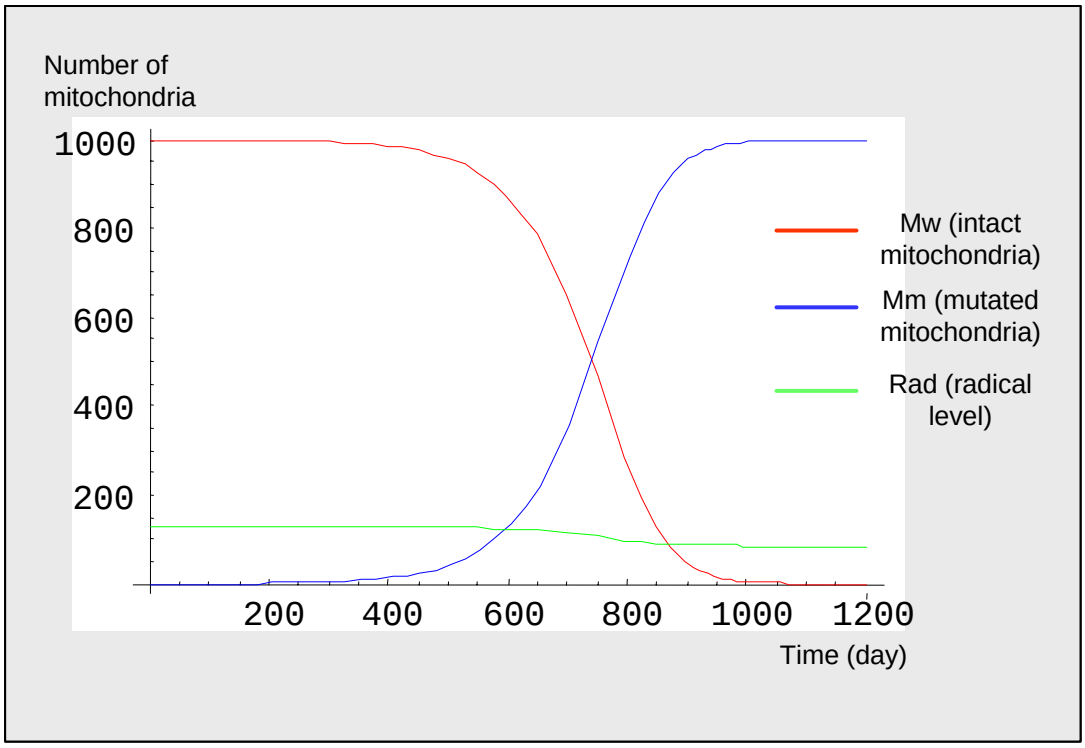

Fig.37: One example of a serious of mathematical simulation results of the model. The population of wild type mitochondria decrease with age, while the number of mutated mitochondria in a cell increase with age. Standard parameters described in table 1 and mutation rate value $k=1.2x10^{-8}$ per gene per day was used to produce these curves. Mw: number of intact mitochondria in a cell; Mm: number of mutated mitochondria in a cell; Rad: concentration of free radicals in the cell.

From the time-dependent curves of wild type mitochondria (Mw), mutated mitochondria (Mm) and free radical (Rad), an expected tendency of the decrease of wild type mitochondria and the accumulation of mutated mitochondria in a cell could be deduced. Varying the mutation rate value “k” from 10^{-3} to 10^{-12} per gene per day, the alteration velocity of intact mitochondria and defective mitochondria could be altered accordingly (fig.38).

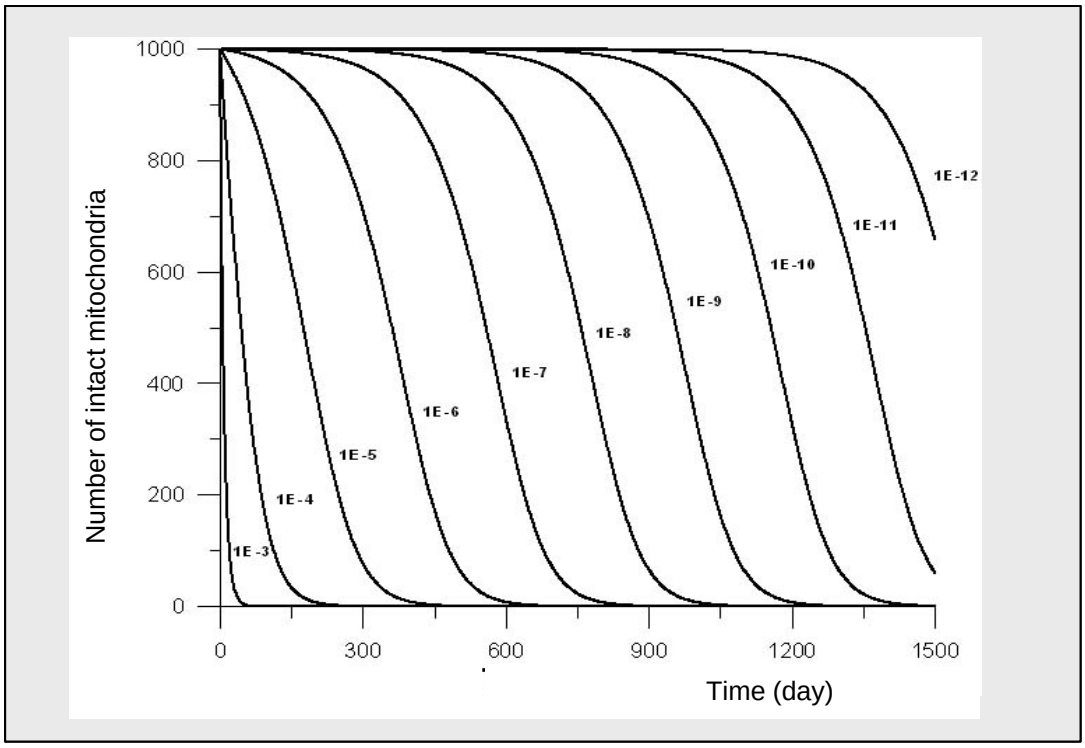

Fit.38: A summary of simulation results by varying the mutation rate "k" from 10^{-3} to 10^{-12} per gene per day. Only the number of intact mitochondria along with time is plotted on the diagram.

In the following table (tab.9), the experimental data are the average concentration ratios of NADH-ubiquinone oxidoreductase 13 kDa-A subunit, NADH-ubiquinone oxidoreductase 1 alpha subcomplex 5 and Cytochrome c oxidase, subunit Vb (see tab.8) in mouse brain and liver mitochondria. These data were obtained from 2D-electrophoresis experiments. As reference time point, the protein concentrations at newborn group were set as one. The values accounted alteration of -0.476% per day and -0.025% per day for mouse brain and liver mitochondria, respectively. In the same table, values calculated from the mathematical model were listed at the right side of the experimental data, with the mtDNA mutation rate at 1.2×10^{-8} per gene per day.

Holding the assumption that the experimental data and modeling data could be closely associated, we applied linear regression analysis to model the relationship between these two time-dependent variables.

Tab.9: Linear regression analysis of experimental data and values calculated from the mathematical model:

	Brain mitochondria		**Liver mitochondria**	
	Experimental data	**Modeling data**	**Experimental data**	**Modeling data**
Newborn	1.0	1.0	1.0	1.0
5-months	0.778 ± 0.104	0.998	0.981 ± 0.060	0.998
10-months	0.911 ± 0.113	0.994	0.995 ± 0.023	0.995
15-months	0.746 ± 0.070	0.973	0.942 ± 0.017	0.983
20-months	0.767 ± 0.064	0.860	0.859 ± 0.026	0.929
24-months	0.610 ± 0.072	0.546	0.854 ± 0.014	0.780
Linear regression analysis	r=0.76		r=0.83	
	p<0.1		p<0.05	
Alteration rate [per day]	-0.476%	-0.319%	-0.025%	-0.023%

After linear regression analysis using the least square model, the data set built from mtDNA mutation rate as $1.2x10^{-8}$ per gene per day gave the best fit (r=0.76, p<0.1 for brain mitochondria, or r=0.83, p<0.05 for liver mitochondria). To view this fit, the computed regression line was plotted, with the experimental data on the Y-axis and the simulation result on the X-axis (fig.39). As can be deduced from the figure, most of the data points were clustered around the regression line. Thus, the mtDNA mutation rate of mouse mitochondrial DNA was determined to be $1.2x10^{-8}$ per gene per day, which was the most suitable value according to our experimental data obtained from 2D-electrophoresis.

.

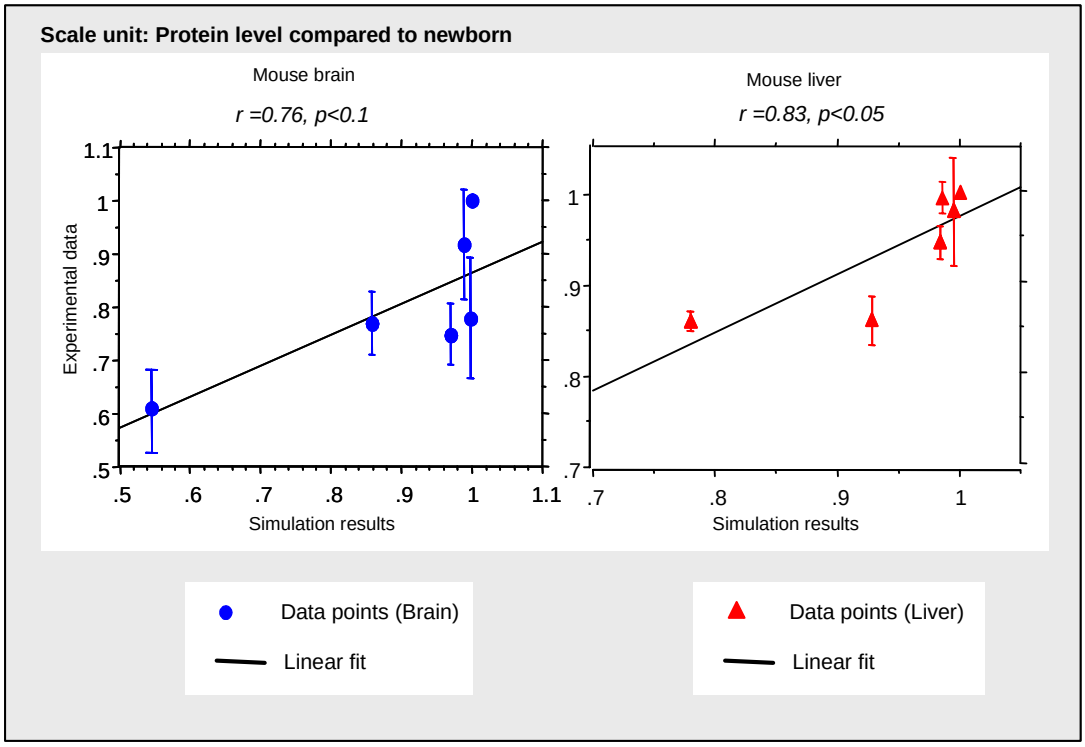

Fig.39: Linear fitting of experimental data gained from the 2D-electrophoresis and modeling result, which was calculated with standard parameter and mutation value of $1.2x10^{-8}$ per gene per day. As reference time points, the protein concentrations at newborn group were set as one.

6 Discussion

6.1 Investigation on mitochondrial theory of aging needs proteomic approaches

As more and more age-related degenerative disease being linked to mitochondrial pathology, mitochondria become viable pharmacological targets for the treatment of numerous diseases, as well as for the possible retardation of aging process (Grad et al., 2001; Morin et al., 2001). In order to develop reliable therapeutic intervention, the age-related mitochondrial change and its mechanism need to be investigated and understood at the first line.

The current study undertaken was for the purpose of getting an insight of the mitochondrial proteome change during the aging process. Driven by the hypothesis of mitochondrial theory of aging, the emphasis of this study was put on the possible effect of mitochondrial somatic mutations which could be responsible for some aspects of the aging process (Harman, 1972; Linnane et al., 1989).

6.2 Mouse has been proven to be pertinent model organism for aging study

For this purpose, we chose an inbred mouse strain as the model of human aging. Advantages of using mouse model include the similar genetic background of inbred strain, the ability to control precisely the developmental and aging stages, as well as the existence of large body of reference data. However, because the phylogenic lineages leading to the human being and the mouse are thought to have diverged about 90 million years ago (Copeland et al., 2002), we first strengthen to validate the mouse model.

Abundant references have verified the close correlation of cytochrome c oxidase activity deficiency in muscle fibre to the extent of mtDNA rearrangements in aged individuals (Brierley et al., 1998; Cooper et al., 1992; Trounce et al., 1989). To the best of our knowledge, however, no respective data on mouse exist.

Thus, we have chosen the histochemical staining of COX-activity on young and old mouse muscle tissue as our criterion of model validation (Sugiyama et al., 1993). As expected, we observed the prominent “mosaic pattern” on COX-stained old muscle tissue, similar to that been described for aged human muscle. This suggests that C57BL/6 strain mouse could be a pertinent model organism for human aging.

6.3 The choice of organs

As to organs of choice in this study, we chose both brain and liver tissues. The brain tissue consume about 20% of the total oxygen in the body (Wade and Bishop, 1962). The relatively high metabolic activity of brain and the low mitotic rate of neuron could possibly accelerate the free radical induced damages (Brierley et al., 1998).

Many age-related diseases affect brain tissue but not liver (Wallace, 1992). Respecting the mitochondrial aspect involved, it is of interest to investigate such tissue-specifity. Using both liver and brain tissues, we could be able to investigate the influence of mitotic rate on mitochondria mutation accumulation.

6.4 The choice of strategy

Characterization of proteins in whole tissues is sometimes difficult to accomplish particularly for low abundant proteins or hydrophobic proteins (Murayama et al., 2001). Sub-cellular fraction of mitochondria permits the isolation of our target organelles in pure form in order to perform relevant studies (Jung et al., 2000; Lopez et al., 2000; Xie, 2003).

In order to further increase sensitivity of our proteomic investigation, we combined sub-cellular fractionation to sub-fractionation of mitochondrial proteins, in order to reveal low abundant proteins, especially to enhance the capacity of membrane protein resolution.

In this study, a total of 116 novel spots or spots with enhanced intensity were present on the mitochondrial 2D-gels compared to 2D-gels of brain whole protein extract. This observation indicates that the sub-cellular fractionation procedure utilized in this study largely depleted the pure mitochondria fraction from other cellular proteins. The reduced spot pattern of mitochondrial gel also facilitated efficient gel evaluation procedure. This demonstrated that sub-cellular fractionation could intensify the low-abundant proteins and facilitate their easier detection and evaluation.

More importantly, the change of mitochondria-associated alpha synuclein that otherwise could have escaped identification demonstrated that the isolation of cell organelle brought us additional cellular location information. This sub-cellular fractionation technique would also be a strategy for the initial identification of previously unknown proteins and for their assignment to particular sub-cellular localization or interaction (Bell et al., 2001; Neubauer et al., 1998).

In the same line, pre-fractionation of proteins using sequential extraction strategy could enrich certain hydrophobic proteins, which were not pronounced in total cell lysates. The detection of seven membrane proteins in “Fraction II” demonstrated the effect of protein pre-fractionation strategy.

6.5 Mitochondrial isolation was successful

It is important for sub-proteomic studies to obtain intact cellular components, so that contamination of irrelevant proteins could be minimized and cellular localization information preserved. The electronic micrographs of isolated mitochondria in this study showed that isolated mitochondria were largely intact, with purity over 94%. The yields of mitochondria from brain and liver tissue were comparable to that of other authors (Fernandez-Vizarra et al., 2002; Jungblut and Klose, 1985). Probably due to the higher water-content of newborn tissue (Holland et al., 1986), the newborn mice materials gave lower mitochondrial yield compared to the remaining aging stages. On the other hand, the detection of 27 protein spots that representing cytosolic contamination showed that minimal cellular contaminations can be revealed by more sensitive analysis methods such like the 2D-electrophoresis analysis.

Comparing the mitochondria isolation from fresh and frozen materials, it was observed that the yield of mitochondria from frozen material was lower compared to that of fresh material, indicating the damage of mitochondrial membrane through freeze-thaw effect. This could have contributed to the possible contamination of 24-months mitochondria samples. On the other hand, the aspiration of only intact mitochondrial band after the gradient centrifugation enabled our investigation of non-damaged mitochondria in the down-stream analyses. The isolation of mitochondria from old organism has been described as difficult in previous literature (Frese and Stahl, 1992). However, this was not validated in our study respecting the quality of mitochondria isolated from young and old mouse tissue.

Notice, however, that there was a much smaller yield of mitochondria from brain tissue, as was also observed by other authors (Jungblut and Klose, 1985). This could be due to the small amount of starting material of brain tissue, as well as the special tissue structure of brain organ (personal communication with Dr. Wallace DC).

Nevertheless, for mouse brain tissue which has a mean weight of about 0.4g, an average amount of 1mg pure mitochondria could be obtained, which corresponds to 280μg total protein (Brown, 1991). This was sufficient for a large-gel 2D-electrophoresis analysis, which needs about 200μg of proteins. Taken together, the successful isolation of mitochondria of

sufficient yield in this study demonstrates that it is feasible to carry out sub-cellular fractionation for proteomic studies.

6.6 Protein fractionation was effective

The dynamic range of protein abundance within the cells has been estimated to be as high as 10^7 (Lopez and Melov, 2002). As approximately 90% of the total protein of a typical cell is made up of only 10% of the 10,000 to 20.000 abundant protein species (Miklos and Maleszka, 2001; Zuo et al., 2001), many low-abundance proteins may not be detectable by conventional methods. In such a complex protein mixture, pre-fractionation has shown be beneficial to facilitate the identification of low-abundant proteins (Lopez and Melov, 2002)

In this study, we have employed a sequential extraction strategy to increase the relative concentration of low abundant proteins in different fractions. Based on Klose (Klose, 1999), combined with different disciplinarians such as from Molloy (Molloy et al., 1999), we separated mitochondrial proteins into three fractions.

Since the capacity of protein solvation in a buffer system is not unlimited (Brown, 1991), the high representation of highly soluble proteins in the solution makes the solution of hydrophobic protein more difficult. Thus, we first applied Tris-buffer to extract most soluble proteins. This “Fraction I” obtained through Tris-buffer extraction contained mostly water-soluble proteins.

By pellet suspension in a buffer containing 0.1% Triton-X100, proteins of intermediate solubility could be released and collected as “Fraction II”. The use of Triton-X100 was borrowed by Villa (Villa et al., 1998), originally aimed at the isolation of a mitochondrial inner membrane protein with calcium transport activity. Combined with a nonionic detergent Triton-X100 in the isoelectric focusing separation (Stephenson et al., 1980), we detected seven membrane proteins with trans-membrane domain on the 2D-gels of “Fraction II”. This suggests that the sequential extraction strategy could be useful for the separation of mitochondrial membrane proteins.

Due to the presence of organic solutions, methanol-chloroform extraction was a selective method favouring hydrophobic proteins, with the aim that membrane protein could be extracted from the phospholipids bilayers (Molloy et al., 1999). Yerushima has described similar method to extract only highly hydrophobic membrane proteins from bacterial membrane (Yerushalmi et al., 1995).

The amount of protein in three different fractions showed that there is still a substantial part (17%) of proteins remained after Triton-buffer extraction (remained in the phospholipids). This justified the use of methanol-chloroform extraction. However, irreversible precipitation of hydrophobic proteins did happen during the resolvation procedure in this study, which resulted in insoluble pellet. This indicates that organic solvents does not provide good results for the resolution of membrane proteins (Kashino, 2003). Together, this sequential extraction protocol allowed us to increase the relative abundance of less soluble proteins, albeit to a limited extent.

6.7 Satisfactory result from 2D-PAGE analysis was obtained

Different proteomic approaches are suitable for different categories of proteins. The 2D-electrophoresis method developed by Klose and O'Farrel has been proved to be superiors for separating soluble proteins (Klose, 1975; O'Farrell, 1975). This method has been widely used for the investigation of the proteomic and genetic changes in a global way. In this study, large-gel 2D-electrophoresis method was successfully applied on "Fraction I" and "Fraction II" protein analysis.

In order to monitor technical variations of the 2D-electrophoresis method undertaken in this study, we controlled the reproducibility of 2D-gels in this study using same samples as well as the experimental samples.

Most of the protein spots achieved satisfactory quantitative reproducibility. This could be concluded through the following points: First, the presence or absence of the majority of spots of different gels was the same, indicating a stable resolution of the gels. Second, the relative positions of the spots were similar on different gels. Thirdly, the relative intensity of the majority of spots was similar on all gels. Theses three criteria could also be deduced from the high value of correlation coefficients.

Although gels from same sample beard higher correlation coefficients over the gels from experimental samples, the variation of all 2D-gels carried out in this study were well under 20%. This indicates that the gel-to-gel variation in our 2D-electrophoresis system was small enough to allow one to analyse changes in mitochondrial protein in the aging process (Chang et al., 2003). This constitutes a solid prerequisite for the subsequent gel image evaluation. Combined with multiple gel runs and appropriate statistical methods, we were able to identify differentially expressed spots at different age groups with statistical confidence.

On the other hand, it was noticed that many spots could not be matched automatically, although they show apparent counterpart property in manual comparison. This indicates that the current software for 2D-gel analysis was still not mature for the automatic gel image evaluations. Thus, manual gel evaluation was conducted before software quantifications in this study.

6.8 Gel image evaluation was successful

Quantitative and qualitative modifications can frequently be reflected on the protein spot pattern change in the 2D-electrophoresis system (O'Farrell, 1975). Electrophoretic mobility changes of proteins in the horizontal direction could be due to difference of amino acid substitutions involving change in charge (Klose et al., 2002), or different protein modifications, such as phosphorylation (Robinson and Pauling, 1974). The vertical shift could result from either molecular mass alterations or changes in protein conformation that affects the shape of the SDS-protein complex (de Jong et al., 1978; Klose et al., 2002). Different post-translational modifications of the same protein commonly lead to spot slitting patterns, which represent different isoforms.

According to these theoretical guidelines and previous experiences, numerous protein spot differences were successfully detected. The underlying cause for protein spot pattern variations may be somatic mutation in the structural gene, or in regulatory sequences (promoter, enhancer etc). Increase or decrease of cellular concentration of certain proteins may either be the result of a decreased synthesis or an increased degradation rate.

6.9 Protein identification was efficient

Protein identification is another factor largely influencing a proteomic study. Although MALDI-TOF-MS identification has been considered to be an effective high-throughput method, it has a certain signal capacity. If two or more proteins present in the same protein spots, the spectra from those overlapping protein peptide mixtures may confuse the database search and largely decrease the search score (Karty et al., 2002). Combined with the ESI Iontrap mass spectrometry which pre-fractionate the peptide mixture using reverse-phase HPLC, this disadvantage can be avoided.

In this study, a satisfactory 72% of the spots were identified, with an average of sequence coverage over 50%. This also validates the effectively of mass spectrometric protein identification and the usefulness of preparative silver staining.

Respecting proteins that were not successfully identified in this study, there are two major points of considerations: either the protein has not been annotated in the data bank, or the MS-spectra data were not accurate or comprehensive enough to distinguish between several entries in the database. If the database search is not fruitful, then further information would be required. This could be achieved by tandem MS experiments to determine the amino acid sequences of the individual proteolytic peptides contained in the digest mixture (Johnson and Biemann, 1987).

6.10 2D-electrophoresis combined with mass spectrometry is an efficient proteomic strategy

The 2D-electrophoresis analysis has undergone a long way of establishing period and is presently a relative matured method (Klose, 1975; O'Farrell, 1975). As an effective hypothesis-less method, large-gel 2D-electrophoresis facilitates the global proteomic comparison through gel evaluation.

Using differential proteomic analysis, it is possible to carry out classical perturbation analysis through the comparison of normal condition to stimulated condition, or the comparison of the time stages. Thus, this system is especially suitable for aging studies. Our data showed that the reproducibility of 2D-PAGE analysis is reliable enough that it can be used to detect protein level variation by demonstrating the qualitative and quantitative changes of protein spots (Klose et al., 2002).

Although the 2D-electrophoresis method is highly effective for soluble proteins, the under-representation of trans-membrane-proteins, especially integrate membrane proteins on the 2D-gel was a serious drawback of the method (Santoni et al., 2000). For this reason, we have applied other proteomic approaches such like Western immunoblotting and Blue-native electrophoresis in parallel.

6.11 Analysis of membrane proteins remains a problem

Big efforts have been paid in the modification of the 2D-electrophoresis method trying to improve the resolution of membrane proteins (Molloy, 2000). Based on previous literatures, we applied Triton-X100 in the isoelectric focusing gel (Stephenson et al., 1980). Including this modification on “Fraction II” proteins, seven membrane proteins were detected, which beard Gravy score ranging from 0.139 to -0.72, with one to two trans-membrane domains. The fact that these spots were available only on 2D-gel patterns of “Fraction II” proteins

suggests the beneficial effects of protein pre-fractionation procedure and/or the use of Triton-X100 in the electrophoresis system.

However, none of the protein identified in this study contained more than two trans-membrane domain, neither were we able to resolve more than one mtDNA-encoded proteins using this system. This indicates that 2D-electrophoresis method is still not powerful enough for the analysis of highly hydrophobic integral membrane proteins, as also been shown by previous studies (Santoni et al., 1999).

The loss of hydrophobic proteins probably occurs during the whole experimental process. It is believed to be due to unable to extract the proteins from membrane double layers; unable to solve these proteins into the solution; and protein precipitation during the transfer from first to second dimension (Adessi et al., 1997; Gygi et al., 2000).

6.12 Mitochondrial protein profile change during the aging process

Respecting our initial goal of accessing age-related changes in mitochondrial proteome, we discuss in the following the ten proteins that were observed to change significantly during the aging process.

6.12.1 Down-regulation of complex I and complex IV subunits indicates mtDNA mutation

In the current study, two nuclear-DNA-encoded subunits of complex I (NADH-ubiquinone oxidoreductase 13 kDa-A subunit and NADH-ubiquinone oxidoreductase 1 alpha subcomplex 5) and one subunit of complex IV (COX Vb in brain) were observed to down regulate during the aging process. As has been suggested by Remacle, this could indicate deficiency of respiratory chain complex subunits induced by abnormalities of mitochondrial DNA (Remacle et al., 2004). A decreased representation of mtDNA-encoded complex I and complex IV subunits could in turn lead to a reduced requirement of other subunits for the protein complex assembly. Nevertheless, other influences such as possible nuclear DNA mutation or post-translational modification are not to be excluded.

Previous works on human material showed that most mtDNA deletions ablate the region between the genes encoding ATP8 and cytochrome b, which codes predominantly for subunits of complex I and complex IV subunit (Cortopassi and Wong, 1999; Vu et al., 2000) (see fig.1). This could imply that complex I and complex IV are the most affected protein complexes through mtDNA mutation. Here we showed that similar phenomenon could also be observed on mouse model at protein level.

In a concert, Bowling showed that there was an age-associated progressive impairment of complex I (over 22% by 80 years) and complex IV activity (Bowling et al., 1993; Yen et al., 1991). Cooper reported activity decrease of complex I (59%) and complex IV (47%) comparing donor groups of 20-30 and 60-90 years (Cooper et al., 1992). In the current study, we observed significant COX-activity deficiency in part of the old mouse myocytes. Together with our current result, these indicate that such activity decrease of complex I and complex IV could be directly linked to the protein steady state concentration decrease.

6.12.2 Increase of complex III and complex V subunits suggest feedback regulation

In a chain of enzyme reaction, if the activity of an up-stream (complex I) enzyme changes, then all of the down-stream metabolite pools and enzyme activities could be altered (Stryer, 1995). As the cell responds to the decrease of complex I and complex IV functionality, increased synthesis of protein of down-stream enzyme complexes in the respiratory chain would soon follow, intending to maintain the required functional levels of the whole respiratory chain.

Two nuclear-encoded proteins localized in the down-stream of respiratory chain reaction, ubiquinol-cytochrome-c binding protein (complex III subunit in liver mitochondria) and ATP F0 (complex V subunit in brain mitochondria) were observed to increase with age. This indicates such a negative feedback mechanism, which is common in metabolic pathway control.

6.12.3 MtDNA-encoded COX subunit I showed only moderate change

In order to verify the proposed decrease of nuclear-DNA-encoded respiratory chain subunits due to mtDNA mutation, it was our interest to investigate the possible alteration of mtDNA-encoded subunits. As a hypothesis-driven investigation, we employed Western immunoblotting to probe the concentration change of an mtDNA-encoded complex IV subunit, COX I, in brain and liver mitochondria.

Interestingly, only a transient up-regulation of COX subunit I at 15-months age group was significant in the WB analysis, the concentration of COX I dropped back to average level at 20-months aging stage. This result did not support our hypothesis. However, as can be deduced from figure 1, COX I is not inside the most deleted region on the mtDNA molecule.

In effect, several authors described that mtDNA encoded COX I and COX II (but not COX III) present at elevated levels in Alzheimer disease patients compared to normal control individual (Hirano et al., 1997; Wallace, 1997). This could indicate enhanced protein

synthesis in the mitochondrial matrix as a response to mtDNA mutation. In this respect, our observation of the up-regulation of mitochondrial ribosomal protein L12 could be considered as such compensatory attempt to enhance the mitochondrial protein expression due to decreased mitochondrial respiratory chain function.

On the other hand, it need be noticed that decrease of protein concentration at 15-months age group is a seldom case in the range of our experimental results. Several other proteins showed also specific lower protein concentration at 15-months age group. This could suggest possible systematic error.

6.12.4 Decrease of a mitochondrial heat-shock protein could suggest the increased consumption of heat shock protein

Respecting the respiratory chain complex I deficiency in old age, Bandy hypothesized that the mitochondrial genome damage would increase the steady-state concentration of reduced intermediate of the respiratory chain, leading to formation of more free radicals through their auto-oxidation (Bandy and Davison, 1990).

Heat-shock responses are a fundamental and widespread type of cellular defense against environmental stress (Hansen et al., 2003). The down-regulation of mitochondrial heat shock protein in both brain and liver mitochondria could be linked to the increased consumption of heat shock proteins. This in turn suggests that mitochondria in aged individual may not be able to deal with oxidative stress in a sufficient scale. Similar results were also reported by other authors (Zabel et al., 2002).

6.12.5 Down-regulation of peroxiredoxin suggest elevated oxidative stress in aged individual

Peroxiredoxins are enzymes catalyzing the destruction of peroxides. The decrease of peroxiredoxin level was commonly discussed as increased oxidation or aggregation of these proteins due to enhanced oxidative stress (Rabilloud et al., 2002). The down-regulation of peroxiredoxin 1 was also observed in this present study. However, so far, no indication of mitochondria-association of peroxiredoxin 1 has been reported.

Because peroxiredoxin is an abundant antioxidant in the cell, we cannot exclude the possibility of contamination of cytoplasmic proteins. Upon performing protein-protein sequence alignment, peroxiredoxin 1 could be aligned to two mitochondria-associated proteins with high similarity scores. We speculate that we could have observed the decrease of certain mitochondria-specific peroxiredoxin, or the protein detected could be a substrate of mitochondria-associated proteinase. More detailed studies in this respect would be obligatory before further discussion.

Several proteins that had previously been located to other cellular compartments were found in yeast or human heart mitochondria (Sickmann et al., 2003; Taylor et al., 2002). This suggests that such proteins may be specifically associated with mitochondria. They could be linked to the mitochondria though either binding to the outer membrane of mitochondria (beta actin), or transport material to the mitochondria. It is not clear how closely these proteins are associated *in vivo* and whether the connection is biologically relevant.

6.12.6 Down-regulation of regucalcin in liver mitochondria indicates a lowered buffering capacity of calcium

In our 2D-electrophoresis analysis of "Fraction I" proteins, we have observed that a calcium-binding protein regucalcin decreased significantly with age in the liver mitochondria. Interestingly, regucalcin, also called senescent marker protein 30 (SMP30), has been intensively investigated since 1992, when it was first identified as an androgen-independent marker protein that is down-regulated during the aging process (Fujita et al., 1998; Fujita et al., 1992). The amount of regucalcin in aged rat liver decreased to 40% of that in adult rat liver (Fujita et al., 1998). In the current study, a similar decrease range of 42% was observed comparing the regucalcin level in mouse liver mitochondria of 5-months group to that of 24-months group.

This decrease of regucalcin was observed only in liver mitochondria, not in brain. This is probably due to the much lower normal concentration of regucalcin in brain compared to liver (Yamaguchi and Isogai, 1993). Andreyev and Fiskum reported that brain and liver possess different mechanism for the calcium induced cytochrome c release (Andreyev and Fiskum, 1999). The treatment of Ca^{2+} induced the mitochondrial membrane permeability transition (MPT) in liver but not in brain. They suggested that the membrane permeability transition is responsible for liver cytochrome c release, while certain MPT-independent mechanism is responsible for the release of cytochrome c from brain mitochondria.

As a second messenger for the common signal transduction elements in a cell, intracellular calcium is a key player in regulation of various cellular functions such as proliferation, differentiation and adhesion (Stryer, 1995). Prolonged elevation of calcium has been suggested to induce apoptosis by stimulating Ca^{2+} Ma^{2+} dependent endonucleases (Kaiser and Edelman, 1977). A low cytoplasmic Ca^{2+} concentration of living cells is maintained by energy-requiring pumps. Theses pumps either remove calcium to the extra-cellular space by transporting it across the plasma membrane or accumulate it inside intracellular

organelles such as the mitochondria and endoplasmic reticulum (Carafoli and Zurini, 1982; van Os, 1987).

Regucalcin has been shown to enhances ATP-dependent calcium pump enzyme activity in both plasma membrane and isolated mitochondria (Takahashi and Yamaguchi, 2000; Xue et al., 2000). Ishigami found that hepatocytes from regucalcin-knock-out mouse were highly susceptible to tumour necrosis factor-alpha- and Fas-mediated apoptosis (Ishigami et al., 2002). The specific binding of regucalcin on a glycoprotein located on the mitochondrial outer membrane has been verified by Panfili (Panfili et al., 1980).

Based on the pure fraction of isolated mitochondria utilized in our proteomic study, we reason that we have measured the change of mitochondria-associated regucalcin concentration (Fountoulakis and Schlaeger, 2003). This could suggest that less amount of regucalcin is bound on liver mitochondrial outer membrane in the aged stages.

Recently, Ishigami A (2004) reported that regucalcin-deficient mice accumulate lipid droplets in liver, while the liver mitochondria were abnormally enlarged. This could suggest that regucalcin-deficiency profoundly affect mitochondrial function or transport of metabolite into mitochondria (which could be ion-dependent).

Taken together, down-regulation of mitochondria-associated regucalcin could be associated with alterations in the mitochondrial buffering capacity of Ca^{2+} and calcium signalling in the aged. However, whether this is a up-stream or down-stream event of mitochondrial dysfunction during aging is still unknown. Further analysis would be required to investigate the detailed mechanism.

6.12.7 Up-regulation of alpha-synuclein in brain mitochondria resembles neuronal degenerative diseases

Another interesting finding using the 2D-electrophoresis is the significant increase of alpha-synuclein level in the brain mitochondrial proteins during the aging process. This finding raised our interest because alpha-synuclein gives also a prominent spot on the 2D-gel pattern of brain total protein extract. Less prominent increase tendency was observed upon comparing the 2D-gels of whole brain proteins in different aging stages (1 week to 25-months, courtesy to Mrs. Herrmann). The differentially pronounced pattern of the same protein on mitochondrial 2D-gels indicates that we have observed the increase of mitochondria-associated alpha-synucleins.

Alpha-synuclein is predominantly a neuron-specific presynaptic protein (Hsu et al., 1998). Among others, it has the function of protecting against oxidative stress via interaction with the stress-signalling pathway in neuronal cells (Hashimoto et al., 2002). Since the identification of alpha-synuclein as a prominent protein component in the aggregates of amyloid bodies (Goedert, 1997; Ueda et al., 1993), it has been intensively studied in the fibrogenesis processes of brain tissue.

The relation of alpha-synuclein to mitochondria first drew attention when it was noticed that MPTP, a toxin specifically inhibiting respiratory chain complex I, was depleted completely of its toxicity in alpha-synuclein knock-out mice (Dauer et al., 2002; Kuhn et al., 2003). Focusing on the role of mitochondria in the neuronal fibrogenesis procedure, Perrin and Dawson & Dawson observed that alpha-synuclein is specifically associated with membrane compartments in cultured cells and brain tissue through interactions with acidic head groups of phospholipids (Dawson and Dawson, 2003; Perrin et al., 2001).

Lately, Song links over-expression of alpha-synuclein to mitochondrial dysfunction *in vivo* (Song et al., 2004). Their morphological study showed that alpha-synuclein-treated mice had significantly greater mitochondrial abnormalities than either saline-treated controls or MPTP-treated wild-types. Hence, they speculated that mitochondria play a role in early stage of neuronal fibrogenesis that could be induced by alpha-synuclein-related protein aggregation.

Our current study showed that the increased level of mitochondria-associated alpha-synuclein could be a common phenomenon in the normal aging process. The translocation of increasing amount of alpha-synuclein proteins to the mitochondrial membrane with time might play an important role in either triggering or perpetuating age-related neuronal fibrogenesis. Our observation thus links the mechanism of aging closer to that of neuronal degenerative disease.

Integrating other observations of this current study, we take one step ahead to speculate that Complex I function deficiency in old age is probably up-stream to aggregation of alpha-synuclein in the aging process. Deficiency of complex I induced by mtDNA mutation could create an elevated oxidative stress that ultimately leads to aggregation of alpha-synuclein and the neuronal apoptosis.

6.12.8 Difference between brain and liver respecting mitochondrial aspect of aging

In this study, the change of NADH-ubiquinone oxidoreductase 13 kDa-A subunit, COXVb and 10kDa heat shock protein were observed in both brain and liver mitochondria, while the change of other proteins were observed in either liver or brain (see tab.8). These observation could suggest tissue-specifity.

The decrease rate of 10kDa mitochondrial heat shock protein was more pronounced in liver than in brain mitochondria. This could be related to the higher metabolic rate of liver tissue compared to brain, which lead to a higher production of reactive oxygen species.

The average decrease rate of both NADH-ubiquinone oxidoreductase 13 kDa-A subunit and COX Vb in brain were higher than that of in liver. The decrease of NADH-ubiquinone oxidoreductase 1 alpha subcomplex 5 was observed in brain tissue only. Taken together, brain mitochondria showed higher decrease rate of protein steady state concentration in both complex I and complex IV subunit. This could indicate that brain is more susceptible to the secondary loss of nuclear DNA encoded complex I and IV protein subunits.

Another phenomenon observed in this study is that the feedback mechanism functions more efficient in liver mitochondria than in brain mitochondria in the respect of protein synthesis machinery. This could be deduced from the following observation: First, there was an increase of mitochondrial ribosomal protein in liver mitochondria, but not in brain; Second, at the presence of complex I deficiency, the up-regulation of complex III subunit was observed in liver mitochondria, while the up-regulation of more down-stream complex V was observed in brain tissue. This could suggest that liver has higher capacity of feedback regulation compared to brain tissue. This less efficient feedback mechanism of brain mitochondria could further contribute to its higher vulnerability.

One possible explanation for the phenomenon mention above could be the influence of mitotic rate. Brain has much lower mitotic rate, which means a reduced rate of mitochondrial renewal. While the liver with higher mitotic rate is able to dilute mutated mitochondria more effectively (Kowald and Kirkwood, 2000).

Respecting the tissue-specific protein profile changes of regucalcin and alpha-synuclein observed in this study, it could be deduced that brain is more susceptible to cellular fibrogenesis, while liver more vulnerable to abnormal calcium buffering.

Brown suggested that the cellular protein concentrations are generally close to the maximum solubility in cells (Brown, 1991). The extraordinary complex cellular structure of brain tissue could mean a frequent violation to the maximal protein concentration. This in turn gives a high susceptibility of brain cells to protein aggregation.

As the central processing field of cellular metabolism, liver cells have been designed against this fault, since the majority of the metabolic functions require ion-formed macromolecules (Stryer, 1995). However, large amount of ions in the cell could means a high ionic strength, which in turn makes the hepatocytes vulnerable for ion management.

Another difference of brain and liver observed in this study is the finding that old-aged mouse brain tissues (20-months and 24-months stage), but not old-aged mouse liver tissue gave significant smaller yield of mitochondria compared to their young counterparts (all other aging stages). Notice that only intact mitochondria with density between 1.09 and 1.13 g/ml could be focussed during the continuous gradient purification method. Damaged mitochondria migrate to other density layer as diffused material. Thus, the possibility remains that the defective mitochondria were not isolated in our sub-cellular fractionation since they bear densities other than that of intact mitochondria.

Based on this reasoning, we speculate that there could be less amount of intact mitochondria in old brain tissue, due to increased representation of defective mitochondria. If this should be the case, its influence should be considered seriously upon interpreting the result of down-stream proteomic analysis.

6.13 Potential of Blue-native electrophoresis analysis

Valuable results have been gained from the 2D-electrophoresis analysis in this study. However, only one mtDNA-encoded subunit has been identified so far. This is largely due to the highly hydrophobic properties of the mtDNA-encoded proteins, that could precipitate at the basic pole during IEF (Hanson et al., 2001; Lopez et al., 2000; Santoni et al., 2000). Although Western immunoblotting remains an effective hypothesis-driven alternative against specific protein targets, the scarity of commercially available antibody against mtDNA-encoded protein stronly obstacate this efforts.

Confronting this serious shortness, we employed Blue-native electrophoresis method as an additional strategy to investigate mitochondrial proteins in the frame of intact protein complex. Another potential advantage of Blue-native electrophoresis is that functional

information regarding protein interactions within the complex could be retained due to the non-denaturing conditions of the first dimension electrophoresis system.

In the preliminary experiment of Blue-native electrophoresis, we were able to resolve four mitochondrial respiratory chain complexes at the first dimension. Only the Complex II, which is the smallest respiratory complex (130 kDa), eluded detection after preparative silver staining. An additional subunit of respiratory chain Complex IV containing two trans-membrane domains was also resolved. This demonstrates the potential usefulness of Blue-native electrophoresis as an additional strategy in further studies focusing on the alteration of mitochondrial respiratory chain proteins. The detection of another calcium binding protein on the Blue-native gel could suggest its functional association with mitochondria.

Due to the small gel format used in this prelimeary experiment, protein subunits in the same protein complex were not optimally resolved at the second dimension (SDS-PAGE). This could be seen from the complex protein mixture property which overstrained the MALDI-TOF-MS measurement. A larger gel format combined with pre-fractionation of MS measurement could lead to the identification of more mitochondrial-specific proteins.

Traditionally, Blue-native electrophoresis is not a quantitative analytical method. However, it could be possible to combine modern techniques, such as the florescent staining method in order to improve the ability of this method respecting protein quantification.

6.14 The accumulation of defective mitochondria with age was simulated

The recognition that aging is mechanistically complex has brought the need for *in silico* approaches. These approaches are following the spirit of Joel Keizer, who first recognized that many problems in molecular biology could be formulated as physical-chemical processes and studied by modern tools of nonlinear dynamical systems (Hastings, 2001).

Among the most controversial hypothesis of aging are those involved in the progressive accumulation of error-bearing or altered macromolecules with advancing age. The model of Kowald has been a theoretical prove of the mitochondrial theory of aging (Kowald and Kirkwood, 2000). However, since the presence of numerous parameters of unknown values, it has not been tractable to prove it experimentally.

Based on the model proposed by Kowald, we have employed a strongly reduced mathematical model for the dynamic discussion of mitochondrial theory of aging. In our current model, the accumulation of mutated mitochondria in the aging process can be

treated as dynamic system containing a collection of components (wild type mitochondria, mutated mitochondria and free radicals), the properties of which change with time as they response to interactions among the components. Our model also included the protein maximum concentration hypothesis by Brown (Brown, 1991) in order to further reduce parameter dimension. Such construct also reflects the mitochondria-host-cell dependency.

As can be seen in figure 37, our model faithfully simulated the accumulation of mutated mitochondria in the aging process. Notice that there exist a “quasi-stable phase” of both curves of intact and defective mitochondria at the beginning of simulation period. Subsequently, the defective mitochondria accumulated dramatically, accompanied by the rash decrease of intact mitochondria. The model allowed us to test the hypothesis of mitochondrial theory of aging by comparing the simulated behaviour of the model with the observed behaviour of the biological subject.

6.15 Mutation rate of mouse mtDNA was estimated

The somatic mutation rate of mtDNA is an important aspect directly influencing the validation of mitochondrial theory of aging. In case the mutation rate is smaller than a certain threshold value, the strength of mutation could be neglected, so the mitochondrial mutation will not be a driving force of the aging process. Unfortunately, It is currently difficult to directly measure the level of mutant mtDNA within living cells (Chinnery and Samuels, 1999; Linnane et al., 1989). The major goal of the utilization of model in this study was to calculate the mouse mtDNA mutation applying our experimental data obtained using proteomic approach.

For the calculation of mtDNA mutation rate, we used data of nuclear-encoded complex I and complex IV subunit alterations. This was based on two considerations: first, the mtDNA mutation affects predominantly respiratory complex I and complex IV genes (Cortopassi and Wong, 1999; Vu et al., 2000); second, the physiological stoimetry of complex assembly deduce that the reduction level of mtDNA-encoded subunit of complex I should be proportional to the reduction of nuclear-encoded subunits (Remacle et al., 2004).

Notice here that we did not use complex III and complex V subunits. This was based on the observation of feedback phenomenon in our experiment, which caused up-regulation in down-stream enzyme complexes in the respiratory chain. Furthermore, the strength of feedback inhibition is not known.

For efficient parameter scanning, we assumed that the change of wild type mitochondria was directly correlated with the change of mean value of the respiratory chain complex I and IV subunits. This was based on the simplified assumption that only wild type contained respiratory complex I and complex IV subunits, wile mutated mitochondria were totally depleted of this subunits (Remacle et al., 2004).

Assembly of the functional respiratory chain complexes requires the coordinated contribution of subunits synthesized in both the cytoplasm and the mitochondria. In case there is a lack of mtDNA-encoded subunits, there should be correlated lack of nuclear DNA-encoded subunits in the same protein complex (di Rago et al., 1997).

Under the current setting of both experiments and mathematical simulation in this study, mtDNA mutation rate of mouse (this strain C57BL/6) could be calculated as 1.2×10^{-8} per gene per day. This corresponds to 1.7×10^{-7} per gene per mitochondrial genome replication. This result is consistent with to the data of Shenkar, who predicted the mutated rate of 4977bp deletion to be 5.95×10^{-8} per mitochondrial genome replication (Shenkar et al., 1996).

With this mutation rate, dramatic accumulation of mutated mitochondria happens at approximately 600 days of age in our mouse model. This ensures that the vast majority of mitochondria remain intact throughout the developmental and reproduction phase of mouse life. According to our simulation result, at the time point of 800 days, which is the average lifespan of the C57BL/6 mouse (Rowlatt et al., 1976), the mitochondria population is consisted of 30% of intact mitochondria and 70% of defective mitochondria. This correlates well with the observation of mitochondrial dysfunction in old age. It also indicates that the mitochondrial somatic mutation is a factor that is not to be neglected respecting aging process.

Interestingly, both brain and liver got the same mutation rate value, in case the mitochondrial turnover rate "α" for liver was set to 0.073 d^{-1}. This corresponds to a replication rate of liver mitochondria to be 9.5 days. This indicates that even with the same mutation rate, the brain tissue could accumulate mutated mitochondria at a higher rate compared to liver. Thus, the faster accumulation of mutated mitochondria in brain could be largely due to the lower mitotic rate.

The purpose of modeling in this study was to use mathematical simulation to test abstract biological hypothesis of the mitochondrial theory of aging. Using the current model, we

were able to estimate the mutation rate of mtDNA of mouse, which is the key player in the whole system. Through more advanced experiments, we could be able to determine additional factors that influence the length of this “quasi-stable phase”. In this way, it would be possible to find intervention strategy in order to retard aging.

6.16 Result of current study is consistent with the mitochondrial theory of aging

About 15 years ago, it was proposed that aging is caused by life-long accumulation of mitochondrial mutations (Linnane et al., 1989), which comprise cellular energy metabolism and increase intracellular oxidative stress. This could result in the development of the multiple degenerative changes in tissues at old age.

The experimental results gained in this study have been consistent with this view. Indirect suggestion of mtDNA mutation was observed by the observation of complex I and complex IV protein down-regulation and the feedback effects of down-stream complex subunits, as well as the up-regulation of mitochondrial protein synthesis machinery. This indicates that the key initiating event of aging and age-related degeneration could be a decline in mitochondrial function, which leads to progressive oxidative damage that is exacerbated along with time.

To the author’s personal opinion, a basic underlying ground for this pivotal role of mitochondria in aging process could lie on the symbiotic nature of the modern eukaryotic cells. Symbiotic of proto-eukaryotic cell and the Rickettsiales-like aerobic bacteria was beneficial for the host cell, since it gained increased energy supply through extensive oxidation of nutrient. This eminently promoted the subsequent evolution. However, this benefit is accompanied by two major disadvantages: First, genome of microorganisms have generally much higher mutation rates than that of eukaryotic organism. MtDNA mutation was observed to occur on a frequent basis (Ferguson and von Borstel, 1992). As a facultative parasitic microorganism, this frequent mutation contributed to their fast adaptation to the environment. However, after becoming an obligatory symbiotic object, this property turns catastrophe for their host cell due to the low selective pressure in the cellular environment.

As can be seen in the mathematical simulation of this study, instead of being depleted, defective mitochondria could achieve homoplasmy state under normal physiological condition, taking the advantage of their slower degradation rate. This accumulation of defective mitochondria constitute as a potential hazard for the cell that manifest with time.

Respecting this problem, the host eukaryotic cell has been transferring the mitochondrial genes into the nuclei, in order to better perpetuate them. However, due to its inability of doing it in a complete manner, this problem has been inherited to date.

Another problem of symbiotic with an aerobic microorganism is their constant generation of free radical. Persistent oxidative stress could in turn cause further damage to DNA, membrane and proteins. It seems that oxidative stress cannot be totally prevented despite the cellular construction of diverse heat shock proteins and antioxidants. The decrease of mitochondrial heat shock protein and peroxiredoxin profiles observed in the current study suggests an elevated oxidative stress level in the mitochondria of the aged individuals.

Oxidative stress commonly acts as signal initiating apoptosis (Chen et al., 2001). It has been suggest that cells harbouring mutant mtDNA are more prompt to apoptosis (Khrapko et al., 1999). In this sense, mitochondrial DNA mutation could play an important role in neurological and other age-related diseases, sharing apoptosis as common feature (Horton et al., 1995).

The observed change of regucalcin and alpha-synuclein suggest that some genetic and environmental factors that increase the susceptibility of cells to apoptosis might interact with common molecular pathways. These include calcium signalling pathway or red-ox cell signalling. The influence of genetic, tissue-specific and epigenetic factors could contribute to the development of different pathologies. The insights obtained from the current proteomic characterization of the aging process may also be applied to the role of mitochondria in other age-related disorders.

Taking together, these finding indicate that, far from being merely an energy supplier of the cell, mitochondria play key roles in red-ox cell signalling and apoptosis (Bogoyevitch et al., 2000; Lai et al., 1996; Levonen et al., 2001; Liu et al., 1996). The emerging paradigm is a complex cross-talk between mitochondrial and cellular functions, with reactive oxygen species playing a key role.

7 Conclusion

In this study, we have put the mitochondrial theory of aging on trial at the proteomic aspect. The mouse model (C57BL/6) was first validated as a suitable model for human aging, and the effect of senescence on brain and liver mitochondria were assessed by proteomic comparisons of different age groups.

Sub-cellular fractionation has been shown to enrich part of the low-abundant mitochondrial proteins in the proteomic analysis. Sequential extraction of proteins, together with the employment of additional detergent improved the resolution of membrane proteins on the 2D-gels to a certain extent. This shows that sub-cellular fractionation and protein pre-fractionation are feasible and effective strategies for proteomic studies. Differential proteomic studies combined with hypothesis-driven method such like immunoblotting was shown to be powerful method to detect global protein profile changes. However, membrane protein remains a problem in proteomic studies.

Numerous protein profile changes during the aging process were observed. They suggest progressive mitochondrial dysfunction and increasing oxidative stress with advancing age. Respecting the difference between post-mitotic and mitotic tissue, an increased susceptibility to protein aggregation in the aged mouse brain was observed; while aged liver tissue showed decreased capacity of calcium buffering. There was indication for more severe mitochondrial abnormality in old brain compared to old liver.

Preliminary experiment showed that Blue-native electrophoresis could be potentially useful for the investigations of respiratory complex subunits and other mitochondria-associated proteins. Further experiments are on the way to improve the quantification capacity of this method.

A mathematical model has been useful for the estimation of mtDNA mutation rate of mouse based on experimental data. The result of the mathematical simulation confirms the mitochondrial somatic mutation as an important factor in the aging process. Further experimental data would be needed to improve the model, so as to further our understanding of aging as a dynamic process. Only theoretical and experimental works in concert can push forward our understanding of the dynamic aging process.

Aging is essentially a gradual decline in an organism’s capacity of responding to environmental stress and return to the resting state. Central to the restoring of resting state are a series of inter-related signaling pathways such as calcium signaling and controlled

protein or organelle degradation. Deficiency of such cellular mechanism will lead to significant alterations in their restoring capacity. Energy deficiency will further exacerbate this situation since most cellular processes are energy-dependent.

The evidence gained from this study was in concert to the mitochondrial theory of aging. By summarizing the major evidences gained in this current study, we conclude that mutated mitochondria can accumulate under normal physical conditions along with time. The mitochondrial somatic mutation could directly lead to respiratory chain complex deficiency. Mitochondrial dysfunction, in turn, causes the elevation of oxidative stress level in the cell. Oxidative damage manifests itself partially through protein aggregation and calcium buffering breakdown (fig.40).

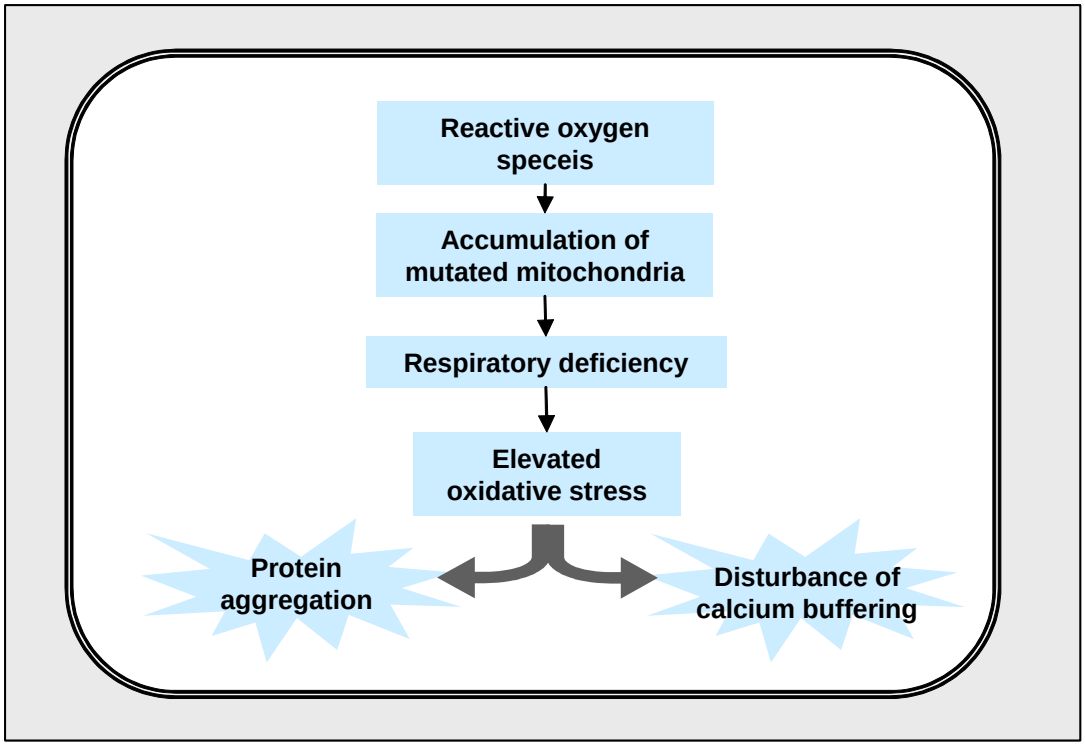

Fig.40: The current study expanded our knowledge respecting mitochondrial theory of aging. The mitochondrial somatic mutation could directly lead to mitochondrial dysfunction. This, in turn, causes the elevation of oxidative stress level in the cell, which manifests itself through protein aggregation and disturbed calcium buffering.

Through this study, we were able to expand our knowledge respecting the mitochondrial theory of aging. This study also demonstrated that aging and age-related diseases could be related through common pathways. It also provides a precondition for further differential proteomic experiments and mathematical simulation. Together, this could ultimately provide

a rationale for mitochondria as a target for preventing from the adverb side effect of aging, as well as to provide valid therapies in age-related diseases.

8 Outlook

Upon completion of this study, some further investigations would be required in the future respecting the following issues. Diverse protein profile changes during the aging process were observed in the current study. As the next step, analysis would be required to investigate whether there exist underlying gene expression alternations, alteration in post-transcriptional modifications or protein degradation control. Gene level control experiments (RT-PCR, northern blot) and protein modification analysis would be helpful in answering these questions. Blue-native gel electrophoresis combined with fluorescent staining could be useful to gather additional information regarding the possible changes in protein complex property.

More importantly, it deserves our understanding of detailed mechanism causing these protein level alternations, to determine the up-stream factors and system interplay. For example, how the proposed mitochondrial somatic mutations possibly lead to a high susceptibility of brain to fibrogenesis, or the vulnerability of liver mitochondria to calcium buffering.

Detailed investigations of the biochemical changes are still hampered by the lack of means for the analysis of hydrophobic membrane proteins. Further improvement will be needed in both protein extraction and protein separation strategy, in order to facilitate the investigation of mtDNA-encoded proteins directly. Alternatively, the employment of profound mass spectrometric and chromatographic strategies, such as multidimensional liquid chromatography coupled online to tandem mass spectrometry could be potentially useful to give indirect quantification of hydrophobic membrane proteins (Rabilloud et al., 2003; Sickmann et al., 2003).

Upon investigating the proteomic alteration of mouse brain and liver mitochondria in this study, the question arose whether and to what extent protein alterations that occur in one organ are valid in other organs. Additionally, whether there is a homogeneous behaviour in the same organ. Especially for highly differentiated tissue like brain, different anatomical and functional areas could be largely heterogeneous (Itoh et al., 1996; Soong et al., 1992). In the future, additional tissue types and tissue fractionations should be analyzed for their proteomic characterization.

Respecting the modest observation of mtDMA-encoded protein alteration in this study, another problem could be the low level of mtDNA mutation of a certain type which requires a high sensitivity of the measurement method. A different picture could emerge if

techniques were used that allow one to investigate individual cells or pure cell subpopulations. Laser capture micro dissection techniques could be methodology of choice in the future.

Studies on whole organism model have been useful to access global changes related to the aging process. Hypothesis-less differential proteomic analysis further reduces the range of key factors in the dynamic system in our study. In the future, hypothesis-driven experiments employing *in vitro* model could be useful to deduce the intrinsic relationship between free-radical induced mitochondrial mutation and oxidative stress in the frame of cellular senescence.

As an example, different oxidative stress accelerator (tert-butyl hydroperoxide (BHP)) or inhibitors, respiratory chain enzyme inhibitors, heat shock treatment could be applied on cell culture model to manipulate the cellular aging process, so as to measure the factors of interests (Rabilloud et al., 2002). Genotoxic stress could be simulated by genetically manipulation of mouse model with increased mtDNA mutation rate (Trifunovic et al., 2004). Such experiments combined with advanced mathematical simulation will help to delineate the contribution of mitochondria in aging process and age-related diseases. In the same context, it would also be of interest to investigate the Influence of epigenetic factors on the heterogeneous outcome of common pathway involved in the aging process, as well as diversity of age-related diseases.

9 Zusammenfassung

Man nimmt an, dass die Anreicherung von Mitochondrien mit mutiertem Genom maßgeblich am Alterungsprozess beteiligt ist (Wallace, 2001). Um die Auswirkung der mtDNA-Veränderungen bei der Alterung auf Proteinebene zu erforschen, wurde das mitochondriale Proteom während des Alterns anhand eines Mausmodells (C57/BL6) untersucht.

Vor der Untersuchung des Proteoms wurde durch histochemische Färbung nachgewiesen, dass die Zytochrome C Oxydase (COX) Aktivität bei alten (24 Monate) im Gegensatz zu jungen Mäusen (2 Woche) im Muskelgewebe abnimmt. Während bei jungen Mäusen keine COX-negativen Muskelzellen gefunden wurden, zeigte ein bedeutender Teil der Myozyten (43%) im Muskel von alten Mäusen eine reduzierte COX-Aktivität. Dies bestätigt, dass die Lebensspanne der Maus für die Untersuchung der mitochondrialen Alterung ausreicht.

Aus dem Gehirn und der Leber von Mäusen wurden Mitochondrien an sechs unterschiedlichen Zeitpunkten (von Neugeboren bis zu einem Alter von 24 Monaten, n=8 bis 13 pro Zeitpunkt) mit Hilfe einer kontinuierlichen Gradienten-Zentrifugation isoliert. Mitochondriale Proteine wurden mit einer sequenziellen Extraktionsstrategie basierend auf Tris-Puffer ("Fraktion I"), Triton-Puffer ("Fraktion II") und Methanol-Chloroform ("Fraktion III") extrahiert. Großgel 2D-Elektrophorese (2DE) und eine modifizierte 2D-Elektrophorese Prozedur (unter Verwendung von Triton-X100) wurden für die Analyse der Proteine aus „Fraktion I", beziehungsweise "Fraktion II", verwendet. Bei "Fraktion III" wurde mit Hilfe von Westernblots Veränderungen im Expressionsniveaus des mtDNA-kodierten Protein COX Untereinheit I untersucht.

Die Expression von zwei Untereinheiten des Komplexes I (NADH-Ubiquinone Oxidoreductase 13 kDa-A Untereinheit und NADH-Ubiquinone Oxidoreductase 1 alpha Subcomplex 5) und einer Untereinheit des Komplexes IV (COX Untereinheit Vb) der Atmungskette nahm mit zunehmendem Alter ab. Eine Untereinheit von Komplex III (Ubiquinol-Zytochrome c Reductase bindendes Protein), eine Untereinheit von Komplex V (ATP F0 Untereinheit F) und ein mitochondrial-ribosomales Protein zeigten ein erhöhtes Expressionsniveau im Alter. Diese Ergebnisse zeigen, dass das Fehlen von Komponenten der Komplexe I und IV der Atmungskette in alterndem Gewebe durch Feedbackregelung anderer Proteinkomplexe in der Atmungskette begleitet wird. Diese Beobachtungen stützen die Hypothese, dass die Ansammlung von mtDNA Mutationen überwiegend Gene für die Komplexe I und IV beeinflusst (Vu et al., 2000).

Die Herunterregulierung des 10 kDa mitochondrialen Hitzeschock-Proteins deutet auf ein erhöhtes Niveau an oxidativem Stress im alternden Mausgehirn und in der Leber hin. Oxidativer Stress tritt sowohl bei der Alterung als auch bei neurodegenerativen Erkrankungen auf (Cottrell et al., 2000, Richter et al., 1988). Die Erhöhung der Expression des mitochondrien-assozierten alpha-Synuclein im Gehirn könnte auf eine erhöhte Anfälligkeit zur Bildung von Proteinaggregaten mit fortschreitendem Alter hindeuten (Goedert, 1997; Ueda et al., 1993). Diese sind ebenfalls einen Kennzeichen von einigen neurodegenerativen Erkrankungen. Die Abnahme des mitochondrien-assoziierten Regucalcin in der Leber weist auf eine gesenkte mitochondriale Pufferungsfähigkeit für Kalziumionen hin (Takahashi und Yamaguchi, 2000; Xue et al., 2000).

Ein mathematisches Modell wurde entwickelt, um die Anhäufung von defekten Mitochondrien während des Alterns zu simulieren. Mit den experimentell erhobenen quantitativen Daten aus der Großgel 2DE wurde eine mtDNA Mutationsrate von $1.2x10^{-8}$ pro Gen und Tag abgeschätzt. Diese Mutationsrate ist groß genug, um eine Anreicherung von defekten Mitochondrien während des Alterns innerhalb der Lebensspanne einer Maus zu verursachen.

Die experimentellen Daten, die durch die Untersuchung des mitochondrialen Proteoms gewonnen wurden, unterstützen die Hypothese, dass sich mitochondriale Veränderungen mit dem Alter anreichern. Dies erklärt mitochondriale Funktionsstörungen und die Zunahme von oxidativen Stresses während des Alterns. Zukünftige Untersuchungen werden sich auf die Identifizierung weiterer, mtDNA-kodierter Proteinexpressionsveränderungen und die Proteininteraktionen während des Alterns konzentrieren.

Schlüsselwörter:
Mitochondiren, Alterung, Proteom, zweidimensionale Proteinelektrophorese, Mathematischemodellierung

10 Reference

Adessi, C., Miege, C., Albrieux, C., and Rabilloud, T. (1997). Two-dimensional electrophoresis of membrane proteins: a current challenge for immobilized pH gradients. Electrophoresis *18*, 127-135.

Ames, B. N., Shigenaga, M. K., and Hagen, T. M. (1993). Oxidants, antioxidants, and the degenerative diseases of aging. Proc Natl Acad Sci U S A *90*, 7915-7922.

Amson, R. B., Nemani, M., Roperch, J. P., Israeli, D., Bougueleret, L., Le Gall, I., Medhioub, M., Linares-Cruz, G., Lethrosne, F., Pasturaud, P., *et al.* (1996). Isolation of 10 differentially expressed cDNAs in p53-induced apoptosis: activation of the vertebrate homologue of the drosophila seven in absentia gene. Proc Natl Acad Sci U S A *93*, 3953-3957.

Anderson, N. G., and Anderson, N. L. (1996). Twenty years of two-dimensional electrophoresis: past, present and future. Electrophoresis *17*, 443-453.

Andreyev, A., and Fiskum, G. (1999). Calcium induced release of mitochondrial cytochrome c by different mechanisms selective for brain versus liver. Cell Death Differ *6*, 825-832.

Arnold, I., Pfeiffer, K., Neupert, W., Stuart, R. A., and Schagger, H. (1998). Yeast mitochondrial F1F0-ATP synthase exists as a dimer: identification of three dimer-specific subunits. Embo J *17*, 7170-7178.

Bandy, B., and Davison, A. J. (1990). Mitochondrial mutations may increase oxidative stress: implications for carcinogenesis and aging? Free Radic Biol Med *8*, 523-539.

Baumer, A., Zhang, C., Linnane, A. W., and Nagley, P. (1994). Age-related human mtDNA deletions: a heterogeneous set of deletions arising at a single pair of directly repeated sequences. Am J Hum Genet *54*, 618-630.

Bell, A. W., Ward, M. A., Blackstock, W. P., Freeman, H. N., Choudhary, J. S., Lewis, A. P., Chotai, D., Fazel, A., Gushue, J. N., Paiement, J., *et al.* (2001). Proteomics characterization of abundant Golgi membrane proteins. J Biol Chem *276*, 5152-5165.

Bodenteich, A., Mitchell, L. G., and Merril, C. R. (1991). A lifetime of retinal light exposure does not appear to increase mitochondrial mutations. Gene *108*, 305-309.

Boffoli, D., Scacco, S. C., Vergari, R., Solarino, G., Santacroce, G., and Papa, S. (1994). Decline with age of the respiratory chain activity in human skeletal muscle. Biochim Biophys Acta *1226*, 73-82.

Bogoyevitch, M. A., Ng, D. C., Court, N. W., Draper, K. A., Dhillon, A., and Abas, L. (2000). Intact mitochondrial electron transport function is essential for signalling by hydrogen peroxide in cardiac myocytes. J Mol Cell Cardiol *32*, 1469-1480.

Boguski, M. S., and Schuler, G. D. (1995). ESTablishing a human transcript map. Nat Genet *10*, 369-371.

Bohr, V. A., and Dianov, G. L. (1999). Oxidative DNA damage processing in nuclear and mitochondrial DNA. Biochimie *81*, 155-160.

Bowen, R. L., and Atwood, C. S. (2004). Living and dying for sex. A theory of aging based on the modulation of cell cycle signaling by reproductive hormones. Gerontology *50*, 265-290.

Bowling, A. C., Mutisya, E. M., Walker, L. C., Price, D. L., Cork, L. C., and Beal, M. F. (1993). Age-dependent impairment of mitochondrial function in primate brain. J Neurochem *60*, 1964-1967.

Brierley, E. J., Johnson, M. A., James, O. F., and Turnbull, D. M. (1997). Mitochondrial involvement in the ageing process. Facts and controversies. Mol Cell Biochem *174*, 325-328.

Brierley, E. J., Johnson, M. A., Lightowlers, R. N., James, O. F., and Turnbull, D. M. (1998). Role of mitochondrial DNA mutations in human aging: implications for the central nervous system and muscle. Ann Neurol *43*, 217-223.

Brockington, M., Sweeney, M. G., Hammans, S. R., Morgan-Hughes, J. A., and Harding, A. E. (1993). A tandem duplication in the D-loop of human mitochondrial DNA is associated with deletions in mitochondrial myopathies. Nat Genet *4*, 67-71.

Brookes, P. S., Pinner, A., Ramachandran, A., Coward, L., Barnes, S., Kim, H., and Darley-Usmar, V. M. (2002). High throughput two-dimensional blue-native electrophoresis: a tool for functional proteomics of mitochondria and signaling complexes. Proteomics *2*, 969-977.

Brown, G. C. (1991). Total cell protein concentration as an evolutionary constraint on the metabolic control distribution in cells. J Theor Biol *153*, 195-203.

Carafoli, E., and Zurini, M. (1982). The Ca2+-pumping ATPase of plasma membranes. Purification, reconstitution and properties. Biochim Biophys Acta *683*, 279-301.

Cartwright, J. H. E., and Piro, O. (1992). The Dynamics of Runge-Kutta Methods. Int J Bifurcations Chaos *2*, 427-449.

Challapalli, K. K., Zabel, C., Schuchhardt, J., Kaindl, A., Klose, J., and Herzel, H. (2004). High reproducibility of large gel two dimensional electrophoresis. Electrophoresis *accepted*.

Chang, J., Van Remmen, H., Cornell, J., Richardson, A., and Ward, W. F. (2003). Comparative proteomics: characterization of a two-dimensional gel electrophoresis system to study the effect of aging on mitochondrial proteins. Mech Ageing Dev *124*, 33-41.

Chen, Y., Stanford, A., Simmons, R. L., Ford, H. R., Hoffman, R. A., Cai, J., Anders, M. W., Stevens, J. L., and Jones, D. P. (2001). Nitric oxide protects thymocytes from gamma-irradiation-induced apoptosis in correlation with inhibition of p53 upregulation and mitochondrial damage. Cell Immunol *214*, 72-80.

Chinnery, P. F., and Samuels, D. C. (1999). Relaxed replication of mtDNA: A model with implications for the expression of disease. Am J Hum Genet *64*, 1158-1165.

Coligan, J. E., Dunn, B. M., and Ploegh, H. L. (1995). Current Protocols in Protein Sciences. In, D. W. Speicher, and P. T. Wingfield, eds. (New York, John Willey & Sons), pp. 94-99.

Coller, H. A., Bodyak, N. D., and Khrapko, K. (2002). Frequent intracellular clonal expansions of somatic mtDNA mutations: significance and mechanisms. Ann N Y Acad Sci *959*, 434-447.

Cooper, J. M., Mann, V. M., and Schapira, A. H. (1992). Analyses of mitochondrial respiratory chain function and mitochondrial DNA deletion in human skeletal muscle: effect of ageing. J Neurol Sci *113*, 91-98.

Copeland, N. G., Jenkins, N. A., and O'Brien, S. J. (2002). Genomics. Mmu 16--comparative genomic highlights. Science *296*, 1617-1618.

Corral-Debrinski, M., Horton, T., Lott, M. T., Shoffner, J. M., Beal, M. F., and Wallace, D. C. (1992). Mitochondrial DNA deletions in human brain: regional variability and increase with advanced age. Nat Genet *2*, 324-329.

Cortopassi, G. A., and Arnheim, N. (1990). Detection of a specific mitochondrial DNA deletion in tissues of older humans. Nucleic Acids Res *18*, 6927-6933.

Cortopassi, G. A., and Arnheim, N. (1992). Using the polymerase chain reaction to estimate mutation frequencies and rates in human cells. Mutat Res *277*, 239-249.

Cortopassi, G. A., and Wong, A. (1999). Mitochondria in organismal aging and degeneration. Biochim Biophys Acta *1410*, 183-193.

Cottrell, D. A., Blakely, E. L., Borthwick, G. M., Johnson, M. A., Taylor, G. A., Brierley, E. J., Ince, P. G., and Turnbull, D. M. (2000). Role of mitochondrial DNA mutations in disease and aging. Ann N Y Acad Sci *908*, 199-207.

Cullinane, C., and Bohr, V. A. (1998). DNA interstrand cross-links induced by psoralen are not repaired in mammalian mitochondria. Cancer Res *58*, 1400-1404.

Dallman, P. R. (1967). Cytochrome oxidase repair during treatment of copper deficiency: relation to mitochondrial turnover. J Clin Invest *46*, 1819-1827.

Dauer, W., Kholodilov, N., Vila, M., Trillat, A. C., Goodchild, R., Larsen, K. E., Staal, R., Tieu, K., Schmitz, Y., Yuan, C. A., *et al.* (2002). Resistance of alpha -synuclein null mice to the parkinsonian neurotoxin MPTP. Proc Natl Acad Sci U S A *99*, 14524-14529.

Dawson, T. M., and Dawson, V. L. (2003). Molecular pathways of neurodegeneration in Parkinson's disease. Science *302*, 819-822.

de Grey, A. D. (1997). A proposed refinement of the mitochondrial free radical theory of aging. Bioessays *19*, 161-166.

de Jong, W. W., Zweers, A., and Cohen, L. H. (1978). Influence of single amino acid substitutions on electrophoretic mobility of sodium dodecyl sulfate-protein complexes. Biochem Biophys Res Commun *82*, 532-539.

di Rago, J. P., Sohm, F., Boccia, C., Dujardin, G., Trumpower, B. L., and Slonimski, P. P. (1997). A point mutation in the mitochondrial cytochrome b gene obviates the requirement for the nuclear encoded core protein 2 subunit in the cytochrome bc1 complex in Saccharomyces cerevisiae. J Biol Chem *272*, 4699-4704.

DiMauro, S., Hirano, M., Schon, E. A., and Andreu, A. L. (2000). Mitochondrial encephalomyopathies: therapeutic approaches. Neurol Sci *21*, S901-908.

Emelyanov, V. V. (2001). Evolutionary relationship of Rickettsiae and mitochondria. FEBS Lett *501*, 11-18.

Feeney, L., and Berman, E. R. (1976). Oxygen toxicity: membrane damage by free radicals. Invest Ophthalmol *15*, 789-792.

Ferguson, L. R., and von Borstel, R. C. (1992). Induction of the cytoplasmic 'petite' mutation by chemical and physical agents in Saccharomyces cerevisiae. Mutat Res *265*, 103-148.

Fernandez, J., Gharahdaghi, F., and Mische, S. M. (1998). Routine identification of proteins from sodium dodecyl sulfate-polyacrylamide gel electrophoresis (SDS-PAGE) gels or polyvinyl difluoride membranes using matrix assisted laser desorption/ionization-time of flight-mass spectrometry (MALDI-TOF-MS). Electrophoresis *19*, 1036-1045.

Fernandez-Vizarra, E., Lopez-Perez, M. J., and Enriquez, J. A. (2002). Isolation of biogenetically competent mitochondria from mammalian tissues and cultured cells. Methods *26*, 292-297.

Finch, C. E. (1993). FRAR course on laboratory approaches to aging. Theories of aging. Aging (Milano) *5*, 277-289.

Finch, C. E., and Tanzi, R. E. (1997). Genetics of aging. Science *278*, 407-411.

Fountoulakis, M., and Schlaeger, E. J. (2003). The mitochondrial proteins of the neuroblastoma cell line IMR-32. Electrophoresis *24*, 260-275.

Frese, D., and Stahl, U. (1992). Oxidative stress and ageing in the fungus Podospora anserina. Mech Ageing Dev *65*, 277-288.

Fujita, T., Shirasawa, T., Inoue, H., Kitamura, T., Maruyama, N., Sato, N., and Shimosawa, T. (1998). Hepatic and renal expression of senescence marker protein-30 and its biological significance. J Gastroenterol Hepatol *13*, S124-131.

Fujita, T., Uchida, K., and Maruyama, N. (1992). Purification of senescence marker protein-30 (SMP30) and its androgen-independent decrease with age in the rat liver. Biochim Biophys Acta *1116*, 122-128.

Giavalisco, P. (2003) Proteomanalyse von Pfanzen, Dissertation, Freien Universität Berlin, Berlin.

Goedert, M. (1997). Familial Parkinson's disease. The awakening of alpha-synuclein. Nature *388*, 232-233.

Grad, J. M., Cepero, E., and Boise, L. H. (2001). Mitochondria as targets for established and novel anti-cancer agents. Drug Resist Updat *4*, 85-91.

Gras, R., Muller, M., Gasteiger, E., Gay, S., Binz, P. A., Bienvenut, W., Hoogland, C., Sanchez, J. C., Bairoch, A., Hochstrasser, D. F., and Appel, R. D. (1999). Improving protein identification from peptide mass fingerprinting through a parameterized multi-level scoring algorithm and an optimized peak detection. Electrophoresis *20*, 3535-3550.

Green, D. R., and Amarante-Mendes, G. P. (1998). The point of no return: mitochondria, caspases, and the commitment to cell death. Results Probl Cell Differ *24*, 45-61.

Gygi, S. P., Corthals, G. L., Zhang, Y., Rochon, Y., and Aebersold, R. (2000). Evaluation of two-dimensional gel electrophoresis-based proteome analysis technology. Proc Natl Acad Sci U S A *97*, 9390-9395.

Hansen, J. J., Bross, P., Westergaard, M., Nielsen, M. N., Eiberg, H., Borglum, A. D., Mogensen, J., Kristiansen, K., Bolund, L., and Gregersen, N. (2003). Genomic structure of the human mitochondrial chaperonin genes: HSP60 and HSP10 are localised head to head on chromosome 2 separated by a bidirectional promoter. Hum Genet *112*, 71-77.

Hanson, B. J., Schulenberg, B., Patton, W. F., and Capaldi, R. A. (2001). A novel subfractionation approach for mitochondrial proteins: a three-dimensional mitochondrial proteome map. Electrophoresis *22*, 950-959.

Harley, C. B., Futcher, A. B., and Greider, C. W. (1990). Telomeres shorten during ageing of human fibroblasts. Nature *345*, 458-460.

Harman, D. (1972). The biologic clock: the mitochondria? J Am Geriatr Soc *20*, 145-147.

Harman, D. (1981). The aging process. Proc Natl Acad Sci U S A *78*, 7124-7128.

Harry, J. L., Wilkins, M. R., Herbert, B. R., Packer, N. H., Gooley, A. A., and Williams, K. L. (2000). Proteomics: capacity versus utility. Electrophoresis *21*, 1071-1081.

Hashimoto, M., Hsu, L. J., Rockenstein, E., Takenouchi, T., Mallory, M., and Masliah, E. (2002). alpha-Synuclein protects against oxidative stress via inactivation of the c-Jun N-terminal kinase stress-signaling pathway in neuronal cells. J Biol Chem *277*, 11465-11472.

Hastie, N. D., Dempster, M., Dunlop, M. G., Thompson, A. M., Green, D. K., and Allshire, R. C. (1990). Telomere reduction in human colorectal carcinoma and with ageing. Nature *346*, 866-868.

Hastings, A. (2001). In memoriam: Joel E. Keizer. J Theor Biol *210*, 133-139.

Hayakawa, M., Hattori, K., Sugiyama, S., and Ozawa, T. (1992). Age-associated oxygen damage and mutations in mitochondrial DNA in human hearts. Biochem Biophys Res Commun *189*, 979-985.

Henshaw, P. S. (1947). The biological effects of pile radiations. Radiology *9*, 349-364.

Herskovits, T. T., Carberry, S. E., and Villanueva, G. B. (1985). Subunit dissociation of Busycon canaliculatum hemocyanin. Biochim Biophys Acta *828*, 278-289.

Heukeshoven, J., and Dernick, R. (1988). Improved silver staining procedure for fast staining in PhastSystem Development Unit. I. Staining of sodium dodecyl sulfate gels. Electrophoresis *9*, 28-32.

Hillenkamp, F., Karas, M., Beavis, R. C., and Chait, B. T. (1991). Matrix-assisted laser desorption/ionization mass spectrometry of biopolymers. Anal Chem *63*, 1193A-1203A.

Hirano, M., Shtilbans, A., Mayeux, R., Davidson, M. M., DiMauro, S., Knowles, J. A., and Schon, E. A. (1997). Apparent mtDNA heteroplasmy in Alzheimer's disease patients and in normals due to PCR amplification of nucleus-embedded mtDNA pseudogenes. Proc Natl Acad Sci U S A *94*, 14894-14899.

Hirokawa, T., Boon-Chieng, S., and Mitaku, S. (1998). SOSUI: classification and secondary structure prediction system for membrane proteins. Bioinformatics *14*, 378-379.

Hobot, J. A., Carlemalm, E., Villiger, W., and Kellenberger, E. (1984). Periplasmic gel: new concept resulting from the reinvestigation of bacterial cell envelope ultrastructure by new methods. J Bacteriol *160*, 143-152.

Holland, B. A., Haas, D. K., Norman, D., Brant-Zawadzki, M., and Newton, T. H. (1986). MRI of normal brain maturation. AJNR Am J Neuroradiol *7*, 201-208.

Horton, T. M., Graham, B. H., Corral-Debrinski, M., Shoffner, J. M., Kaufman, A. E., Beal, M. F., and Wallace, D. C. (1995). Marked increase in mitochondrial DNA deletion levels in the cerebral cortex of Huntington's disease patients. Neurology *45*, 1879-1883.

Hsu, L. J., Mallory, M., Xia, Y., Veinbergs, I., Hashimoto, M., Yoshimoto, M., Thal, L. J., Saitoh, T., and Masliah, E. (1998). Expression pattern of synucleins (non-Abeta component of Alzheimer's disease amyloid precursor protein/alpha-synuclein) during murine brain development. J Neurochem *71*, 338-344.

Ishigami, A., Fujita, T., Handa, S., Shirasawa, T., Koseki, H., Kitamura, T., Enomoto, N., Sato, N., Shimosawa, T., and Maruyama, N. (2002). Senescence marker protein-30 knockout mouse liver is highly susceptible to tumor necrosis factor-alpha- and Fas-mediated apoptosis. Am J Pathol *161*, 1273-1281.

Itoh, K., Weis, S., Mehraein, P., and Muller-Hocker, J. (1996). Cytochrome c oxidase defects of the human substantia nigra in normal aging. Neurobiol Aging *17*, 843-848.

Jazin, E. E., Cavelier, L., Eriksson, I., Oreland, L., and Gyllensten, U. (1996). Human brain contains high levels of heteroplasmy in the noncoding regions of mitochondrial DNA. Proc Natl Acad Sci U S A *93*, 12382-12387.

Joenje, H. (1989). Genetic toxicology of oxygen. Mutat Res *219*, 193-208.

Joenje, H., Gille, J. J., Oostra, A. B., and Van der Valk, P. (1985). Some characteristics of hyperoxia-adapted HeLa cells. A tissue culture model for cellular oxygen tolerance. Lab Invest *52*, 420-428.

Johnson, R. S., and Biemann, K. (1987). The primary structure of thioredoxin from Chromatium vinosum determined by high-performance tandem mass spectrometry. Biochemistry *26*, 1209-1214.

Jung, E., Heller, M., Sanchez, J. C., and Hochstrasser, D. F. (2000). Proteomics meets cell biology: the establishment of subcellular proteomes. Electrophoresis *21*, 3369-3377.

Jungblut, P., and Klose, J. (1985). Genetic variability of proteins from mitochondria and mitochondrial fractions of mouse organs. Biochem Genet *23*, 227-245.

Jungblut, P. R., and Seifert, R. (1990). Analysis by high-resolution two-dimensional electrophoresis of differentiation-dependent alterations in cytosolic protein pattern of HL-60 leukemic cells. J Biochem Biophys Methods *21*, 47-58.

Kaindl, A. (2001) Genetic analysis of mouse proteome in two-dimensional protein patterns of heart and liver, Dissertation, Humboldt Universität zu Berlin, Berlin.

Kaiser, N., and Edelman, I. S. (1977). Calcium dependence of glucocorticoid-induced lymphocytolysis. Proc Natl Acad Sci U S A *74*, 638-642.

Karas, M., and Hillenkamp, F. (1988). Laser desorption ionization of proteins with molecular masses exceeding 10,000 daltons. Anal Chem *60*, 2299-2301.

Karty, J. A., Ireland, M. M., Brun, Y. V., and Reilly, J. P. (2002). Defining absolute confidence limits in the identification of Caulobacter proteins by peptide mass mapping. Artifacts and unassigned masses encountered in peptide mass mapping. J Proteome Res *1*, 325-335.

Kashino, Y. (2003). Separation methods in the analysis of protein membrane complexes. J Chromatogr B Analyt Technol Biomed Life Sci *797*, 191-216.

Khrapko, K., Bodyak, N., Thilly, W. G., van Orsouw, N. J., Zhang, X., Coller, H. A., Perls, T. T., Upton, M., Vijg, J., and Wei, J. Y. (1999). Cell-by-cell scanning of whole mitochondrial genomes in aged human heart reveals a significant fraction of myocytes with clonally expanded deletions. Nucleic Acids Res *27*, 2434-2441.

Kirkwood, T. B., and Holliday, R. (1979). The evolution of ageing and longevity. Proc R Soc Lond B Biol Sci *205*, 531-546.

Klement, P., Nijtmans, L. G., Van den Bogert, C., and Houstek, J. (1995). Analysis of oxidative phosphorylation complexes in cultured human fibroblasts and amniocytes by blue-native-electrophoresis using mitoplasts isolated with the help of digitonin. Anal Biochem *231*, 218-224.

Klose, J. (1975). Protein mapping by combined isoelectric focusing and electrophoresis of mouse tissues. A novel approach to testing for induced point mutations in mammals. Humangenetik *26*, 231-243.

Klose, J. (1999). Large-gel 2-D electrophoresis. Fractionated extraction of total tissue proteins from mouse and human for 2-D electrophoresis. Methods Mol Biol *112*, 147-172.

Klose, J., and Kobalz, U. (1995). Two-dimensional electrophoresis of proteins: an updated protocol and implications for a functional analysis of the genome. Electrophoresis *16*, 1034-1059.

Klose, J., Nock, C., Herrmann, M., Stuhler, K., Marcus, K., Bluggel, M., Krause, E., Schalkwyk, L. C., Rastan, S., Brown, S. D., *et al.* (2002). Genetic analysis of the mouse brain proteome. Nat Genet *30*, 385-393.

Kopsidas, G., Kovalenko, S. A., Heffernan, D. R., Yarovaya, N., Kramarova, L., Stojanovski, D., Borg, J., Islam, M. M., Caragounis, A., and Linnane, A. W. (2000). Tissue mitochondrial DNA changes. A stochastic system. Ann N Y Acad Sci *908*, 226-243.

Kopsidas, G., Kovalenko, S. A., Kelso, J. M., and Linnane, A. W. (1998). An age-associated correlation between cellular bioenergy decline and mtDNA rearrangements in human skeletal muscle. Mutat Res *421*, 27-36.

Kovalenko, S. A., Kopsidas, G., Kelso, J., Rosenfeldt, F., and Linnane, A. W. (1998). Tissue-specific distribution of multiple mitochondrial DNA rearrangements during human aging. Ann N Y Acad Sci *854*, 171-181.

Kowald, A., and Kirkwood, T. B. (1999). The mitochondrial theory of aging: do damaged mitochondria accumulate by delayed degradation? Exp Gerontol *34*, 605-612.

Kowald, A., and Kirkwood, T. B. (2000). Accumulation of defective mitochondria through delayed degradation of damaged organelles and its possible role in the ageing of post-mitotic and dividing cells. J Theor Biol *202*, 145-160.

Kraytsberg, Y., Nekhaeva, E., Bodyak, N. B., and Khrapko, K. (2003). Mutation and intracellular clonal expansion of mitochondrial genomes: two synergistic components of the aging process? Mech Ageing Dev *124*, 49-53.

Kuhn, K., Wellen, J., Link, N., Maskri, L., Lubbert, H., and Stichel, C. C. (2003). The mouse MPTP model: gene expression changes in dopaminergic neurons. Eur J Neurosci *17*, 1-12.

Kyte, J., and Doolittle, R. F. (1982). A simple method for displaying the hydropathic character of a protein. J Mol Biol *157*, 105-132.

Laemmli, U. K., Amos, L. A., and Klug, A. (1976). Correlation between structural transformation and cleavage of the major head protein of T4 bacteriophage. Cell *7*, 191-203.

Lai, Y. K., Lee, W. C., Hu, C. H., and Hammond, G. L. (1996). The mitochondria are recognition organelles of cell stress. J Surg Res *62*, 90-94.

Le Bourg, E. (1998). Evolutionary theories of aging: handle with care. Gerontology *44*, 345-348.

Lee, H. C., Pang, C. Y., Hsu, H. S., and Wei, Y. H. (1994). Differential accumulations of 4,977 bp deletion in mitochondrial DNA of various tissues in human ageing. Biochim Biophys Acta *1226*, 37-43.

Levonen, A. L., Patel, R. P., Brookes, P., Go, Y. M., Jo, H., Parthasarathy, S., Anderson, P. G., and Darley-Usmar, V. M. (2001). Mechanisms of cell signaling by nitric oxide and peroxynitrite: from mitochondria to MAP kinases. Antioxid Redox Signal *3*, 215-229.

Lindop, P. J., and Rotblat, J. (1961a). Long-term effects of a single whole-body exposure of mice to ionizing radiations. I.Life shortening. ProcRoySoc *154*, 332-349.

Lindop, P. J., and Rotblat, J. (1961b). Shortening of life and causes of death in mice exposed to a single whole-body dose of radiation. Naturwissenschaften *189*, 645-648.

Lindsey, J., McGill, N. I., Lindsey, L. A., Green, D. K., and Cooke, H. J. (1991). In vivo loss of telomeric repeats with age in humans. Mutat Res *256*, 45-48.

Linnane, A. W., Baumer, A., Maxwell, R. J., Preston, H., Zhang, C. F., and Marzuki, S. (1990). Mitochondrial gene mutation: the ageing process and degenerative diseases. Biochem Int *22*, 1067-1076.

Linnane, A. W., Marzuki, S., Ozawa, T., and Tanaka, M. (1989). Mitochondrial DNA mutations as an important contributor to ageing and degenerative diseases. Lancet *1*, 642-645.

Linnane, A. W., Zhang, C., Baumer, A., and Nagley, P. (1992). Mitochondrial DNA mutation and the ageing process: bioenergy and pharmacological intervention. Mutat Res *275*, 195-208.

Liu, V. W., Zhang, C., Pang, C. Y., Lee, H. C., Lu, C. Y., Wei, Y. H., and Nagley, P. (1998). Independent occurrence of somatic mutations in mitochondrial DNA of human skin from subjects of various ages. Hum Mutat *11*, 191-196.

Liu, X., Kim, C. N., Yang, J., Jemmerson, R., and Wang, X. (1996). Induction of apoptotic program in cell-free extracts: requirement for dATP and cytochrome c. Cell *86*, 147-157.

Lopez, M. F., Kristal, B. S., Chernokalskaya, E., Lazarev, A., Shestopalov, A. I., Bogdanova, A., and Robinson, M. (2000). High-throughput profiling of the mitochondrial proteome using affinity fractionation and automation. Electrophoresis *21*, 3427-3440.

Lopez, M. F., and Melov, S. (2002). Applied proteomics: mitochondrial proteins and effect on function. Circ Res *90*, 380-389.

Lottspeich, F., and Zorbas, H. (1998). Bioanalytik (Heidelberg. Berlin, Spektrum Akademischer Verlag).

Ludwig, J., Kerscher, S., Brandt, U., Pfeiffer, K., Getlawi, F., Apps, D. K., and Schagger, H. (1998). Identification and characterization of a novel 9.2-kDa membrane sector-associated protein of vacuolar proton-ATPase from chromaffin granules. J Biol Chem *273*, 10939-10947.

Mann, M., Hendrickson, R. C., and Pandey, A. (2001). Analysis of proteins and proteomes by mass spectrometry. Annu Rev Biochem *70*, 437-473.

Mann, M., and Wilm, M. (1994). Error-tolerant identification of peptides in sequence databases by peptide sequence tags. Anal Chem *66*, 4390-4399.

Manzelmann, M. S., and Harmon, H. J. (1987). Lack of age-dependent changes in rat heart mitochondria. Mech Ageing Dev *39*, 281-288.

Menzies, R. A., and Gold, P. H. (1971). The turnover of mitochondria in a variety of tissues of young adult and aged rats. J Biol Chem *246*, 2425-2429.

Miklos, G. L., and Maleszka, R. (2001). Integrating molecular medicine with functional proteomics: realities and expectations. Proteomics *1*, 30-41.

Mita, S., Schmidt, B., Schon, E. A., DiMauro, S., and Bonilla, E. (1989). Detection of "deleted" mitochondrial genomes in cytochrome-c oxidase-deficient muscle fibers of a patient with Kearns-Sayre syndrome. Proc Natl Acad Sci U S A *86*, 9509-9513.

Molloy, M. P. (2000). Two-dimensional electrophoresis of membrane proteins using immobilized pH gradients. Anal Biochem *280*, 1-10.

Molloy, M. P., Herbert, B. R., Walsh, B. J., Tyler, M. I., Traini, M., Sanchez, J. C., Hochstrasser, D. F., Williams, K. L., and Gooley, A. A. (1998). Extraction of membrane proteins by differential solubilization for separation using two-dimensional gel electrophoresis. Electrophoresis *19*, 837-844.

Molloy, M. P., Herbert, B. R., Williams, K. L., and Gooley, A. A. (1999). Extraction of Escherichia coli proteins with organic solvents prior to two-dimensional electrophoresis. Electrophoresis *20*, 701-704.

Molloy, M. P., Phadke, N. D., Maddock, J. R., and Andrews, P. C. (2001). Two-dimensional electrophoresis and peptide mass fingerprinting of bacterial outer membrane proteins. Electrophoresis *22*, 1686-1696.

Morin, D., Hauet, T., Spedding, M., and Tillement, J. (2001). Mitochondria as target for antiischemic drugs. Adv Drug Deliv Rev *49*, 151-174.

Motsenbocker, M. A. (1988). Sensitivity limitations encountered in enhanced horseradish peroxidase catalysed chemiluminescence. J Biolumin Chemilumin *2*, 9-16.

Munscher, C., Rieger, T., Muller-Hocker, J., and Kadenbach, B. (1993). The point mutation of mitochondrial DNA characteristic for MERRF disease is found also in healthy people of different ages. FEBS Lett *317*, 27-30.

Murayama, K., Fujimura, T., Morita, M., and Shindo, N. (2001). One-step subcellular fractionation of rat liver tissue using a Nycodenz density gradient prepared by freezing-thawing and two-dimensional sodium dodecyl sulfate electrophoresis profiles of the main fraction of organelles. Electrophoresis *22*, 2872-2880.

Nagley, P., and Wei, Y. H. (1998). Ageing and mammalian mitochondrial genetics. Trends Genet *14*, 513-517.

Nekhaeva, E., Bodyak, N. D., Kraytsberg, Y., McGrath, S. B., Van Orsouw, N. J., Pluzhnikov, A., Wei, J. Y., Vijg, J., and Khrapko, K. (2002). Clonally expanded mtDNA point mutations are abundant in individual cells of human tissues. Proc Natl Acad Sci U S A *99*, 5521-5526.

Neubauer, G., King, A., Rappsilber, J., Calvio, C., Watson, M., Ajuh, P., Sleeman, J., Lamond, A., and Mann, M. (1998). Mass spectrometry and EST-database searching allows characterization of the multi-protein spliceosome complex. Nat Genet *20*, 46-50.

Neubert, D., Bass, R., and Helge, H. (1966). [Conversion rate of DNA in the mitochondria of warm-blooded animals]. Naturwissenschaften *53*, 23-24.

O'Farrell, P. H. (1975). High resolution two-dimensional electrophoresis of proteins. J Biol Chem *250*, 4007-4021.

Osiewacz, H. D., and Hamann, A. (1997). DNA reorganization and biological aging. A review. Biochemistry (Mosc) *62*, 1275-1284.

Panfili, E., Sottocasa, G. L., Sandri, G., and Liut, G. (1980). The Ca2+-binding glycoprotein as the site of metabolic regulation of mitochondrial Ca2+ movements. Eur J Biochem *105*, 205-210.

Pang, C. Y., Lee, H. C., Yang, J. H., and Wei, Y. H. (1994). Human skin mitochondrial DNA deletions associated with light exposure. Arch Biochem Biophys *312*, 534-538.

Pappin, D. J. C., Hojrup, P., and Bleasby, A. J. (1993). Rapid identification of proteins by peptide-mass fingerprinting. Curr Biol *3*, 327-332.

Pascale, R. M., De Miglio, M. R., Muroni, M. R., Simile, M. M., Daino, L., Seddaiu, M. A., Pusceddu, S., Gaspa, L., Calvisi, D., Manenti, G., and Feo, F. (1998). Transferrin and transferrin receptor gene expression and iron uptake in hepatocellular carcinoma in the rat. Hepatology *27*, 452-461.

Perrin, R. J., Woods, W. S., Clayton, D. F., and George, J. M. (2001). Exposure to long chain polyunsaturated fatty acids triggers rapid multimerization of synucleins. J Biol Chem *276*, 41958-41962.

Pirt, S. J. (1991). Genome project. Nature *350*, 104.

Rabilloud, T. (1990). Mechanisms of protein silver staining in polyacrylamide gels: a 10-year synthesis. Electrophoresis *11*, 785-794.

Rabilloud, T., Brodard, V., Peltre, G., Righetti, P. G., and Ettori, C. (1992). A comparison between low background silver diammine and silver nitrate protein stains. Modified silver staining for immobilized pH gradients. Electrophoresis *13*, 429-439.

Rabilloud, T., Heller, M., Gasnier, F., Luche, S., Rey, C., Aebersold, R., Benahmed, M., Louisot, P., and Lunardi, J. (2002). Proteomics analysis of cellular response to oxidative stress. Evidence for in vivo overoxidation of peroxiredoxins at their active site. J Biol Chem *277*, 19396-19401.

Rabilloud, T., Heller, M., Gasnier, F., Luche, S., Rey, C., Aebersold, R., Benahmed, M., Louisot, P., and Lunardi, J. (2003). Membrane proteins ride shotgun. Nat Biotechnol *21*, 508-510.

Rabilloud, T., Kieffer, S., Procaccio, V., Louwagie, M., Courchesne, P. L., Patterson, S. D., Martinez, P., Garin, J., and Lunardi, J. (1998). Two-dimensional electrophoresis of human placental mitochondria and protein identification by mass spectrometry: toward a human mitochondrial proteome. Electrophoresis *19*, 1006-1014.

Ramsby, M. L., Makowski, G. S., and Khairallah, E. A. (1994). Differential detergent fractionation of isolated hepatocytes: biochemical, immunochemical and two-dimensional gel electrophoresis characterization of cytoskeletal and noncytoskeletal compartments. Electrophoresis *15*, 265-277.

Remacle, C., Gloire, G., Cardol, P., and Matagne, R. F. (2004). Impact of a mutation in the mitochondrial LSU rRNA gene from Chlamydomonas reinhardtii on the activity and the assembly of respiratory-chain complexes. Curr Genet *45*, 323-330.

Richter, C. (1988). Do mitochondrial DNA fragments promote cancer and aging? FEBS Lett *241*, 1-5.

Richter, C., Park, J. W., and Ames, B. N. (1988). Normal oxidative damage to mitochondrial and nuclear DNA is extensive. Proc Natl Acad Sci U S A *85*, 6465-6467.

Robinson, A. B., and Pauling, L. (1974). Evolution and the distribution of glutaminyl and asparaginyl residues in proteins. Clin Chem *20*, 961-965.

Rotilio, G., Bray, R. C., and Fielden, E. M. (1972). A pulse radiolysis study of superoxide dismutase. Biochim Biophys Acta *268*, 605-609.

Rowlatt, C., Chesterman, F. C., and Sheriff, M. U. (1976). Lifespan, age changes and tumour incidence in an ageing C57BL mouse colony. Lab Anim *10*, 419-442.

Rustin, P., von Kleist-Retzow, J. C., Vajo, Z., Rotig, A., and Munnich, A. (2000). For debate: defective mitochondria, free radicals, cell death, aging-reality or myth-ochondria? Mech Ageing Dev *114*, 201-206.

Santoni, V., Doumas, P., Rouquie, D., Mansion, M., Rabilloud, T., Rossignol, M., Kieffer, S., and Garin, J. (1999). Large scale characterization of plant plasma membrane proteins. Towards the recovery of hydrophobic proteins on two-dimensional electrophoresis gels. Biochimie *81*, 655-661.

Santoni, V., Molloy, M., and Rabilloud, T. (2000). Membrane proteins and proteomics: un amour impossible? Electrophoresis *21*, 1054-1070.

Schagger, H., and von Jagow, G. (1991). Blue native electrophoresis for isolation of membrane protein complexes in enzymatically active form. Anal Biochem *199*, 223-231.

Seglen, P. O. (1976). Preparation of isolated rat liver cells. Methods Cell Biol *13*, 29-83.

Seligman, A. M., Karnovsky, M. J., Wasserkrug, H. L., and Hanker, J. S. (1968). Nondroplet ultrastructural demonstration of cytochrome oxidase activity with a polymerizing osmiophilic reagent, diaminobenzidine (DAB). J Cell Biol *38*, 1-14.

Shenkar, R., Navidi, W., Tavare, S., Dang, M. H., Chomyn, A., Attardi, G., Cortopassi, G., and Arnheim, N. (1996). The mutation rate of the human mtDNA deletion mtDNA4977. Am J Hum Genet *59*, 772-780.

Shevchenko, A., Wilm, M., Mann, M., Jensen, O. N., Podtelejnikov, A. V., Sagliocco, F., Vorm, O., Mortensen, P., and Boucherie, H. (1997). Mass spectrometric sequencing of proteins silver-stained polyacrylamide gels. J Protein Chem *16*, 481-490.

Shibutani, S., Takeshita, M., and Grollman, A. P. (1991). Insertion of specific bases during DNA synthesis past the oxidation-damaged base 8-oxodG. Nature *349*, 431-434.

Shoubridge, E. A., Karpati, G., and Hastings, K. E. (1990). Deletion mutants are functionally dominant over wild-type mitochondrial genomes in skeletal muscle fiber segments in mitochondrial disease. Cell *62*, 43-49.

Sickmann, A., Reinders, J., Wagner, Y., Joppich, C., Zahedi, R., Meyer, H. E., Schonfisch, B., Perschil, I., Chacinska, A., Guiard, B., *et al.* (2003). The proteome of Saccharomyces cerevisiae mitochondria. Proc Natl Acad Sci U S A *100*, 13207-13212.

Sims, N. R. (1990). Rapid isolation of metabolically active mitochondria from rat brain and subregions using Percoll density gradient centrifugation. J Neurochem *55*, 698-707.

Smith, P. K., Krohn, R. I., Hermanson, G. T., Mallia, A. K., Gartner, F. H., Provenzano, M. D., Fujimoto, E. K., Goeke, N. M., Olson, B. J., and Klenk, D. C. (1985). Measurement of protein using bicinchoninic acid. Anal Biochem *150*, 76-85.

Song, D. D., Shults, C. W., Sisk, A., Rockenstein, E., and Masliah, E. (2004). Enhanced substantia nigra mitochondrial pathology in human alpha-synuclein transgenic mice after treatment with MPTP. Exp Neurol *186*, 158-172.

Soong, N. W., Hinton, D. R., Cortopassi, G., and Arnheim, N. (1992). Mosaicism for a specific somatic mitochondrial DNA mutation in adult human brain. Nat Genet *2*, 318-323.

Stephenson, G., Marzuki, S., and Linnane, A. W. (1980). Biogenesis of mitochondria. Two-dimensional electrophoretic analysis of mitochondrial translation products in yeast. Biochim Biophys Acta *609*, 329-341.

Storm, T., Rath, S., Mohamed, S. A., Bruse, P., Kowald, A., Oehmichen, M., and Meissner, C. (2002). Mitotic brain cells are just as prone to mitochondrial deletions as neurons: a large-scale single-cell PCR study of the human caudate nucleus. Exp Gerontol *37*, 1389-1400.

Stryer, L. (1995). Biochemistry, 4th edn (New York, W.H. Freeman and Company).

Sugiyama, S., Takasawa, M., Hayakawa, M., and Ozawa, T. (1993). Changes in skeletal muscle, heart and liver mitochondrial electron transport activities in rats and dogs of various ages. Biochem Mol Biol Int *30*, 937-944.

Swain, M., and Ross, N. W. (1995). A silver stain protocol for proteins yielding high resolution and transparent background in sodium dodecyl sulfate-polyacrylamide gels. Electrophoresis *16*, 948-951.

Switzer, R. C., 3rd, Merril, C. R., Shifrin, S., Switzer, R. C., and Van Keuren, M. L. (1979). A highly sensitive silver stain for detecting proteins and peptides in polyacrylamide gels. Anal Biochem *98*, 231-237.

Takahashi, H., and Yamaguchi, M. (2000). Stimulatory effect of regucalcin on ATP-dependent Ca(2+) uptake activity in rat liver mitochondria. J Cell Biochem *78*, 121-130.

Taylor, R. W., Wardell, T. M., Connolly, B. A., Turnbull, D. M., and Lightowlers, R. N. (2001). Linked oligodeoxynucleotides show binding cooperativity and can selectively impair replication of deleted mitochondrial DNA templates. Nucleic Acids Res *29*, 3404-3412.

Taylor, S. W., Warnock, D. E., Glenn, G. M., Zhang, B., Fahy, E., Gaucher, S. P., Capaldi, R. A., Gibson, B. W., and Ghosh, S. S. (2002). An alternative strategy to determine the mitochondrial proteome using sucrose gradient fractionation and 1D PAGE on highly purified human heart mitochondria. J Proteome Res *1*, 451-458.

Tengan, C. H., Gabbai, A. A., Shanske, S., Zeviani, M., and Moraes, C. T. (1997). Oxidative phosphorylation dysfunction does not increase the rate of accumulation of age-related mtDNA deletions in skeletal muscle. Mutat Res *379*, 1-11.

Timmons, T. M., and Dunbar, B. S. (1990). Protein blotting and immunodetection. Methods Enzymol *182*, 679-688.

Towbin, H., and Gordon, J. (1984). Immunoblotting and dot immunobinding--current status and outlook. J Immunol Methods *72*, 313-340.

Trifunovic, A., Wredenberg, A., Falkenberg, M., Spelbrink, J. N., Rovio, A. T., Bruder, C. E., Bohlooly, Y. M., Gidlof, S., Oldfors, A., Wibom, R., *et al.* (2004). Premature ageing in mice expressing defective mitochondrial DNA polymerase. Nature *429*, 417-423.

Trounce, I., Byrne, E., and Marzuki, S. (1989). Decline in skeletal muscle mitochondrial respiratory chain function: possible factor in ageing. Lancet *1*, 637-639.

Ueda, K., Fukushima, H., Masliah, E., Xia, Y., Iwai, A., Yoshimoto, M., Otero, D. A., Kondo, J., Ihara, Y., and Saitoh, T. (1993). Molecular cloning of cDNA encoding an unrecognized component of amyloid in Alzheimer disease. Proc Natl Acad Sci U S A *90*, 11282-11286.

van Os, C. H. (1987). Transcellular calcium transport in intestinal and renal epithelial cells. Biochim Biophys Acta *906*, 195-222.

Villa, A., Garcia-Simon, M. I., Blanco, P., Sese, B., Bogonez, E., and Satrustegui, J. (1998). Affinity chromatography purification of mitochondrial inner membrane proteins with calcium transport activity. Biochim Biophys Acta *1373*, 347-359.

Vu, T. H., Tanji, K., Pallotti, F., Golzi, V., Hirano, M., DiMauro, S., and Bonilla, E. (2000). Analysis of mtDNA deletions in muscle by in situ hybridization. Muscle Nerve *23*, 80-85.

Wade, O. L., and Bishop, J. M. (1962). Cardiac output and Regional Blood Flow (Philadelphia, Oxford Blackwell Scientific).

Wallace, D. C. (1992). Mitochondrial genetics: a paradigm for aging and degenerative diseases? Science *256*, 628-632.

Wallace, D. C. (1997). Mitochondrial DNA in aging and disease. Sci Am *277*, 40-47.

Wallace, D. C. (2001). Mitochondrial genes in degenerative disease and aging. ScientificWorldJournal *1*, 83.

Wasinger, V. C., Cordwell, S. J., Cerpa-Poljak, A., Yan, J. X., Gooley, A. A., Wilkins, M. R., Duncan, M. W., Harris, R., Williams, K. L., and Humphery-Smith, I. (1995). Progress with gene-product mapping of the Mollicutes: Mycoplasma genitalium. Electrophoresis *16*, 1090-1094.

Wei, Y. H. (1998). Mitochondrial DNA mutations and oxidative damage in aging and diseases: an emerging paradigm of gerontology and medicine. Proc Natl Sci Counc Repub China B *22*, 55-67.

Weiss, W., Postel, W., and Gorg, A. (1992). Application of sequential extraction procedures and glycoprotein blotting for the characterization of the 2-D polypeptide patterns of barley seed proteins. Electrophoresis *13*, 770-773.

Wessel, D., and Flugge, U. I. (1984). A method for the quantitative recovery of protein in dilute solution in the presence of detergents and lipids. Anal Biochem *138*, 141-143.

Westermann, B., and Neupert, W. (2003). 'Omics' of the mitochondrion. Nat Biotechnol *21*, 239-240.

Whitehead, T. P., Kricka, L. J., Carter, T. J., and Thorpe, G. H. (1979). Analytical luminescence: its potential in the clinical laboratory. Clin Chem *25*, 1531-1546.

Wilkins, M. R., Pasquali, C., Appel, R. D., Ou, K., Golaz, O., Sanchez, J. C., Yan, J. X., Gooley, A. A., Hughes, G., Humphery-Smith, I., *et al.* (1996). From proteins to proteomes: large scale protein identification by two-dimensional electrophoresis and amino acid analysis. Biotechnology (N Y) *14*, 61-65.

Wilm, M., and Mann, M. (1996). Analytical properties of the nanoelectrospray ion source. Anal Chem *68*, 1-8.

Xie, J. (2003) Establishment of a two-dimensional electrophoresis map of human mitochondrial proteins, Dissertation, Humboldt-Universität zu Berlin, Berlin.

Xue, J. H., Takahashi, H., and Yamaguchi, M. (2000). Stimulatory effect of regucalcin on mitochondrial ATP-dependent calcium uptake activity in rat kidney cortex. J Cell Biochem *80*, 285-292.

Yamaguchi, M., and Isogai, M. (1993). Tissue concentration of calcium-binding protein regucalcin in rats by enzyme-linked immunoadsorbent assay. Mol Cell Biochem *122*, 65-68.

Yen, T. C., King, K. L., Lee, H. C., Yeh, S. H., and Wei, Y. H. (1994). Age-dependent increase of mitochondrial DNA deletions together with lipid peroxides and superoxide dismutase in human liver mitochondria. Free Radic Biol Med *16*, 207-214.

Yen, T. C., Su, J. H., King, K. L., and Wei, Y. H. (1991). Ageing-associated 5 kb deletion in human liver mitochondrial DNA. Biochem Biophys Res Commun *178*, 124-131.

Yerushalmi, H., Lebendiker, M., and Schuldiner, S. (1995). EmrE, an Escherichia coli 12-kDa multidrug transporter, exchanges toxic cations and H+ and is soluble in organic solvents. J Biol Chem *270*, 6856-6863.

Zabel, C., Chamrad, D. C., Priller, J., Woodman, B., Meyer, H. E., Bates, G. P., and Klose, J. (2002). Alterations in the mouse and human proteome caused by Huntington's disease. Mol Cell Proteomics *1*, 366-375.

Zeviani, M., Moraes, C. T., DiMauro, S., Nakase, H., Bonilla, E., Schon, E. A., Rowland, L. P., Tiranti, V., and Piantadosi, C. (1998). Deletions of mitochondrial DNA in Kearns-Sayre syndrome. Neurology *51*, 1525-1533.

Zhang, C., Bills, M., Quigley, A., Maxwell, R. J., Linnane, A. W., and Nagley, P. (1997a). Varied prevalence of age-associated mitochondrial DNA deletions in different species and tissues: a comparison between human and rat. Biochem Biophys Res Commun *230*, 630-635.

Zhang, C., Liu, V. W., Addessi, C. L., Sheffield, D. A., Linnane, A. W., and Nagley, P. (1998). Differential occurrence of mutations in mitochondrial DNA of human skeletal muscle during aging. Hum Mutat *11*, 360-371.

Zhang, C., Liu, V. W., and Nagley, P. (1997b). Gross mosaic pattern of mitochondrial DNA deletions in skeletal muscle tissues of an individual adult human subject. Biochem Biophys Res Commun *233*, 56-60.

Zhao, W., Devamanoharan, P. S., and Varma, S. D. (2000). Fructose-mediated damage to lens alpha-crystallin: prevention by pyruvate. Biochim Biophys Acta *1500*, 161-168.

Zuo, X., Echan, L., Hembach, P., Tang, H. Y., Speicher, K. D., Santoli, D., and Speicher, D. W. (2001). Towards global analysis of mammalian proteomes using sample prefractionation prior to narrow pH range two-dimensional gels and using one-dimensional gels for insoluble and large proteins. Electrophoresis *22*, 1603-1615.

Curriculum vitae

Mao Lei (Mrs.)
Seidenbau str. 6
D-12489 Berlin, Germany

Professional Experience

January 2002 – present:
Research assistant and doctoral student at the Institute of Human Genetics, University hospital Campus Virchow-Klinikum Charité, worked on the dissertation project under supervision of Prof. Dr. Dr. Klose.

January 1997 – December 2001:
Research assistant at the Department of Experimental Surgery, University hospital Campus Virchow-Klinikum Charité, worked on the projects of "Development of hepatocyte bioreactors as an alternative to animal experiments" and "Improvement of liver preservation solutions for liver transplantation".

August 1995 – December 1995:
Visiting scholar and interpreter at the Marmara Research Center, Gebze-Istanbul, Turkey. Worked on a Sino-Turkish cooperation research project entitled "Trans-gene laboratory animals by human gene microinjection".

August 1991 – August 1995:
Research fellow of Biotechnology Research Center, Chinese Academy of Agricultural Sciences, Beijing, China, focusing on the national project "Scale-up of monoclonal antibody vaccine production for agricultural and veterinary usages". Project manager in establishment and management of a complete set of specific pathogen free (SPF) standard laboratory animal facilities.

Education

October 2002 – July 2004:
Graduate study at University of Applied Sciences Berlin, ***Master of Computer Sciences in Bioinformatics*** pursued. Graduate thesis titled "Mathematical simulation of the accumulation of defective mitochondria during the aging process", supervised by Dr. Kowald and Prof. I. Koch.

October 1996 – December 2001:
Graduate study at the Department of biotechnology, Technical University Berlin. ***Dipom Engineer of Biotechnology*** pursued. Graduate thesis titled "Simultaneous isolation of hepatocytes and nonparenchymal cells from adult rat and human liver", supervised by Uni. Prof. Dipl. -Ing. Dr. U. Stahl and Dr. K. Zeilinger.

September 1987 – July 1991:
Undergraduate study at Beijing Agricultural University. ***Bachelor of Science in Agronomy*** (majoring laboratory animal Sciences) awarded in July 1991. Undergraduate thesis titled "The establishment of a diabetes animal using mini-pig".

August 1991 – December 1991:

National certification courses in technology of germ-free laboratory animal husbandry and National workshop on Specific-pathogen-free (SPF) animal facility management. Provided by the Chinese Academy of Medical Sciences.

Publication:

1. Zeilinger K, Sauer IM, Pless G, Strobel C, Rudzitis J, Wang A, Nussler AK, Grebe A, Mao L, Auth SH, Unger J, Neuhaus P, Gerlach JC.Three-dimensional co-culture of primary human liver cells in bioreactors for in vitro drug studies: effects of the initial cell quality on the long-term maintenance of hepatocyte-specific functions. Altern Lab Anim. 2002 Sep-Oct; 30(5):525-38.

2. Zeilinger K, Auth SHG, Unger J, Grebe A, Mao L. Standardisierung eines Hepatozyten-bioreaktorsystemes für in vitro-Metabolismusstudien als Alternative zum Tierversuch. In: Schöffl H, Spielmann H, Tritthart HA, eds. Ersatz- und Ergänzungsmethoden zu Tierversuchen. Springer-Verlag. 2000: 1-7.

3. Zeilinger K, Auth SHG, Unger J, Grebe A, Mao L, Petrik M, Holland G, Appel K, Nüssler AK, Neuhaus P, Gerlach JC. Leberzellkultur in Bioreaktoren für in vitro Studien zum Arzneimittelmetabolismus als Alternative zum Tierversuch. ALTEX 2000; 17:3-10.

4. Mao L, Zeilinger K, Roth S, Gerlach JC, Neuhaus P. Gleichzeitige Isolierung von Hepatozyten, Itozellen und Simusendothelzellen der Leber aus dem selben Organ. Z. Gastroenterol. 2000; 39:94.

5. Mao L, Zeilinger K, Auth S, Grebe A, Petrik M, Appel D, Schonoy N, Holland G, Jennings G, Gerlach JC. Immortalisierte Hepatozyten: Zukunftsmodell zum Ersatz von Metabolismusstudien am Tier? In: Schöffl H, Spielmann H, Tritthart HA, eds. Ersatz- und Ergänzungsmethoden zu Tierversuchen. Springer-Verlag. 2000: 450.

6. Grebe A, Zeilinger K, Auth SHG, Mao L, Schonoy N, Holland G, Appel K, Jennings G, Gerlach JC. Kultur primärer und immortalisierter humaner Hepatozyten in einem Bioreaktor-Perfusionssystem. Z. Gastroenterol. 1999; 37: 71.

Acknowledgments

The work with this dissertation has been extensive and trying, but in the first place exciting, instructive, and fun. Without help, support, and encouragement from some persons, I would never have been able to finish this work.

First of all, I would like to express my deep gratitude to the unselfish effort of my external examiner, Prof. Dipl.-Ing. Dr. Ulf Stahl and his untiring guidance and help throughout the years.

I would like to thank my supervisor Prof. Dr. Dr. Joachim Klose for making possible the conduct of this research, for his inspiring and encouraging way to guide me to a deeper understanding of knowledge, and for his invaluable comments during the whole work. His constructive comments and invaluable suggestions have significantly improved the contents of this dissertation.

I would also like to acknowledge Professor Dr. Karl Sperling, Director General of our institute for coming up with such a distinguished program.

I will also give a special thanks to Dr. Katrin Zeilinger, whose voices I always recall, especially during the writing and proofreading of this work. It was she who led me grasp the spirit of discover.

I am very grateful to Prof. Sebastian Bachmann, Mrs. Petra Schrade and Dr. Kerim Mutig, who have worked with the histopathological techniques of the biopsies. Thank you all for dedicating their valuable time for my curiosity.

Priv.-Doz. Dr. Grosse-Siestrup and his co-workers, especially Melanie are appreciated for a fruitful and agreeable collaboration.

I am also very grateful to everyone who has proofread parts of the manuscript, especially Dr. Claus Zabel and Dr. Jin Xie, for their helpful advice and criticism throughout the course of this work. Dr. Patrick Giavalisco is consistently appreciated for the exciting and endless discussions concerning the work.

My thanks also go to all my colleagues at the Institute of Human Genetics for providing a superior working atmosphere, especially Mrs. Grit Nebrich, Mr. Maik Wacker and Mrs. Silke Becker in the core facility for their assistance of Mass spectrometry measurements. Mrs. Marion Herrmann is acknowledged for allowing the use of relevant data for this study. Mr. Ingo Seefeldt is appreciated for his assistance of ProteinWeaver software. Mrs. Bettina Esch, Mrs. Yvonne Kläre and Mrs. Janine Stuwe are appreciated for their assistance of the laboratory works. Dr. Dijana Sagi is given thanks for sharing her valuable experimental data relating to this study and fruitful discussion.

Support of mathematical modeling has been provided by Dr. Axel Kowald from Max Plank institute for Molecular Genetics, and from Mr. Maciej Swat from the Institute of Theoretical Biology. I appreciate their invaluable help and suggestions.

At last, I wish to express my heartiest gratitude and respect to a special person who is always there for me: Mr. Rudi Beichel, to whom this work is dedicated.

Erklärung
Hiermit erkläre ich, Lei Mao, geboren am 29.04.1970 in Shanghai (China), an Eides Statt, dass meine Dissertation mit dem Thema “The Mitochondrial Protein Profile Change during the Aging Process” von mir selbst und ohne Hilfe Dritter verfasst wurde, auch in Teilen keine Kopie andere Arbeiten darstellt und die benutzen Hilfsmittel sowie die Literatur vollständig angegeben sind. Ich habe mich anderwärtig nicht um einen Doktorgrad beworben und besitze einen entsprechenden Doktorgrad nicht. Ich erkläre die Kenntnisnahme der dem Verfahren zugrunde liegenden Promotionsordnung der Technischen Universität zu Berlin.

Berlin, den _____

_____
Unterschrift

Appendix:

Tab.A1: Protein spots on the large-gel 2D-gels that have been identified in our study:

Spot	Hit*	gi-Nr.	Probability based Mowse Score	Matched Peptide	Sequence coverage [%]	MW [kDa]	pI	Protein name
9		gi|18655687	99	15	90	16	7..27	Chain B, Chimeric MOUSE CARBONMONOXY HEMOGLOBIN
		gi|553919	59	5	63	13	6.78	alpha-1-globin
16		gi|13654245	77	10	65	21	5.02	major urinary protein 1 [Mus musculus]
17		gi|6677739	76	12	39	33	5.15	regucalcin [Mus musculus]
		gi|6754976	132	15	50	22	8.26	peroxiredoxin 1; proliferation-associated gene A; osteoblast specific factor 3
37e		gi|8393343	84	11	68	14	8.59	fatty acid binding protein 1, liver; fatty acid binding protein liver [Mus musculus]
41	1.Hit	gi|12842467	64	7	29	14	8.34	unnamed protein product [Mus musculus]
	2.Hit	gi|6753500	62	7	29	14	8.69	cytochrome c oxidase, subunit Vb [Mus musculus]
81		sgi|127134	63	9	48	17	4.62	Myosin light chain 3, skeletal muscle isoform (A2 catalytic) (Alkali) (MLC3F)
96		gi|7949078	164	20	74	19	4.82	myosin light chain 2, phosphorylatable, fast skeletal muscle [Mus musculus]
126		gi|127134	70	10	55	17	4.62	Myosin light chain 3, skeletal muscle isoform (A2 catalytic) (Alkali) (MLC3F)
128b		gi|7949078	149	13	63	19	4.82	myosin light chain 2, phosphorylatable, fast skeletal muscle [Mus musculus]
173b		gi|4506741	156	12	43	22	10.09	ribosomal protein S7; 40S ribosomal protein S7 [Homo sapiens]
173e		gi|31560385	98	13	46	19	10.49	ribosomal protein L21 [Mus musculus]
175b		gi|18079339	202	26	36	85	8.08	aconitase 2, mitochondrial [Mus musculus]
300		gi|20818892	96	9	41	22	8.25	similar to FLJ23469 protein [Mus musculus]
301		gi|18250284	132	17	36	40	6.27	isocitrate dehydrogenase 3 (NAD+) alpha [Mus musculus]
302		gi|18152793	122	22	60	39	6.41	pyruvate dehydrogenase (lipoamide) beta [Mus musculus]
303		gi|18152793	197	23	48	39	6.41	pyruvate dehydrogenase (lipoamide) beta [Mus musculus]
304		gi|18250284	141	19	40	40	6.27	isocitrate dehydrogenase 3 (NAD+) alpha [Mus musculus]
305		gi|18250284	74	11	31	40	6.27	isocitrate dehydrogenase 3 (NAD+) alpha [Mus musculus]
407(18)	1.Hit	gi|12846314	150	15	48	22	8.26	unnamed protein product [Mus musculus]
	2.Hit	gi|6754976	150	15	48	22	8.26	peroxiredoxin 1; proliferation-associated gene A; osteoblast specific factor 3

Spot	Hit*	gi-Nr.	Probability based Mowse Score	Matched Peptide	Sequence coverage [%]	MW [kDa]	pI	Protein name
406		gi|8393343	143	22	91	14	8.59	fatty acid binding protein 1, liver; fatty acid binding protein liver [Mus musculus]
405(17)		gi|6677739	155	22	63	33	5.15	regucalcin [Mus musculus]
404_1	1.Hit	gi|226471	80	10	57	16	6.03	Cu/Zn superoxide dismutase
	2.Hit	gi|20896095	80	10	57	16	6.02	superoxide dismutase 1, soluble [Mus musculus]
404_2	1.Hit	gi|226471	127	12	64	16	6.03	Cu/Zn superoxide dismutase
	2.Hit	gi|20896095	126	12	63	16	6.02	superoxide dismutase 1, soluble [Mus musculus]
403	1.Hit	gi|26324826	96	20	27	73	8.47	unnamed protein product [Mus musculus]
	2.Hit	gi|6429156	86	19	24	75	8.64	peroxisomal acyl-CoA oxidase [Mus musculus]
402		gi|21313138	154	19	65	26	8.97	glutathione S-transferase class kappa [Mus musculus]
401		gi|31981724	161	27	64	25	8.76	glutathione S-transferase, alpha 3 [Mus musculus]
79		gi|7949005	92	6	54	12	9.36	ATP synthase, H+ transporting, mitochondrial F0 complex, subunit F; mitochondrial ATP synthase coup
142		gi|18655687	69	5	43	16	7.27	Chain B, Chimeric HumanMOUSE CARBONMONOXY HEMOGLOBIN
175b		gi|18079339	164	21	25	85	8.08	aconitase 2, mitochondrial [Mus musculus]
152		gi|6679299	81	12	47	30	5.57	prohibitin [Mus musculus]
154b	1.Hit	gi|6679583	98	14	51	24	5.64	RAB11B, member RAS oncogene family [Mus musculus]
	2.Hit	gi|7108528	95	14	53	24	6.23	small GTPase [Mus musculus]
154d	1.Hit	gi|18390323	133	15	64	24	5.85	RAB14, member RAS oncogene family [Mus musculus]
	2.Hit	gi|6679583	86	10	38	24	5.64	RAB11B, member RAS oncogene family [Mus musculus]
	3.Hit	gi|34147513	58	8	45	23	6.4	RAB7, member RAS oncogene family; Ras-associated protein RAB7
	4.Hit	gi|6679599	48	7	41	24	7.53	RAB7, member RAS oncogene family [Mus musculus]
		gi|229552	123	35	54	66	5.76	albumin
160	1.Hit	gi|547679	87	12	55	23	6.12	Heat shock 27 kDa protein (HSP 27)
	2.Hit	gi|91319	77	11	42	23	5.86	stress protein, 25K - mouse
180		gi|6680836	77	12	25	48	4.33	calreticulin [Mus musculus]
117a		gi|13385268	65	5	35	15	4.96	cytochrome b-5 [Mus musculus]

Spot	Hit*	gi-Nr.	Probability based Mowse Score	Matched Peptide	Sequence coverage [%]	MW [kDa]	pI	Protein name
126		gi|127134	184	12	59	17	4.62	Myosin light chain 3, skeletal muscle isoform (A2 catalytic) (Alkali) (MLC3F)
137a		gi|13385260	81	9	71	15	8.95	thioesterase superfamily member 2 [Mus musculus]
137b		gi|13385726	126	12	72	14	9.1	ubiquinol-cytochrome c reductase binding protein [Mus musculus]
144		gi|38075371	67	9	50	18	10.32	similar to NADH-ubiquinone oxidoreductase 13 kDa-A subunit, mitochondrial (Complex I-13KD-A) (CI-13KD-A) [Mus musculus]
153a	1.Hit	gi|6755963	183	18	48	31	8.62	voltage-dependent anion channel 1 [Mus musculus]
	2.Hit	gi|10720404	180	18	46	32	8.55	Voltage-dependent anion-selective channel protein 1 (VDAC-1) (mVDAC1) (Outer mitochondrial membrane protein porin 1)
153c	1.Hit	gi|13435636	101	10	30	25	6.67	2400003B06Rik protein [Mus musculus]
	2.Hit	gi|26368202	97	10	27	27	8.49	unnamed protein product [Mus musculus]
155		gi|6679583	151	10	38	24	5.64	RAB11B, member RAS oncogene family [Mus musculus]
164		gi|38082750	67	9	37	27	7.63	NADH dehydrogenase (ubiquinone) flavoprotein 2 [Mus musculus]
173c	1.Hit	gi|27679110	109	19	58	21	10.2	similar to 60S RIBOSOMAL PROTEIN L17 (L23) (ASI) [Rattus norvegicus]
	2.Hit	gi|22001904	109	19	58	21	10.2	60S ribosomal protein L17 (L23)
173d		gi|20899100	170	19	82	21	8.19	NADH dehydrogenase (ubiquinone) 1 beta subcomplex, 10 [Mus musculus]
174	1.Hit	gi|2501472	107	13	30	60	8.87	UDP-glucuronosyltransferase 1-1 precursor, microsomal (UDPGT)
	2.Hit	gi|31324690	107	13	30	60	8.94	UDP glycosyltransferase 1 family polypeptide A1 [Mus musculus]
179	1.Hit	gi|14714615	80	15	23	92	4.74	Tumor rejection antigen gp96 [Mus musculus]
	2.Hit	gi|729425	89	16	24	92	4.78	Endoplasmin precursor (94 kDa glucose-regulated protein) (GRP94)
12c		gi|7440317	176	16	53	16	10.14	ribosomal protein S14 - mouse
13b		gi|13384608	160	12	74	12	6.28	6-pyruvoyl-tetrahydropterin synthase (TCF1)
14		gi|22164792	109	9	35	22	9.34	mitochondrial ribosomal protein L12 [Mus musculus]
37a		gi|1708292	100	10	56	18	8.52	HEAT-RESPONSIVE PROTEIN 12
37c		gi|38075371	90	8	61	18	10.32	similar to NADH-ubiquinone oxidoreductase 13 kDa-A subunit, mitochondrial precursor (Complex I-13KD-A) (CI-13KD-A) [Mus musculus]

Spot	Hit*	gi-Nr.	Probability based Mowse Score	Matched Peptide	Sequence coverage [%]	MW [kDa]	pI	Protein name
51b	1.Hit	gi|12852348	83	7	51	12	9.24	unnamed protein product [Mus musculus]
	2.Hit	gi|6678047	79	7	45	14	4.74	synuclein, alpha; alpha SYN; alpha-synuclein [Mus musculus]
113		gi|31980806	108	8	35	22	4.57	progesterone receptor membrane component [Mus musculus]
114		gi|31980806	89	9	35	22	4.57	progesterone receptor membrane component [Mus musculus]
164a		gi|6680674	85	12	21	56	5.98	thymoma viral proto-oncogene 2; RAC-beta serine/threonine protein kinase; protein kinase B, beta [Mus musculus]
172b	1.Hit	gi|4506741	176	22	61	22	10.09	ribosomal protein S7; 40S ribosomal protein S7 [Homo sapiens]
	2.Hit	gi|38081187	80	14	58	25	10.12	similar to 40S ribosomal protein S7 (S8) [Mus musculus]
9		gi|18655687	150	12	84	16	7.27	Chain B, Chimeric HumanMOUSE CARBONMONOXY HEMOGLOBIN
10	1.Hit	gi|12833511	127	7	58	15	7.96	unnamed protein product [Mus musculus]
	2.Hit	gi|553919	110	6	58	13	6.78	alpha-1-globin
16		gi|13654245	179	18	80	21	5.02	major urinary protein 1 [Mus musculus]
17		gi|6677739	278	24	74	33	5.15	regucalcin [Mus musculus]
27	1.Hit	gi|193761	79	6	89	6	6.82	alpha-globin
	2.Hit	gi|553919	65	6	42	13	6.78	alpha-1-globin
33	1.Hit	gi|12859535	131	12	78	13	6.31	unnamed protein product [Mus musculus]
	2.Hit	gi|13386100	130	12	78	13	7.82	NADH dehydrogenase (ubiquinone) 1 alpha subcomplex, 5 [Mus musculus]
37e		gi|8393343	148	15	76	14	8.59	fatty acid binding protein 1, liver; fatty acid binding protein liver [Mus musculus]
37f		gi|18655687	235	15	84	16	7.27	Chain B, Chimeric HumanMOUSE CARBONMONOXY HEMOGLOBIN
81		gi|127134	96	11	43	17	4.62	Myosin light chain 3, skeletal muscle isoform (A2 catalytic) (Alkali) (MLC3F)
85	1.Hit	gi|117097	103	8	58	12	5.01	Cytochrome c oxidase polypeptide VA
	2.Hit	gi|6680986	76	7	34	16	6.08	cytochrome c oxidase, subunit Va [Mus musculus]
94		gi|127134	93	11	50	17	4.62	Myosin light chain 3, skeletal muscle isoform (A2 catalytic) (Alkali) (MLC3F)
95		gi|7949078	70	7	41	19	4.82	myosin light chain 2, phosphorylatable, fast skeletal muscle [Mus musculus]
96		gi|7949078	205	22	80	19	4.83	myosin light chain 2, phosphorylatable, fast skeletal muscle [Mus musculus]
128b		gi|19880190	102	14	17	69	9.31	DNA topoisomerase I [Mus musculus]

Spot	Hit*	gi-Nr.	Probability based Mowse Score	Matched Peptide	Sequence coverage [%]	MW [kDa]	pI	Protein name
177b		gi|18250284	99	10	21	40	6.27	isocitrate dehydrogenase 3 (NAD+) alpha [Mus musculus]
175a		gi|28279468	158	25	30	81	7.52	leucine zipper-EF-hand containing transmembrane protein 1 [Mus musculus]
172d		gi|25051141	204	14	63	21	10.73	RIKEN cDNA 2510019J09 [Mus musculus]
122	1.Hit	gi|12842467	66	8	29	14	8.34	unnamed protein product [Mus musculus]
	2.Hit	gi|6753500	64	8	29	14	8.69	cytochrome c oxidase, subunit Vb [Mus musculus]
128a		gi|7949078	108	12	74	19	4.82	myosin light chain 2, phosphorylatable, fast skeletal muscle [Mus musculus]
139		gi|13385322	104	9	59	16	8.35	NADH dehydrogenase (ubiquinone) 1 beta subcomplex, 7 [Mus musculus]
145		gi|6680309	105	10	81	11	7.93	heat shock protein 1 (chaperonin 10); heat shock 10 kDa protein 1 (chaperonin 10); mitochondrial chaperonin 10 [Mus musculus]
157b		gi|30794280	85	17	25	69	5.82	albumin
159		gi|20913657	150	14	83	19	5.52	RIKEN cDNA 0610009D10 [Mus musculus]
172a	1.Hit	gi|26333821	88	10	18	75	8.24	unnamed protein product [Mus musculus]
	2.Hit	gi|6429156	75	9	15	75	8.64	peroxisomal acyl-CoA oxidase [Mus musculus]
176b	1.Hit	gi|12805431	107	15	43	35	5.63	Pdhb protein [Mus musculus]
	2.Hit	gi|18152793	101	15	40	39	6.41	pyruvate dehydrogenase (lipoamide) beta [Mus musculus]
181		gi|31980648	186	26	52	56	5.19	ATP synthase, H+ transporting mitochondrial F1 complex, alpha subunit [Mus musculus]
		gi|6754976	197	19	60	22	8.26	peroxiredoxin 1; proliferation-associated gene A; osteoblast specific factor 3; macrophage 23 Kd stress protein; macrophase stress protein 23 kd; Trx dependent
19		gi|21703976	316	36	68	60	6.44	cDNA sequence BC021917 [Mus musculus]
26	1.Hit	gi|18655687	147	15	84	16	7.27	Chain B, Chimeric HumanMOUSE CARBONMONOXY HEMOGLOBIN
	2.Hit	gi|16741459	79	10	61	19	5.52	RIKEN cDNA 0610009D10 [Mus musculus]
29		gi|18655687	192	16	84	16	7.27	Chain B, Chimeric HumanMOUSE CARBONMONOXY HEMOGLOBIN
37b	1.Hit	gi|12859535	103	8	73	13	6.31	unnamed protein product [Mus musculus]
	2.Hit	gi|13386100	103	8	73	13	7.82	NADH dehydrogenase (ubiquinone) 1 alpha subcomplex, 5 [Mus musculus]
46		gi|1841387	62	7	34	28	4.72	14-3-3 zeta [Mus musculus]

Spot	Hit*	gi-Nr.	Probability based Mowse Score	Matched Peptide	Sequence coverage [%]	MW [kDa]	pI	Protein name
47		gi|1346412	78	13	27	74	6.54	Lamin A
49		gi|37589957	92	11	36	36	6.16	Malate dehydrogenase, soluble [Mus musculus]
61		gi|6753500	62	8	36	14	8.69	cytochrome c oxidase, subunit Vb [Mus musculus]
62		gi|6680986	66	8	28	16	6.08	cytochrome c oxidase, subunit Va [Mus musculus]
63		gi|6680986	86	14(Me18)	62	16	6.08	cytochrome c oxidase, subunit Va [Mus musculus]
75		gi|2253399	79	8	56	13	7.85	vesicle associated membrane protein 2 [Mus musculus]
78		gi|7949005	91	9	55	12	9.36	ATP synthase, H+ transporting, mitochondrial F0 complex, subunit F; mitochondrial ATP synthase coupling factor 6 [Mus musculus]
80	1.Hit	gi|12847456	66	5	22	18	5.03	unnamed protein product [Mus musculus]
	2.Hit	gi|20806153	66	5	22	18	5.16	ATP synthase, H+ transporting, mitochondrial F1 complex, delta subunit
88		gi|6680309	173	14	91	11	7.93	heat shock protein 1 (chaperonin 10); heat shock 10 kDa protein 1 (chaperonin 10); mitochondrial chaperonin 10 [Mus musculus]
98		gi|6679299	224	18	61	30	5.57	prohibitin [Mus musculus]
99		gi|20913657	129	15	90	19	5.52	RIKEN cDNA 0610009D10 [Mus musculus]
100		gi|21759114	127	16	61	27	8.57	Electron transfer flavoprotein beta-subunit (Beta-ETF)
102		gi|21759114	131	16	52	27	8.57	Electron transfer flavoprotein beta-subunit (Beta-ETF)
103	1.Hit	gi|21313618	112	13	62	26	8.56	RIKEN cDNA 0610041L09 [Mus musculus]
	2.Hit	gi|12805413	90	14	38	31	8.76	Echs1 protein [Mus musculus]
104	1.Hit	gi|12850643	96	9	43	27	9.1	unnamed protein product [Mus musculus]
	2.Hit	gi|13182962	96	9	43	27	8.89	short chain L-3-hydroxyacyl-CoA dehydrogenase
111		gi|31980806	104	10	36	22	4.57	progesterone receptor membrane component [Mus musculus]
112		gi|31980806	132	14	51	22	4.57	progesterone receptor membrane component [Mus musculus]
115d		gi|31542438	88	10	41	16	4.79	cytochrome b5 outer mitochondrial membrane precursor [Mus musculus]
117b		gi|13385268	87	9	56	15	4.96	cytochrome b-5 [Mus musculus]
117c		gi|13385268	154	11	58	15	4.96	cytochrome b-5 [Mus musculus]

Spot	Hit*	gi-Nr.	Probability based Mowse Score	Matched Peptide	Sequence coverage [%]	MW [kDa]	pI	Protein name
20		gi|15679953	140	14	51	33	6.75	Glycine N-methyltransferase [Mus musculus]
35		gi|38075371	93	11	61	18	10.32	similar to NADH-ubiquinone oxidoreductase 13 kDa-A subunit, mitochondrial precursor (Complex I-13KD-A) (CI-13KD-A) [Mus musculus]
40a		gi|6996913	63	9	21	50	7.55	annexin A2; calpactin I heavy chain; annexin II; lipocortin II; chromobindin 8
41		gi|29789345	79	15	30	50	5.73	2410153K17 protein [Mus musculus]
43	1.Hit	gi|20913929	264	32	58	57	4.77	prolyl 4-hydroxylase, beta polypeptide [Mus musculus]
	2.Hit	gi|129729	264	32	58	57	4.79	Protein disulfide isomerase precursor (PDI) (Prolyl 4-hydroxylase beta subunit) (Cellular thyroid hormone binding protein) (P55) (ERP59)
	2.Hit	gi|21746161	161	30	56	50	4.78	tubulin, beta [Mus musculus]
45		gi|21311901	472	54	65	97	7.67	dimethylglycine dehydrogenase precursor [Mus musculus]
67	1.Hit	gi|1174621	80	12	26	60	5.44	T-COMPLEX PROTEIN 1, THETA SUBUNIT (TCP-1-THETA) (CCT-THETA)
	2.Hit	gi|31560613	80	12	26	60	5.57	chaperonin subunit 8 (theta) [Mus musculus]
71a	1.Hit	gi|12859535	97	10	77	13	6.31	unnamed protein product [Mus musculus]
	2.Hit	gi|13386100	96	10	77	13	7.82	NADH dehydrogenase (ubiquinone) 1 alpha subcomplex, 5 [Mus musculus]
71c		gi|38075371	103	9	61	18	10.32	similar to NADH-ubiquinone oxidoreductase 13 kDa-A subunit, mitochondrial precursor (Complex I-13KD-A) (CI-13KD-A) [Mus musculus]
		gi|5834958				8	9.88	ATP synthase F0 subunit 8
		gi|12643945				31	8.84	Voltage-dependent anion-selective channel protein 3 (VDAC-3)

**Hit: Mascot search hit number*

Tab.A2: Protein spots on the Blue-native gels that have been identified in this study:

Spot	Mix*	gi-Nr.	Probability based Mowse Score	Matched Peptide	Sequence coverage [%]	MW [kDa]	pI	Protein name
26		gi|15489120	205	42	34	116	6.36	Ogdh protein [Mus musculus]
27		gi|18079339	96	21	27	85	8.08	aconitase 2, mitochondrial [Mus musculus]
28	Mix1	gi|33859811	82	23	33	83	9.24	hydroxyacyl-Coenzyme A dehydrogenase
	Mix2	gi|21704020	68	20	28	80	5.51	NADH dehydrogenase (ubiquinone) Fe-S protein 1 [Mus musculus]
29	Mix1	gi|27369581	73	26	41	75	8.43	solute carrier family 25 (mitochondrial carrier, Aralar), member 12 [Mus musculus]
	Mix2	gi|12597627	66	25	35	80	6.15	kinesin family member C3 [Mus musculus]
30	Mix1	gi|31980648	105	32	49	56	5.19	ATP synthase, H+ transporting mitochondrial F1 complex, beta subunit
	Mix2	gi|6680748	103	24	49	60	9.22	ATP synthase, H+ transporting, mitochondrial F1 complex, alpha subunit [Mus musculus]
31	Mix1	gi|2690302	129	36	66	47	9.05	aspartate aminotransferase precursor [Mus musculus]
	Mix2	gi|38259206	74	31	52	47	8.64	creatine kinase, mitochondrial 2 [Mus musculus]
35		gi|21704020	94	27	37	80	5.51	NADH dehydrogenase (ubiquinone) Fe-S protein 1 [Mus musculus]
36		gi|23346461	66	21	46	53	6.52	NADH dehydrogenase (ubiquinone) Fe-S protein 2 [Mus musculus]
38		gi|20839603	104	20	50	30	6.67	NADH dehydrogenase (ubiquinone) Fe-S protein 3 [Mus musculus]
41	Mix1	gi|31980648	193	44	69	56	5.19	ATP synthase, H+ transporting mitochondrial F1 complex, beta subunit
	Mix2	gi|6680748	175	35	56	60	9.22	ATP synthase, H+ transporting, mitochondrial F1 complex, alpha subunit [Mus musculus]
45		gi|16741459	136	19	95	19	5.52	ATP synthase, H+ transporting, mitochondrial F0 complex, subunit d [Mus musculus]
46	Mix1	gi|22267442	113	31	53	48	9.26	RIKubiquinol cytochrome c reductase core protein 2 [Mus musculus]
	Mix2	gi|12846081	93	30	47	53	5.81	unnamed protein product [Mus musculus]
	Mix3	gi|13384794	79	28	46	53	5.75	ubiquinol-cytochrome c reductase core protein 1 [Mus musculus]
49	Mix1	gi|18250284	88	18	41	40	6.27	isocitrate dehydrogenase 3 (NAD+) alpha [Mus musculus]

Spot	Mix*	gi-Nr.	Probability based Mowse Score	Matched Peptide	Sequence coverage [%]	MW [kDa]	pI	Protein name
	Mix2	gi|126897	66	12	47	36	8.83	Malate dehydrogenase, mitochondrial precursor
54		gi|387422	76	6	26	36	8.93	malate dehydrogenase
55		gi|1372988	80	10	49	20	9.10	cytochrome c oxidase subunit IV
58	Mix1	gi|13096984	82	23	45	57	5.88	Glucose regulated protein [Mus musculus]
	Mix2	gi|563510	68	25	48	63	5.85	epoxide hydrolase 2, cytoplasmic [Mus musculus]
60	Mix1	gi|6680836	208	40	61	48	4.33	calreticulin [Mus musculus]
	Mix2	gi|38511616	62	19	32	49	9.16	Myef2 protein [Mus musculus]
57		gi|42415475	205	34	53	57	4.77	prolyl 4-hydroxylase, beta polypeptide; protein disulfide isomerase [Mus musculus]
56	Mix1	gi|6680836	89	22	39	48	4.33	calreticulin [Mus musculus]
	Mix2	gi|42415475	74	19	37	57	4.77	prolyl 4-hydroxylase, beta polypeptide; protein disulfide isomerase [Mus musculus]
52		gi|6680027	104	29	47	61	8.05	glutamate dehydrogenase [Mus musculus]
50	Mix1	gi|31981562	135	31	54	58	7.18	pyruvate kinase 3 [Mus musculus]
	Mix2	gi|6680027	123	31	55	61	8.05	glutamate dehydrogenase [Mus musculus]
48	Mix1	gi|18700024	127	25	51	42	8.76	isocitrate dehydrogenase 3, beta subunit; isocitrate dehydrogenase 3 beta
	Mix2	gi|18250284	76	20	42	40	6.27	isocitrate dehydrogenase 3 (NAD+) alpha [Mus musculus]
	Mix3	gi|6680345	67	16	31	43	9.17	isocitrate dehydrogenase 3 (NAD+), gamma [Mus musculus]
43		gi|53450	94	18	56	25	8.80	manganese superoxide dismutase [Mus musculus]

**Mix: Protein mixtures in the same protein spots.*